NOBLE METALS IN SULFIDE AND OXIDE MINERALS,

STRATHCONA MINE, SUDBURY

DISTRIBUTION OF SOME NOBLE METALS IN SULFIDE AND OXIDE MINERALS IN STRATHCONA MINE, SUDBURY

By

Lindgren Lin Chyi, B.Sc., M.Sc.

A Thesis

Submitted to the School of Graduate Studies

in Partial Fulfilment of the Requirements

for the Degree

Doctor of Philosophy

McMaster University

August, 1972

DOCTOR OF PHILOSOPHY (1972)
(Geology)

McMASTER UNIVERSITY
Hamilton, Ontario.

TITLE: Distribution of Some Noble Metals in Sulfide and Oxide Minerals in Strathcona Mine, Sudbury

AUTHOR: Lindgren Lin Chyi, B.Sc. (National Taiwan University)
M.Sc. (McMaster University)

SUPERVISOR: Dr. J. H. Crocket

NUMBER OF PAGES: xviii, 183.

SCOPE AND CONTENTS: Neutron activation analysis has been carried out to determine the concentrations of Pd, Ir, Pt, and Au in coexisting pyrrhotite-magnetite-chalcopyrite-pentlandite from deep zone ore of Strathcona mine, Sudbury. The concentration profiles of Pd, Ir, and Au from disseminated sulfide along the 2750 cross-cut of the mine were also measured.

It has been shown that the dominant mode of occurrence of these metals is solid solution in host sulfide and oxide minerals at average concentration ranges from 1.5 p.p.m. for Pt to 3 p.p.b. for Ir. The distribution of the noble metals is considered in terms of

magmatic temperature and subsolidus events. At magmatic temperatures, all four noble metals are found to fractionate fairly strongly into pyrrhotite solid solution; at subsolidus conditions, Pt strongly prefers chalcopyrite and Pd and Au, pentlandite. The basis of these effects are discussed in the light of thermodynamic, molecular orbital, and diffusion theories.

The implications of the concentration profiles of Pd, Ir, and Au in the petrogenesis and origin of the Strathcona sulfides are discussed.

ACKNOWLEDGEMENTS

I wish to express my sincere gratitude to Professor J. H. Crocket for his guidance and assistance throughout the work. My thanks are also extended to my supervisory committee, including Professors K. Fritze and H. D.Grundy.

I am grateful to Dr. A. R. Graham and Mr. M. K. Abel for their permission and assistance to collect underground samples, and making assay data and geological maps available.

My special thanks go to Professor D. M. Shaw, Professor P. M. Maitlis, and many graduate students of Geology, Chemistry, and Physics Departments for their generous time, and many stimulating and critical discussions.

The essential financial support was provided by the National Research Council of Canada, Falconbridge Nickel Mines Limited, and McMaster Graduate Fellowships.

CONTENTS

LIST OF TABLES

LIST OF FIGURES

LIST OF PLATES

ABSTRACT

The concentrations of four noble metals, Pd, Ir, Pt, and Au have been determined by neutron activation on carefully separated coexisting minerals - including pyrrhotite, magnetite, chalcopyrite, and pentlandite from the deep zone ore of the Strathcona mine, Sudbury. The proportions of Pt:Pd:Au:Ir are approximately 500:250:10:1 with average concentrations ranging from 1.5 p.p.m. for Pt to 3 p.p.b. for Ir. It has been shown that at this concentration level the dominant mode of occurrence of these metals is solid solution in host sulfide and oxide minerals.

The distribution of the noble metals is considered in terms of an initial high temperature event where fractionation between pyrrhotite solid solution and magnetite has been of importance, and in terms of subsolidus events where distribution between pyrrhotite solid solution and exsolved chalcopyrite below 450°C and pyrrhotite solid solution and pentlandite below 300°C has affected noble metal distribution.

At magmatic temperatures, all four noble metals are found to fractionate fairly strongly into pyrrhotite solid solution:

Pd by 26; Pt by 6; Au by 5; Ir by 2.

This large fractionation is probably due to the highly covalent bond type of pyrrhotite solid solution and the possibility of the noble metals forming π-bonds with chalcogen or pnigogen anions isomorphously held in pyrrhotite solid solution.

There is a general enrichment of Pd in pentlandite relative to chalcopyrite, pyrrhotite, and magnetite by ratios of 6, 13, and 140 respectively; Pt in chalcopyrite relative to pentlandite, pyrrhotite, and magnetite by ratios of 9, 9, and 18 respectively; Au in pentlandite relative to chalcopyrite, pyrrhotite, and magnetite by ratios of 8, 11, and 28 respectively. Because of the strong preference of Pt for chalcopyrite and Pd and Au for pentlandite, it is concluded that under subsolidus conditions these metals diffuse from pyrrhotite solid solution at temperatures similar to those at which Cu and Ni exsolve, probably 450°C or less. Grain boundary diffusion processes which would prevail at these low temperatures are probably dominant. The enrichment of Pd and Au in pentlandite is also probably related to the transition of ferrous iron from a high- to low-spin state.

Concentration profiles for Pd, Ir, and Au measured along the 2750 level cross-cut include the border group of the Irruptive (mafic norite), the mafic sub-layer including part of the main zone ore, and the leucocratic sub-layer. The Ir profile indicates that the Irruptive proper, the main zone ore, and the deep zone ore represent three different intrusions. The Au profile suggests that secondary dispersion of Au due to intrusion of diabase dike is likely.

The noble metal data from the 2750 cross-cut do not support a cosmogenic origin of the Sudbury copper-nickel sulfides because the noble metals are not arranged in a density sequence away from the center of the Irruptive as required by the impact hypothesis. Further, the noble metal ratios of the sub-layer sulfides do not indicate that they were derived directly from the siderophyllic phase of a differentiated meteorite.

CHAPTER I

INTRODUCTION

Mining of the nickel-copper deposits of the Sudbury district, Ontario, began in 1887. The first recognized platinum metal recovery in the area, however, was in 1919. Because of the increasing platinum metal demand, the recovery from this area had made Canada the first platinum metal producer by 1936. This status continued until 1956 and 1957, when the South African output from the deposits of the Bushveld Complex outstripped Sudbury. Russia for a long time ranked third, but as the Uralian placers became depleted, deposits were found in Siberia that by 1961 raised the Russian output to first rank. Canada has ranked third since that time.

The total production of platinum metals from Canada before 1962 came almost exclusively from Sudbury, but since 1962 the nickel-copper mine at Thompson, and lately the similar ore body near Lynn Lake, Manitoba, have added a minor sum.

In Sudbury, the tenor of the platinum metals are generally low, and they are recovered only as by-products of the production of nickel and copper in contrast to the Bushveld where the platinum metals are the major product, and copper and nickel are by-products. Other major by-products are selenium, tellurium, gold, silver, cobalt, and iron.

The first platinum mineral discovered in the Sudbury area was that of a platinum diarsenide at Vermilion mine in 1885. The mineral was named sperrylite by Wells (1889) after F. L. Sperry, a chemist of the Canada Copper Co. C. E. Michener isolated two palladium bismuthides in 1939, they were named by Hawley and Berry (1958) as michenerite and froodite. Unfortunately, there has been little major platinum metal research since then.

The low tenor of the metals in the ore has traditionally presented considerable analytical difficulty. Hence, their relative amounts, their abundances in various ore types and mineral phases are all indefinite. The production of these metals over a long period of years can give an average ratio for the metals, although the figures from different workers are rather inconsistent. Their abundances in various ore types and mineral phases was very poorly known until Hawley and coworkers (1951-1953) started analyzing for the metals,

utilizing a fire-assay method with gold or silver as collectors. Their analyses referred only to the relative proportions of the platinum metals in the three ore-bearing minerals - pyrrhotite, chalcopyrite, and pentlandite, and did not at all indicate the abundances of the individual elements. The efficiency of the collecting bead and the low sensitivity of the method itself limit their abundance determinations.

In order to study the platinum metals, methods with better reliability and sensitivity are required. Colorimetry, atomic absorption, and neutron activation analysis meet these requirements (see Table 1-1).

Table 1-1. Sensitivity limits for platinum metal determination by various techniques

Techniques	Sensitivity in ugm metal per gm sample, p.p.m.					
	Ru	Rh	Pd	Os	Ir	Pt
d-c arc emission spectrography	10	10	10	50	50	50
X-ray spectrometry	5	8	10	10	15	15
Neutron activation	0.04	-	0.0005	0.005	0.00004	0.015
Colorimetric	0.01	0.07	0.04	0.1	0.04	0.03
Atomic absorption	3	0.3	0.2	5	20	1

After Crocket (1969), Handbook of Geochemistry; also Perkin-Elmer (1971) with a dilution factor of 10

Crocket et al. (1968) developed a method for simultaneous determination of some noble metals, including Au, Pt, Os, Ru, Pd, and Ir by neutron activation analysis, and Keays and Crocket (1970), and Hsieh (1967) applied the method to the sulfide ores of Sudbury. Noble metal contents ranged in general from several p.p.m. to less than one p.p.b.

The method was applied to a study of the noble metal enrichment trends in the Strathcona mine - a new mine on the north margin of the Sudbury basin, and to the distribution of the metals between the major coexisting sulfides, chalcopyrite and pyrrhotite. The major uncertainties in their analyses were the beta counting of gold and the single-channel gamma counting of iridium where a relatively large error could result from radiochemical contaminants. The large fluctuation of the noble metal content in profiles across the Strathcona orebody also indicated that sampling was not adequate for a study of noble metal variation on this scale.

It is generally accepted that the nickel-copper ores of the different mines in the Sudbury district have different platinum metal tenor. As shown by Keays and Crocket (1970), and Hsieh (1967) these differences remain true within a single mine or even within different mining stopes. With such variances, the noble metal output does not have to follow the output of the base metal closely as pointed

out by Mertie (1969). By mining ores of higher or lower content of the platinum metals, the output of the noble metals may be regulated.

The Strathcona mine is an excellent deposit for such a study. Its mining geology has been studied by Cowan (1968) and its petrology and some aspects of its geochemistry by Naldrett and Kullerud (1967). Preliminary noble metal geochemistry was done by Keays and Crocket (1970). Continuing geological studies by Greenman (1970) and Hewins (1971) have added greatly to our knowledge of the sublayer rocks.

In the present work the use of a 1600 channel gamma counting system with 3"x3" NaI(Tl) scintillation and 30cm^3 Ge(Li) diode detectors has made the determination of gold and iridium more accurate. The counter also enables Au^{199} determination of Pt through the $Pt^{198}(n,\gamma)$ $Pt^{199}\xrightarrow{\beta^-} Au^{199}$ reaction. Platinum, iridium, and palladium are the three platinum metals chosen for study as well as gold which is included because it is a major by-product recovered together with platinum group metals.

In addition to the two major sulfide phases studied by Keays and Crocket (1970), magnetite and pentlandite are also incorporated in the present program. The study attempts a genetic interpretation of the partition of the noble metals between the most common Sudbury copper-nickel sulfide mineral assemblage - pyrrhotite, chalcopyrite, magnetite, and pentlandite. Composite chip samples were collected from the

2750 level cross-cut to provide an interpretation of the origin of the copper-nickel sulfide.

CHAPTER 2

GEOLOGY OF THE SUDBURY BASIN

2-1. General Statement

The general geological setting of the Sudbury basin is shown in figure 2-1. The rim of the basin is defined by a norite-micropegmatite unit known as the Nickel Irruptive. It outcrops as an oval ring 37 to 17 miles in diameter, and 1 mile to 3.6 miles in width. The outer part of the ring is norite, and the inner, micropegmatite, with a fairly gradational change from one to the other.

Below the norite is a discontinuous layer of sulfide- and inclusion bearing noritic rock, which was termed by Souch et al. (1969) as the sub-layer. The sub-layer and the associated offset dikes form the most favorable environments for the nickel-copper deposits. Inside the Irruptive, the Whitewater series outcrop in concentric oval rings. Wide dikes of olivine diabase cut indiscriminately through the Nickel Irruptive and the Whitewater series.

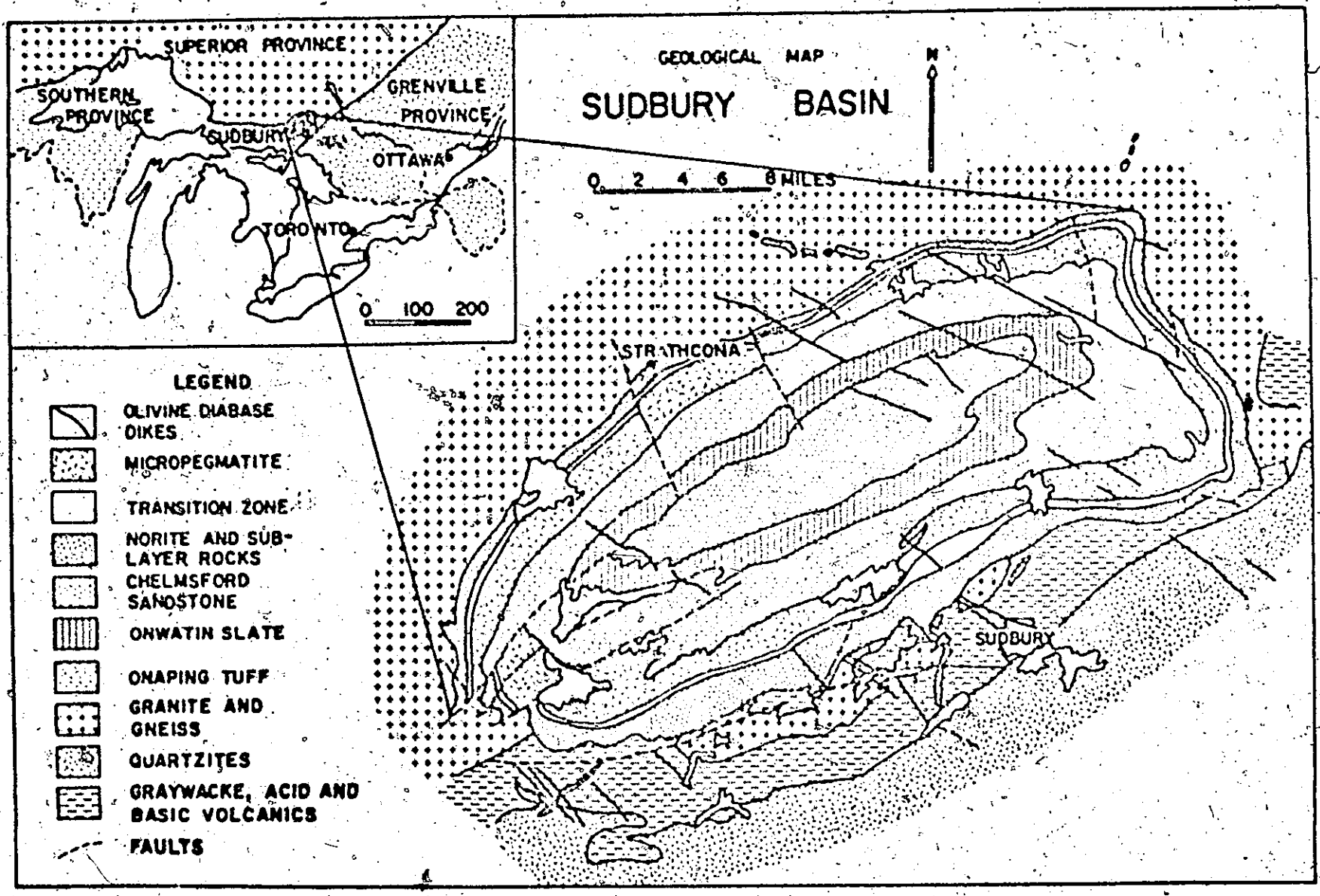

Figure 2-1: General Geological Settings of the Sudbury Basin

Extending southwestward outside the basin is an apparently conformable series of steeply southward dipping graywacke, acid and basic volcanics of middle and early Precambrian age. To the northwestern, the basin is bounded by Precambrian granite and gneiss.

The basin lies near the junction of the Superior, Southern, and Grenville structural provinces. Regionally it is divided by the Cameron Creek fault and the Airport fault into the north and the south ranges with a vertical displacement which exceeds 3 miles (Souch et al., 1969), north side up relative to south. A series of northerly trending and steeply dipping faults cut across the north range between the Levack and Maclennan mines with an accumulated vertical displacement at one-half miles, west side up relative to east. The Maclennan block is thus the highest stratigraphic segment of the Irruptive, and the south range the lowest.

2-2. The Nickel Irruptive

The present near surface outer contact of the Irruptive dips toward the center of the basin with weighted average dips for the north and the south range about 40° and 60° respectively. In the southeast and southwest corners, however, the dips are much steeper, approaching vertical in the southwest and as much as 65° away from the basin in the southeast. The inner contact against the Whitewater group always dips towards the center.

The north and the south range of the Irruptive are petrographically dissimilar, although they have been mapped as a single stratigraphic group. Naldrett et al. (1970) discussed the cryptic variation and petrology of the Irruptive in detail.

On the north range, the inner micropegmatite is a uniform rock about 4500 feet thick consisting of approximately three parts micrographic intergrowth to one part plagioclase with minor augite, biotite, hornblende and secondary minerals. The outer norite has two distinct phases - 1500 feet of light felsic norite and a thin but variable thickness of dark mafic norite. The latter was originally regarded as a sub-layer member (Naldrett and Kullerud, 1967) but recently detailed study (Hewins, 1971) has shown it is part of the main Irruptive. Felsic norite is a coarse grained hypidiomorphic granular rock made up of two parts plagioclase to one part hypersthene and augite with interstitial micrographic intergrowth and minor biotite, apatite, iron oxide and sulfide. The mafic norite is essentially an ortho-pyroxene-rich rock, variable in composition. The contact between these two units varies from transitional to relatively abrupt. An oxide-rich gabbro which overlies the felsic norite, and separates it from the micropegmatite contains up to eight percent opaque oxides, largely ulvospinel, and has an apatite-rich zone in the central part.

On the south range, the inner micropegmatite has been extensively metamorphosed with development of pronounced gneissic foliation marked by the orientation of biotite. The outer norite consists of two facies including the south range norite and the quartz-rich norite. The former is a medium to coarse grained rock containing plagioclase, hypersthene, augite, titaniferous magnetite, quartz, and hornblende as primary minerals, but with extensive secondary alteration particularly uralite and secondary hornblende. The quartz-rich norite is similar to the south range norite except for its high quartz content. There are trends of increasing quartz content and decreasing grain size towards the outer margin of the Irruptive. The south range norite is overlain by upper gabbro which is similar to the oxide-rich gabbro of the north range and grades upwards into micropegmatite.

The Irruptive has been variously interpreted as (1) a folded differentiated-sill, (2) a ring-dike complex, and (3) a differentiated, funnel-shaped intrusion.

The differentiated-sill hypothesis was first proposed by Walker (1897) to explain the upward gradation from norite to micropegmatite. The hypothesis received much support from Coleman (1905, 1913) and Collins (1934, 1935, 1936, 1937). They considered the Irruptive to have been intruded along the unconformity at the base

of the Whitewater group, and the differentiation of magma in situ to have produced norite and micropegmatite with contemporaneous segregation of immiscible sulfide liquids to the base forming sulfide deposits in favorable embayments or offsets. Hawley (1962) favoured this hypothesis because of its successful explanation of the sulfide deposits.

Knight (1917, 1923), who was skeptical of the differentiated-sill hypothesis because the volume of the micropegmatite is much in excess of that to be expected from differentiation of an original gabbroic magma, suggested the multiple ring-dike hypothesis. The strongest evidence for this hypothesis was the fine grained contact facies of norite and micropegmatite, the steep dips both at the southwest and southeast ends of the Irruptive, and the lack of post-intrusive folding. Phemister (1925) further suggested that the transition zone, an oxide-rich gabbro on the north range and the upper gabbro on the south range, was formed by the mixing of the two magmas. This hypothesis was later supported by Yates (1938, 1948) and Thomson (1956, 1969).

These two schools dominated geological interpretations of the Nickel Irruptive until Wilson (1956) demonstrated that the Sudbury Irruptive is similar to the Bushveld complex and other lopoliths in having inward dipping surfaces and layering which dips inward at a more gentle angle than the footwall rock. This led to his further suggestions

that the ultramafic members are at deeper levels, and that the presently exposed proportions of micropegmatite and norite are not necessarily representative of true volumes. Naldrett et al. (1970) presented a revised funnel-shaped intrusion model based on their studies of petrographic texture, the phase layering of various rock-forming minerals, and the cryptic variations of the three cumulus minerals - plagioclase, hypersthene, and augite. They argued that the folding of the inside Whitewater series implied a change of the shape of the Irruptive from circular to oval.

The model of Naldrett et al. (1970) is shown in figure 2-2. They suggested that a somewhat silica-rich magma was emplaced as a funnel-shaped body beneath the Onaping formation. After the intrusion, assimilation of the roof rock took place, the quartz-rich norite formed around the margin and the south range norite accumulated gravitationally. Disturbances during the subsequent cooling caused the remaining magma to intrude farther along the base of the Onaping formation and gave rise to a peripheral sill-like body. Continuous fractionation produced the felsic norite and micropegmatite. Although the model accommodated all the apparent controversies and received popularity, it did not give a satisfactory account of the ultramafic layers at depth common to many funnel-shaped layered intrusions.

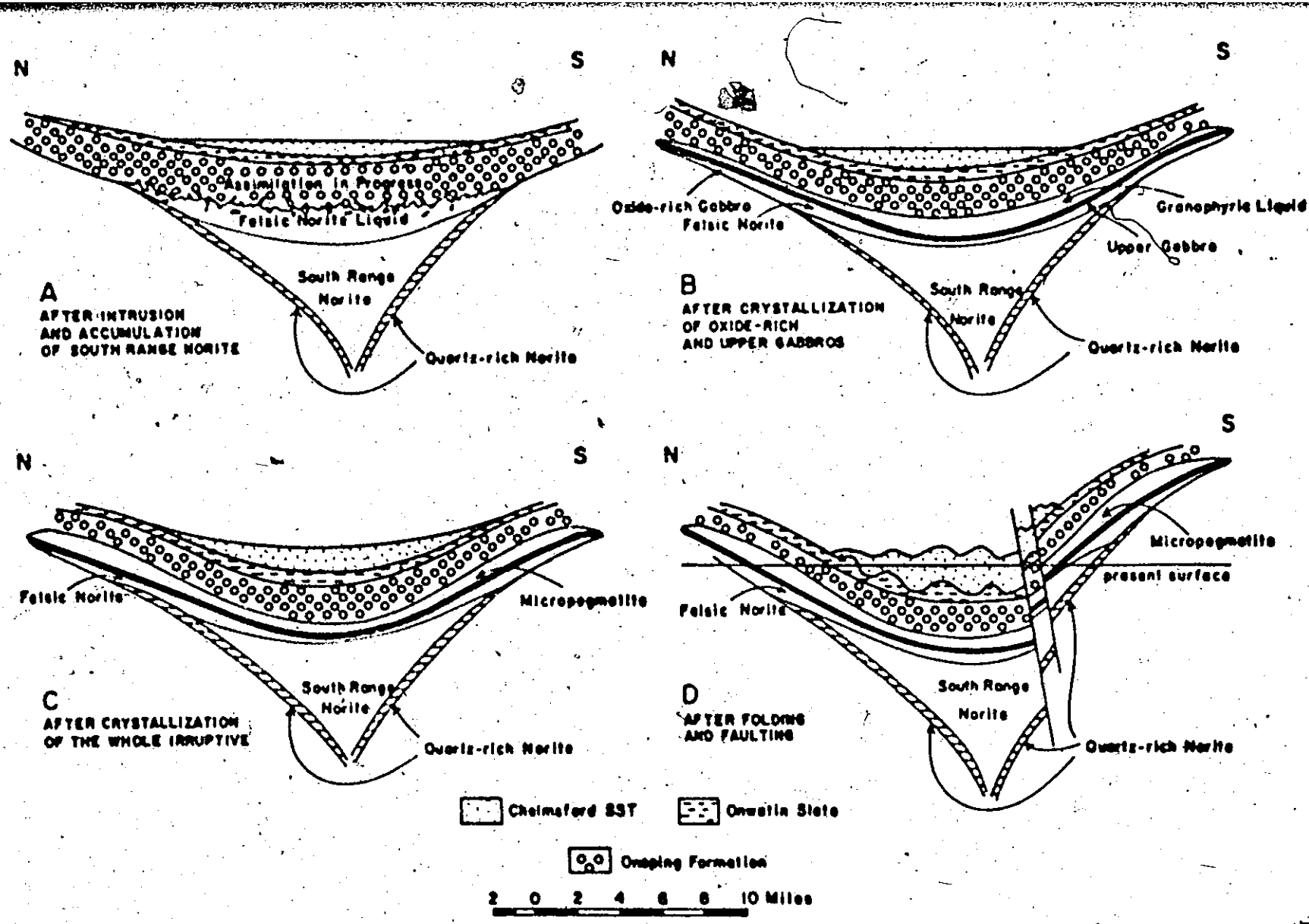

Figure 2-2. A Model for the Crystallization, Folding and Faulting of the Nickel Irruptive (after Naldrett et al., 1970).

Rb-Sr age determinations give 1.70 b.y. for micropegmatite, and between 1.93 and 2.07 b.y. for the south and the north range norite (Gibbins and McNutt, 1972).

2-3. The Sub-layer

A discontinuous layer of sulfide- and inclusion-bearing noritic rock underlying the Irruptive and known as the sub-layer has been described by Souch et al. (1969). They divided the sub-layer environment into north range, south range, and offset dikes as shown in figure 2-3.

The north range environment is characterized by a medium- to fine-grained, inclusion-rich and sulfide-bearing basic norite. The inclusions are either of angular country rocks or a rounded suite of ultramafic and mafic rocks including peridotite, pyroxenite, and gabbro. The silicate mineralogy of the matrix varies from augite norite to hypersthene gabbro in the vicinity of the Strathcona-Fecunis mines (Naldrett et al., 1971). The basic norite may grade downward into finer grained sulfide bearing leucocratic sub-layer breccias which contain abundant footwall rock inclusions and are the hosts of the ore between Levack and Hardy mines. The contact of the sub-layer with the overlying norite is generally abrupt.

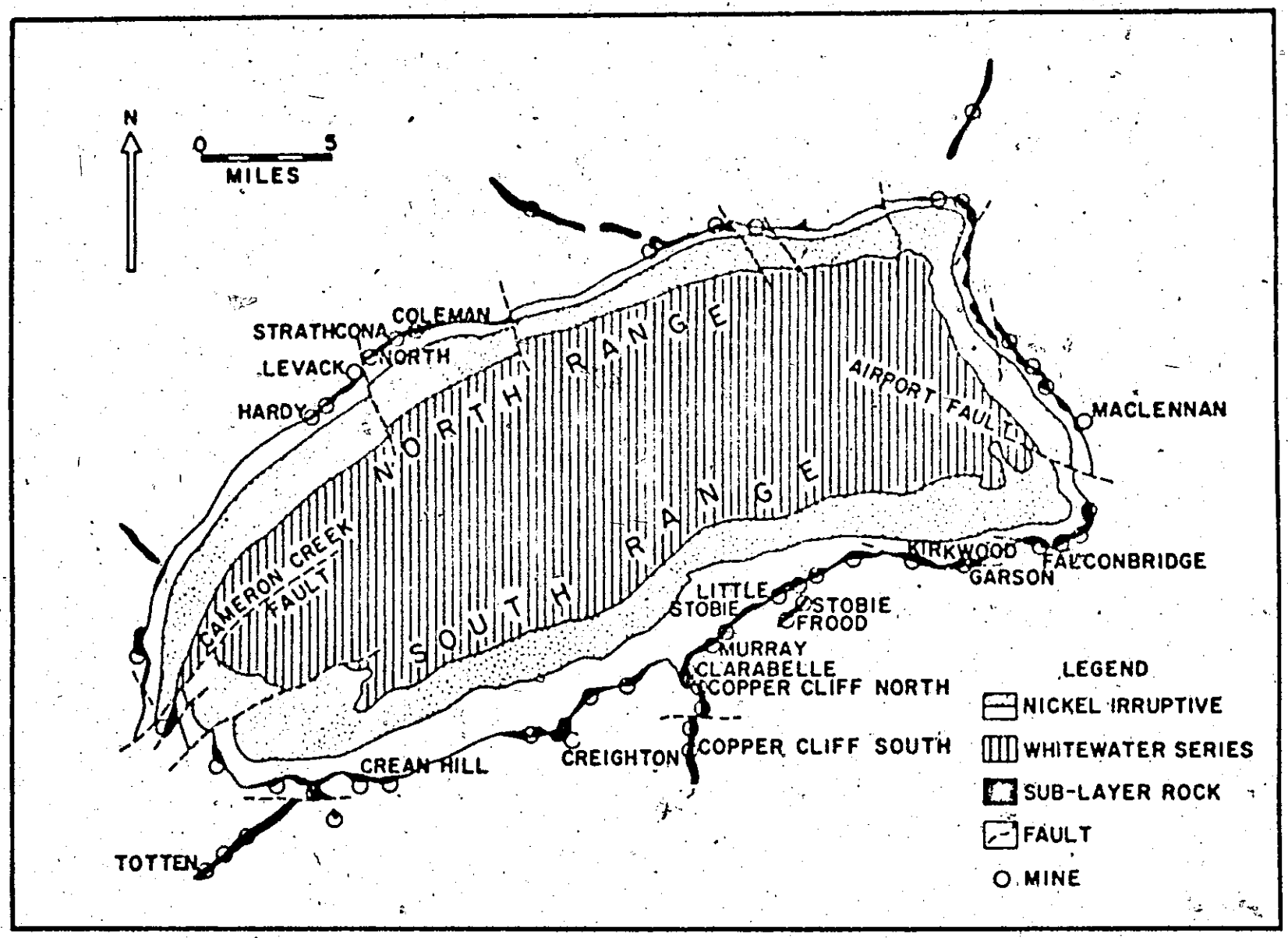

Figure 2-3. The Irruptive, Showing Major Faults and Structural Divisions, and the Relationship between Mines and the Sub-layer.

The south range environment is similar to the north petrologically and petrographically. The inclusions are also country rocks or an exotic suite. The matrix consists of varying amounts of noritic material and sulfide. The contact relation between the sub-layer and the main norite is very difficult to establish.

The offset dikes are steeply dipping bodies that project away from the outer contact of the Irruptive as far as 8 miles. The dominant rock type is quartz diorite which contains quartz, plagioclase, primary hornblende, and biotite; noritic rocks occur occasionally.

In contrast to the main body of the Irruptive, the sub-layer is extraordinarily rich in sulfide. The sulfide is usually limited to the matrix, and may vary from a few to almost one hundred percent. The ores, however, do not alter the proportions of the silicate minerals (Souch et al., 1969).

There is no agreement on the age relations between the sub-layer and the overlying main Irruptive. Isotopic age determinations have not yet yielded reliable ages. Naldrett and Kullerud (1967) argued that the sub-layer is younger based on the petrological information from the Strathcona mine which will be discussed in the following chapter. Dietz (1972) considered that it was formed during a meteorite impact which triggered intrusion of the Irruptive.

2-4. The Ore Deposits

The close association of the Sudbury ore deposits with the sub-layer is very clear as shown in figure 2-3, although the genesis of the Sudbury ore deposits has long been a topic of controversy. The early workers (Bell, 1891; Coleman, 1905) thought that the ores were direct, in situ, gravitational segregations from the main body of the Irruptive. Some of the later workers (Howe, 1914; Bateman, 1917; Collins, Moore, and Walker, 1929; Hawley, 1962) believed that the ores were later injections of sulfide or sulfide-silicate magma; others (Dickson, 1904; Knight, 1919; Wadke and Hoffman, 1924; Phemister, 1925) maintained that they formed from hydrothermal solutions.

One group of recent workers (Naldrett and Kullerud, 1967; Cowan, 1968) impressed by the intermixed nature of the ore bodies and the sub-layer, thought that they were post-Irruptive injections of magmatic sulfide liquids. Dietz (1972), who was also impressed by the intermixed nature, suggested that they were pre-Irruptive and a mixture of Apollo or differentiated asteroid and country rocks. The noble metal information from the present study provides new information bearing on these mutually exclusive hypotheses.

Despite the different interpretations of the genesis of the ores, the close association of the ore deposits with the sub-layer allows a similar genetic classification for the deposits. This classification was attempted in the work of Souch et al. (1969), and again in Naldrett et al. (1971). Following a review of the existing evidence, particularly that of Hawley (1962), Naldrett (1969), and Souch et al. (1969), a detailed genetic classification is summarized as table 2-1.

Naldrett's experimental work (1969) indicates that the emplacement temperature of the ore decreases with increasing copper content with a minimum at 1000°C.

Structurally, the north and the south range deposits may be classified as marginal types. The majority of the marginal deposits occupy structural embayments, form lenticular or sheet-like ore bodies, and are arranged en echelon and more or less parallel to the footwall contact. The off-set types, however, occur as sheet-like, or pipe-like steeply dipping bodies in the quartz diorite beyond the margin of the Nickel Irruptive.

Cowan (1967) and Souch et al., (1969) recognized two types of cryptic metal zoning in the marginal deposits. Copper, nickel, and the Cu/Ni ratio increase towards the footwall, but show little variation with depth. The off-set deposits usually show mineral zoning with an upper disseminated ore-bearing quartz diorite and a lower siliceous zone rich in arsenides, bismuthides, noble metals, and secondary silicates.

The normal ore mineralogy at Sudbury is quite simple. It consists almost entirely of pyrrhotite, pentlandite, and chalcopyrite with variable but closely associated magnetite. Cubanite may become abundant in off-set deposits, but never in the marginal environment. According to Hawley (1962), arsenides and bismuthides occur as minor minerals in the siliceous zones of the off-set environment, and occasionally are encountered in the south range but are never reported in the north range. Secondary nickel minerals like millerite, violarite are sometimes observed in the off-set and south range environments but are only reported as rare minerals in the north range.

The gangue minerals in the marginal environments are mainly primary silicates present in various mafic and ultramafic inclusions and the noritic matrix. Secondary silicates, like epidote, chlorite, and poikiloblastic green and brown biotite occur as reaction rims around sulfides. The gangue mineral assemblages in the off-set environment, however, are quite variable and usually include quartz and carbonate in addition to the secondary silicates.

Souch et al. (1969) classified the Sudbury ore into two groups and eight major types. The two groups are (1) disseminated sulfide, and (2) inclusion bearing sulfide ores. Disseminated sulfide makes up

two-thirds of the production of the district, and comprises (1) sulfide as blebs in quartz diorite known as "buck-shot" ore, (2) blebs in granite breccia, (3) an interstitial phase in norite, and (4) discontinuous patches between fragments in a closely packed inclusion rock. The inclusion bearing sulfide ores comprise (1) gabbro-peridotite inclusion massive sulfide (G. P. I. S.), (2) contorted schist inclusion sulfide, (3) inclusion massive sulfide, and a rare (4) massive sulfide with quartz diorite blebs. Both the disseminated and the inclusion-bearing sulfide ore may vary widely in appearance and grade into massive sulfide as the inclusion material decreases. The distribution of the eight types in the three environments are listed in decreasing order of abundance in table 2-1.

2-5. Rock Units Inside and Outside the Nickel Irruptive

The rocks inside the basin comprise the Whitewater series made up of, in ascending order, the Onaping formation, the Onwatin slate, and the Chelmsford sandstone.

The Onaping formation has great lateral extent and tremendous volume of almost unsorted breccia composed of fragments of various country rocks in a mainly dark, fine grained, carbonaceous matrix characterized by numerous shard-like fragments of devitrified glassy material. This grades upward through a mixed zone into the siltstone and slate of the overlying Onwatin slate.

Table 2-1. Classification of the Environments of the Sudbury Copper-Nickel Deposits

Environment	North Range	South Range	Off-set
Minimum Emplacement Temperature	1000°	1000°	1000°
Pressure	Medium total pressure; low water pressure	High total pressure; medium water pressure	Medium to high total pressure; high water pressure; high As, high CO_2
Ore Mineralogy Major	Pyrrhotite-pentlandite-chalcopyrite-magnetite assemblage;	Pyrrhotite-pentlandite-chalcopyrite-magnetite assemblage;	Pyrrhotite-pentlandite-chalcopyrite-magnetite assemblage;
Minor	rare secondary minerals	arsenides and minor secondary minerals	arsenides, bismuthides, precious metal minerals and secondary minerals
Structure Control	Lenticular, sheet-like; en echelon and moderate dipping	Lenticular, sheet-like; en echelon and moderate dipping	Sheet-like, pipe-like; steeply dipping
Zoning	Cryptic Cu and Ni zoning increasing concentration towards footwall	Cryptic Cu and Ni zoning increasing concentration towards footwall	Mineral phase zoning
Gangue Minerals	Primary silicates and minor secondary silicates	Primary silicates and minor secondary silicates	Secondary silicates, quartz, and carbonates
Ore Types	Disseminated sulfide, inclusion massive sulfide	Disseminated sulfide, G.P.I.S., contorted schist, inclusion sulfide	Disseminated sulfide, inclusion massive sulfide, contorted schist, inclusion sulfide, massive sulfide with quartz diorite blebs

There are two views on the origin of the formation. Thomson (1956), Williams (1956), and Stevenson (1972) think that it is of volcanic origin with feeder vents of the fissure type. Dietz (1964) suggested a meteorite impact origin with the Onaping formation representing an accumulation of material excavated by the impact, the quartzite breccia representing fallback breccia. French (1968) presented some petrographic evidence and supported this view. Less familiar volcanogenic lead-zinc-copper deposits occur at the contact with the overlying Onwatin slate.

The Onwatin slate is a fine grained carbonaceous, pyritic argillite with local thinly laminated limestones and cherts. It has a thickness of at least 1000 feet. It is entirely waterlain and grades upward into the Chelmsford sandstone, which is a carbonaceous subgraywacke and considered by Bouma (1962) as a turbidite bed.

There is no agreement on the age of the Onaping formation. Williams (1956), Thomson (1956), and Phemister (1956) concluded that it was coeval with so-called Keewatin-type volcanism represented by the Stobie formation to the south of the basin. Some workers arguing mainly on isotopic determinations contend that it was Late Precambrian (1.4 b.y., Fullagar et al., 1971) in age. And Dietz (1972) believed it was fallback microbreccias of meteorite impact and slightly earlier than the Irruptive.

Outside the basin, there are thick successions of Huronian sediments and metavolcanics of the Southern Province to the south of the basin. According to Card & Hutchinson (1972), they were deposited about 2.3 b.y. ago. This succession faces south stratigraphically and ranges upwards from greenstone (Stobie formation) to a conglomerate (Ramsey Lake conglomerate) and an overlying quartzite (Wanapitei quartzite). They strike east-northeast and dip at steep angles but mainly to the north. The series has been intruded by the Copper Cliff rhyolite and granite at 2.1 b.y. ago (Fairbairn et al., 1965).

The Irruptive is bound to the north by Archean granite and quartz-plagioclase-augite gneisses. A belt about ten miles wide, occurs below the Irruptive and around the basin, and contains shatter cones (Guy-Bray et al., 1966), with planar features in quartz and kink bands in biotite (Greenman, 1970). The former are developed around the outer contact of the Irruptive and considered diagnostic of impact, while the latter are generated during both shock metamorphism and tectonism (Bunch, 1968).

2-6. Cosmogenic Ore Hypothesis

Dietz postulated in 1962 that the Sudbury structure was an ancient meteorite impact scar. The discovery of shatter cones around the basin (Guy-Bray et al, 1966), and planar structures in quartz and feldspar (French, 1967, 1968) gave this hypothesis petrological and petrographical support.

Based on this background, he postulated further in 1971 that the Sudbury nickel copper sulfide ores might also be meteoritic parenthood.

The main points of his new hypothesis are summarized below and presented in figure 2-4:

1. Impact of a 4-km-diameter Sudbury "moon" probably an Apollo asteroid 1.7 b.y. ago on 2.2 b.y. Huronian sediments.
2. Hemispherical spreading of the impact shock wave, creating shatter cones pointing towards ground zero.
3. Formation of an impact crater about 40 km in diameter and 4 km deep. Upheaval of the country rock with simultaneous emplacement of the sub-layer as the impacting bolide literally turned inside out and swept up the side walls of the crater. The sub-layer must include sulfide of meteoritic origin as well as country rock melt which filled the concave swales in the crater wall and was injected into spoke-like radial tension cracks. The iron-nickel-copper rich phase of the differentiated bolide provided the parental substances for the Sudbury sulfide deposits.

4. Fallback into the crater of the Onaping microbreccias as a suevite.

5. Emplacement of the Irruptive melt rock guided by the saucer-shaped crater. The magma would result primarily from a conventional magmatism triggered at depth by the shock decay heat and static offloading of the deep crust and upper mantle after the impact. Modification of magma composition would result from partial assimilation of shock-produced micro-breccias of the Onaping Formation roof rocks.

6. Differentiation of the Irruptive into micropegmatite and norite on gradual cooling.

7. Modification of the crater's bowl-shaped form by collapse over a magma chamber and by isostatic adjustments.

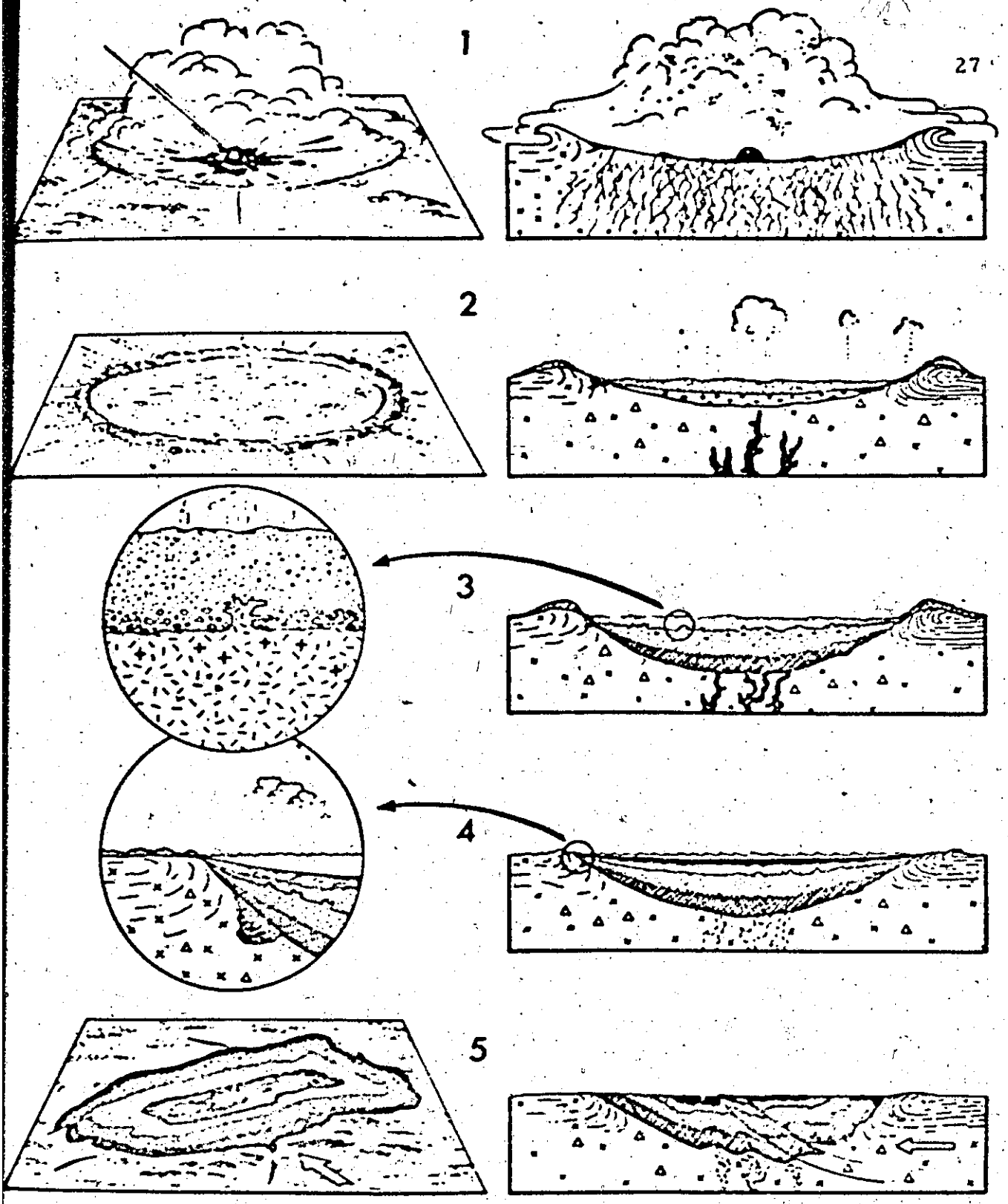

Figure 2-4. A time sequence diagram of the development of the Sudbury Basin by asteroidal impact (after Dietz, 1972).

CHAPTER 3

GEOLOGY OF THE STRATHCONA MINE

3-1. General Statement

The Strathcona mine lies on the northwest rim of the basin (figure 2-1). It is one of the newest mines in the area. The underground pre-production development started in 1965 and partial operation commenced late 1967 with full production achieved only mid-1969. It is, by far, the largest producing mine owned by Falconbridge Nickel Mines Limited in the area.

The newness of the mine allows the application of both traditional and modern investigations. Naldrett and Kullerud (1967) studied its silicate mineralogy and petrology; Cowan (1968) studied the general mining geology, and metal and mineral zoning; Keays and Crocket (1970) studied the noble metal distribution; Greenman (1970) studied the petrology and mineralogy of the footwall breccias, and Hewins (1971) examined the mafic noritic and the sub-layer rocks. The information accumulated has aided not only the develop-

ment of the mine but also the understanding of the regional geology of the Sudbury basin.

The mine is a typical north range mine (see Table 2-1). It is closely associated with the sub-layer (figure 2-5) and has a typical major and minor ore mineralogy, general structural control, and cryptic zoning. Disseminated sulfide is the most important ore type in the upper portion of the mine with chalcopyrite-rich massive stringers increase downwards.

According to their relation to the host rock, the ores are subdivided into three zones - the hanging-wall zone, the main zone, and the deep zone. They are similar in ore mineralogy, but different in metal content. There is no agreement so far on the origin of the three ore zones.

3-2. The Rock Units

There are four groups of rock in the vicinity of the Strathcona mine. They are, in ascending order, the granitic gneiss complex, the southward dipping sub-layer, the Nickel Irruptive, and the younger dikes which cut through all the above units. The general relations of the rock units are shown in figures 3-1 and 3-2.

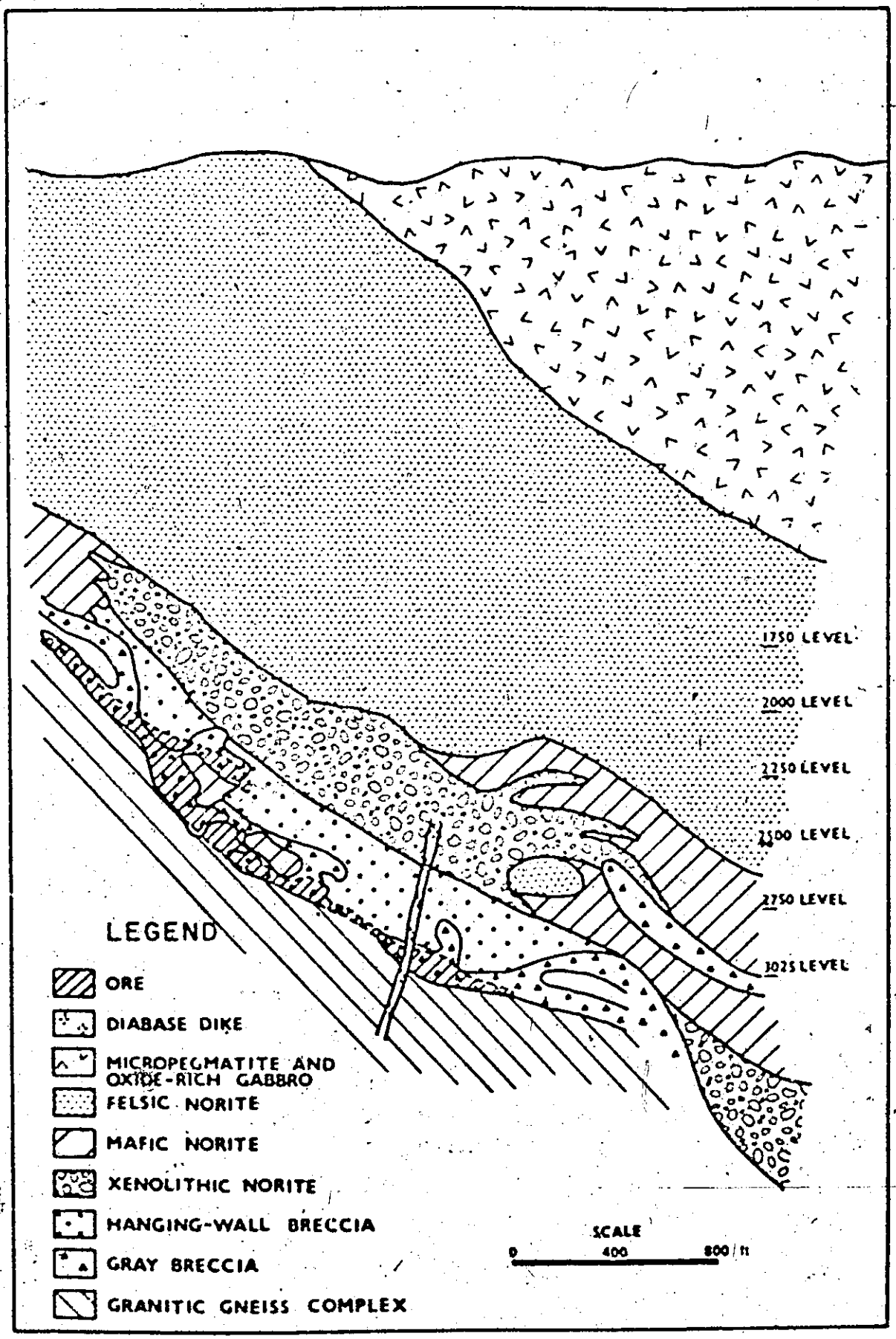

Figure 3-1. Vertical Geological Section (21, 200E) of the Strathcona Mine (after Naldrett and Kullerud, 1967).

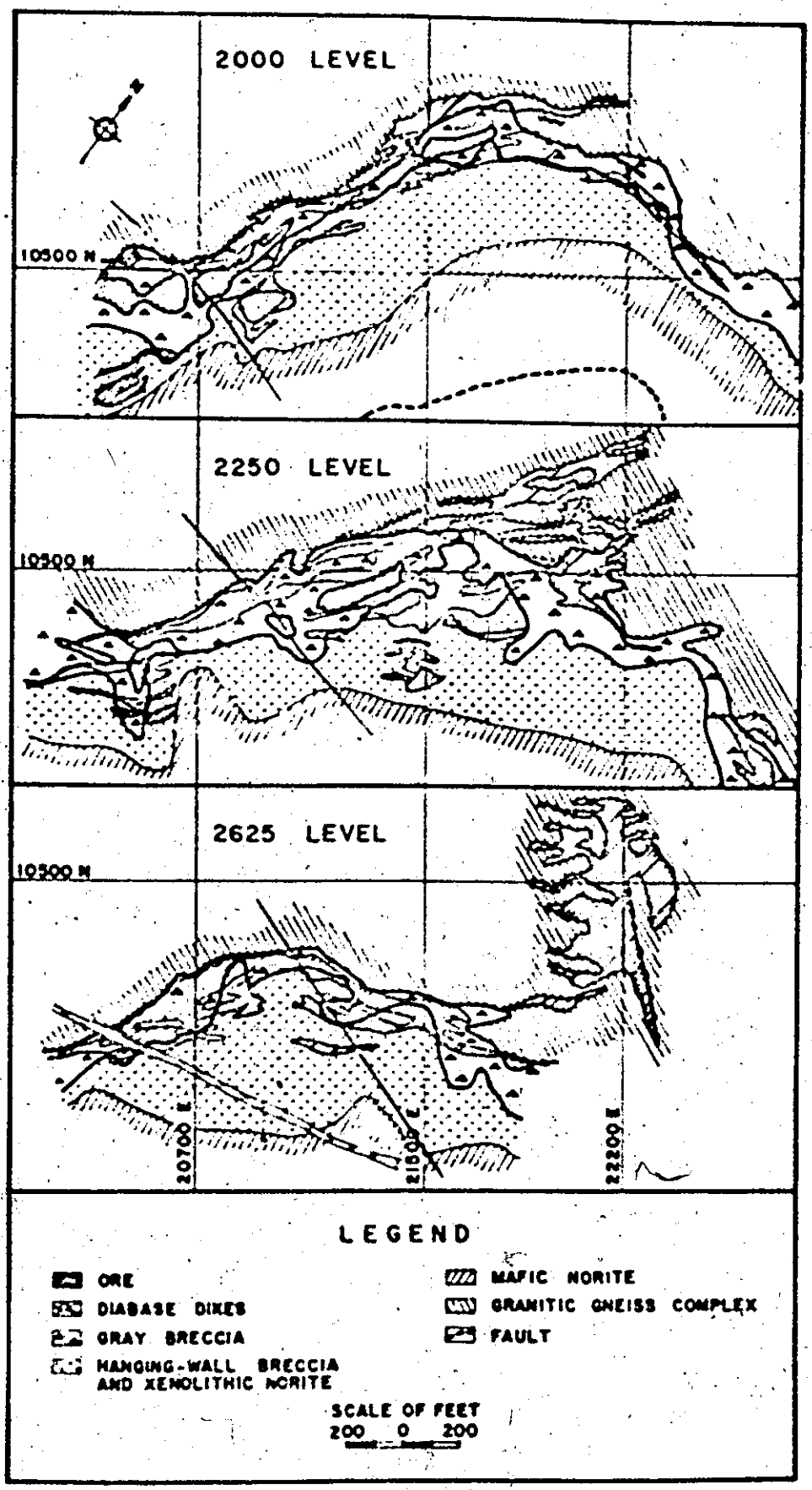

Figure 3-2. Horizontal Geological Sections of Strathcona Mine (after Cowan, 1968).

3-2-1. Granitic Gneiss Complex

In the vicinity of the mine, the granitic gneiss complex is composed of an Archean tonalitic and mafic gneiss known as the Levack complex of Superior structural province. Details of the complex are discussed in Greenman's Ph. D. thesis.

3-2-2. The Sub-layer

The sub-layer composes two phases - the mafic sub-layer and the leucocratic sub-layer as termed by Naldrett et al. (1971). The leucocratic sub-layer or gray breccia as termed by Greenman (1970) overlies the Levack complex while the mafic sub-layer overlies the leucocratic sub-layer.

The ore-bearing gray breccia is dike-like in character, has a metamorphic matrix texture, and contains most of the nickel-copper sulfide ore of the mine. Based on the distribution of the oxides and sulfides in the silicate matrix, Greenman (1970) interpreted the breccias as having been intruded in a fluidized state shortly after the injection of the mafic sub-layer. Based on similarity in form and composition with their counterparts in the hanging-wall breccia, the oxides, sulfides, and many of the inclusions were derived from the mafic sub-layer.

Cowan (1968) mapped the mafic sub-layer as two separate units distinguished on a basis of volume of xenoliths. Rock with less than 30 percent xenoliths he termed xenolithic norite or basic norite, whereas rock with more than 30 percent xenoliths was called hanging-wall breccia. Cowan grouped basic and mafic norite together as dark norite. These terms contradict the genetic interpretation of Hewins (1971) who demonstrated that the mafic norite is an integral part of the Irruptive while the xenolithic norite and hanging-wall breccia belong to a separate intrusion. We will adapt the terms used by Hewins.

The matrix of the hanging-wall breccia has been more or less altered and strongly mineralized so that it constitutes a major host of the ore. It is best developed in embayments where the Irruptive protrudes into the footwall rocks as shown particularly clearly on the 2250 level (figure 3-2).

The probe studies of Hewins (1971) indicate that the mafic sub-layer is a separate intrusion from the main Irruptive and is contaminated by mafic norite. Important evidence supporting this viewpoint is that the basic rocks in the mafic sub-layer lack the cryptic variation shown by mafic norite. The average plagioclase is more calcic whereas the pyroxenes are more iron-rich than those in mafic norite. The xenocrysts and anomalously magnesium-rich ortho-

pyroxene at the top of the mafic sub-layer gabbro indicate that the mafic sub-layer was contaminated by the mafic norite which is interpreted as a border group of the Irruptive.

3-2-3. The Irruptive

Felsic norite is 1800 feet thick in this area. Usually it is a coarse-grained, light colored rock composed of 50 percent subhedral, zoned plagioclase, 30 percent highly altered clinopyroxene and orthopyroxene, and 10 percent micrographic intergrowth. Sulfide is usually less than 2 percent and thus the rock is not a host of mineralization. Light colored inclusions, mainly altered plagioclase, minor pyroxene and quartz, commonly form 10 percent of the lower part of the felsic rock.

The underlying mafic norite is a medium grained, gray to black colored rock with a thickness varying from 0 to 400 feet. The contact with the overlying felsic norite can be sharp or gradational with inter-fingering lenses of the two phases. It is composed of 40 percent zoned plagioclase, 30 percent hypersthene, and 1 percent clinopyroxene. It has been subdivided into poikilitic and hypidiomorphic mafic norite according to whether pyroxene is enclosed in plagioclase poikilitically or forms hypidiomorphic granular texture with it. The former passes up into the latter in all the sections studied by Hewins.

The felsic norite approaches a mesocumulate at Strathcona because of the zoned plagioclase; the hypidiomorphic and the underlying poikilitic mafic norite, on the other hand, are orthocumulates. The decreasing Fe/Fe+Mg ratios and a change in the character of zoning in orthopyroxene with height indicate a change from an in situ crystallized border to a poikilitic and largely gravitationally accumulated hypidiomorphic mafic norite. Both cryptic variation of Fe/Fe+Mg in orthopyroxene and Cr_2O_3 in orthopyroxene and magnetite suggest that the mafic norite is a part of a sequence continuous with the felsic norite.

Hewins revised the funnel-shaped intrusion model of Naldrett in order to accommodate the mafic norite as an integral part of the Irruptive. His model is reproduced in figure 3-3. Poikilitic mafic norite is considered a border group formed by crystallization in situ while hypidiomorphic mafic norite is a later gravitational accumulate in a funnel-shaped chamber. Felsic norite was formed by a rapid crystallization in a sill environment during later resurgence of the magma.

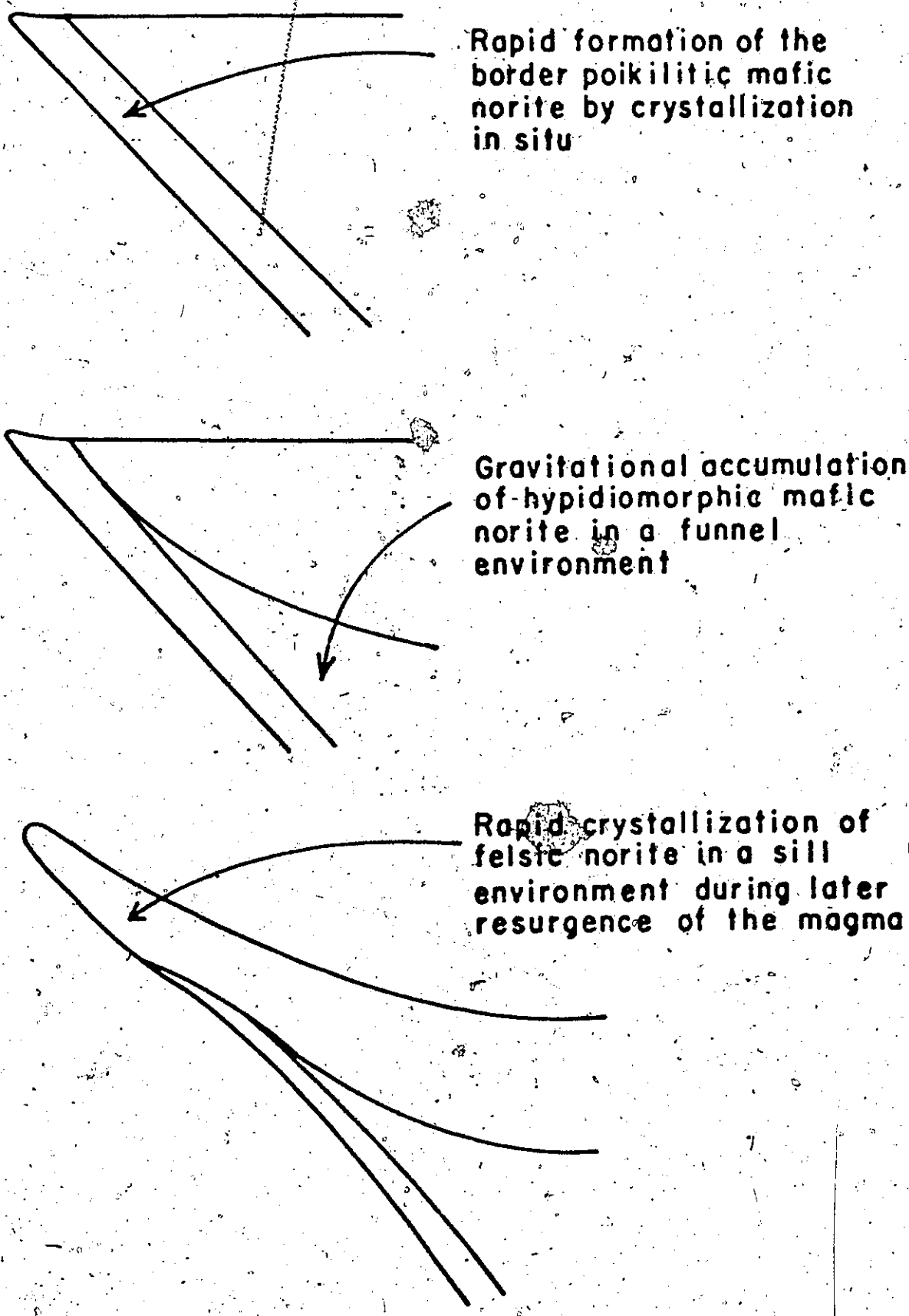

Figure 3-3. Hewins' model for the North range Irruptive

3-2-4. The Diabase Dikes

There are two types of diabase dike at Strathcona - quartz diabase and olivine diabase. These dikes cut through all the other rocks and represent the last stage of igneous activity and are post-ore in age. Olivine diabase, dated at 1.02 b.y. (Fairbairn et al, 1960), is the younger of the two types and cuts the quartz diabase dike.

The quartz diabase is a medium-grained, non-porphyritic rock in which the principal minerals are altered laths of labradorite, subhedral uralitized clinopyroxene, and about 2 percent quartz as interstices. The dikes average 40 feet in width, have a sharp contact with the enclosing rock, and appear to have some degree of grain gradation.

The olivine diabase is a fine-grained, porphyritic rock and is composed of 30 percent phenocrysts of labradorite and olivine set in a fine-grained intergranular matrix of labradorite, augite, and opaque oxides. The dikes have a variable width from a few inches to a maximum of 10 feet. They are commonly strongly sheared and jointed, have a sharp contact with the enclosing rock, and a thin chilled margin.

3-3. The Ore Zones

The Strathcona ore bodies are a series of lenticular sub-parallel ore lenses, arranged en echelon over a vertical extension of 1800 feet and a strike length of 2600 feet (figure 3-1). These ore

lenses are subdivided into the hanging-wall, the main, and the deep zone with respect to their relation to the enclosing rock. The hanging-wall zone is enclosed entirely in xenolithic norite and hanging-wall breccia near the base of the Irruptive. The main zone is largely in the late gray granitic breccia and the deep zone is completely enclosed in the granitic gneiss complex and lies up to 1200 feet below the base of the Irruptive.

The major ore mineralogy is similar to other deposits of the Sudbury basin commonly consisting of 3/4 pyrrhotite, 1/4 pentlandite, chalcopyrite, and magnetite in variable proportions. In general, the pentlandite and chalcopyrite content and the chalcopyrite/pentlandite ratio increase downward parallel to the base of the Irruptive. The minor sulfide minerals include pyrite, millerite, bornite, cubanite, and galena. Disseminated and inclusion massive sulfide are the major ore types.

3-3-1. The Hanging-wall Zone

The hanging-wall ore constitutes 10 percent of the ore reserve. The sulfides occur as disseminated blebs, composite grains, and patches within the matrix of xenolithic norite and hanging-wall breccia. The ore bodies commonly occur in embayments along the strike and above flattenings of the base of the hanging-wall breccia.

Alteration of the silicate gangue by sulfides is minor, but silicates enclosed in sulfides sometimes exhibit thin reaction rims which suggest that minor amounts of water were associated with the sulfide phase.

Pentlandite, which exhibits typical net and flame structure is interstitial to and rims the larger pyrrhotite grains. Chalcopyrite which is usually less than 3 percent, mantles and embays both pyrrhotite and pentlandite. The hanging-wall ore contains up to 15 percent rounded magnetite grains which may contain up to 30 percent oriented ilmenite blades. Pyrite, usually less than 2 percent, occurs as large grains cut by chalcopyrite or as small euhedra of reaction origin (Cowan, 1968).

3-3-2. The Main Zone

The main zone represents 70 percent of the ore reserve. The sulfides commonly occur as either inclusion massive or as disseminated sulfide in the matrix of the gray granitic breccia.

Replacement is a much more important feature in the main zone and sulfides replace both fragments and matrix in the breccia ore. Reaction rims of hydrous minerals, including biotite, chlorite, and epidote adjacent to sulfide patches and indicate the presence of water at the time of sulfide introduction. Small quartz, calcite, and epidote veinlets have been observed, although they are not common.

The main zone has the same mineralogy as the hanging-wall zone, but the chalcopyrite content is higher. Veinlets composed of 80 percent chalcopyrite often occur adjacent to the footwall of the main zone. These veinlets may represent a later stage liquid fraction which equilibrated with a pyrrhotite-rich melt at around 700°C and which was expelled into fractures of the granitic gneiss complex. Magnetite is a common mineral, but when contrasted to the hanging-wall zone, it contains few ilmenite blades. Minor pyrite occurs as euhedra in bands within massive sulfides or as rounded grains enclosed in pyrrhotite.

3-3-3. The Deep Zone

The deep zone comprises 20 percent of the mine reserves. The sulfides occur as arcuate, flat-lying, en echelon bands of massive veins in sharp contact with the host granitic gneiss, and plunging as deep as 300 feet below the gray granitic breccia contact.

There is no evidence of replacement or alteration of the granitic gneiss host rock. But the disorientation of the gneissosity and the presence of rounded rock fragments in granitic blocks indicate there was a certain degree of movement.

As compared to the main zone, the deep zone has increased grain size and contains more magnetite and chalcopyrite. Magnetite is often locally concentrated into irregular bands up to 8 inches in

width with individual euhedra averaging 0.5 mm in diameter. As in the main zone, magnetite contains few ilmenite intergrowths.

Several minor millerite-bearing stringers occur below the footwall of the deep zone in the granitic gneiss host. The stringers fill fractures in the complex which have been altered to quartz-epidote with scattered coarse brown garnet and amphibole. They are believed (Cowan, 1968) to have been formed by late stage sulfide-bearing fluids related to the formation of the main zone ore. Microprobe studies show that minute grains of unidentified platinoid minerals are associated with these stringers. The unidentified minerals are rich in platinum and palladium as well as bismuth, tellurium, and selenium. An analysis by Keays (1968) showed that millerite stringers contained 11.4 p.p.m. Pd.

3-4. Distribution of Metals and Minerals in the Ore

3-4-1. Distribution of Nickel

Pentlandite contains about 35 percent nickel while pyrrhotite and chalcopyrite usually contain less than 1 percent. However, because of the abundance of pyrrhotite, the overall contribution of pyrrhotite to the production of nickel is still significant. Figure 3-4 shows the distribution of nickel in the sulfide ore. The contours show a pronounced zoning. Values of nickel in the hanging-wall zone are low and uniform and vary between 2.5 and 3.0 percent. In contrast, nickel is strongly

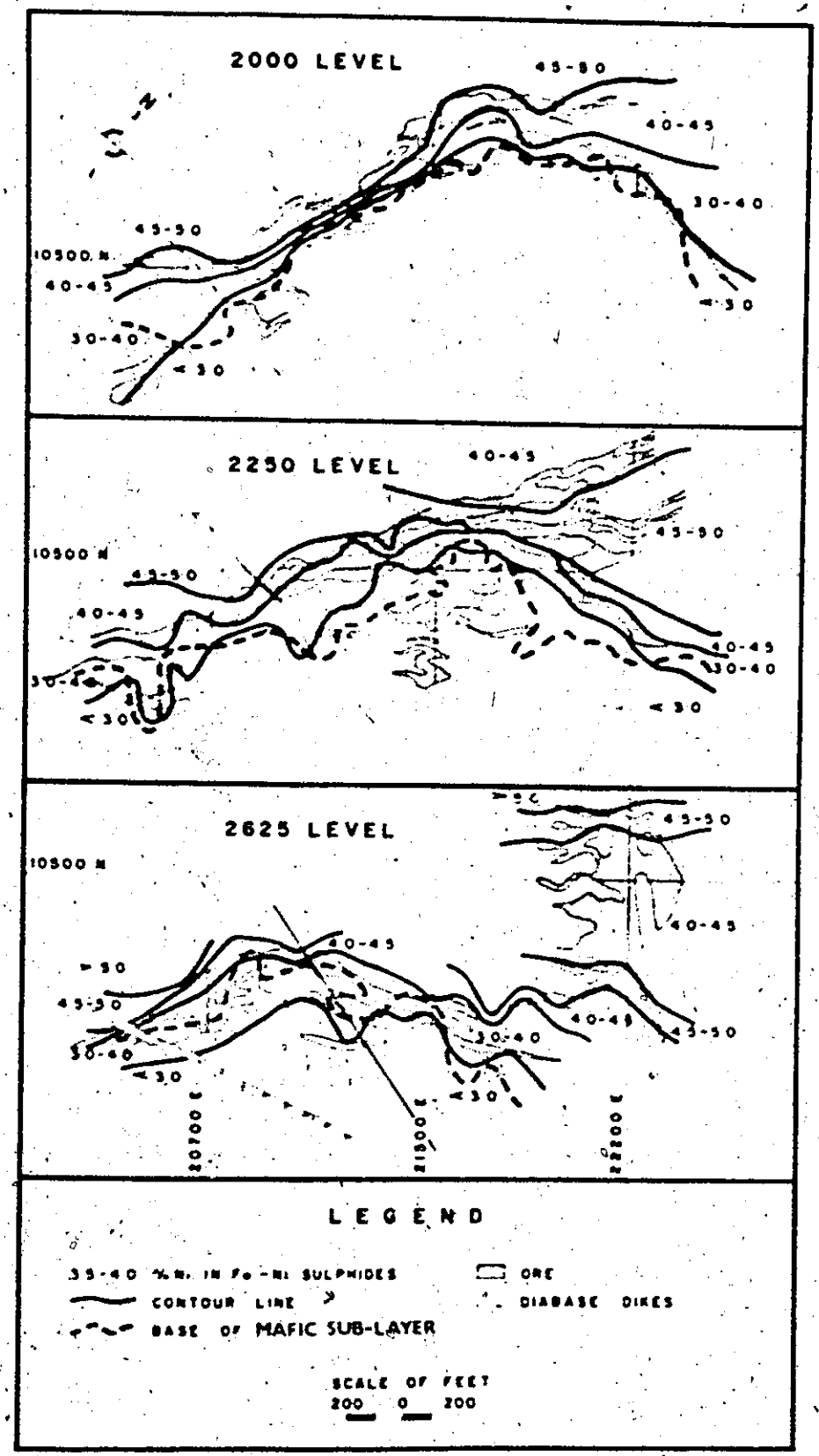

Figure 3-4. Contour plans showing the percentage and distribution of Nickel in Copper-Nickel Sulfides (after Cowan, 1968)

zoned in the main zone as indicated by the closely spaced contours. The value of nickel increases from a minimum of 3.0 percent adjacent to the hanging-wall breccia to a maximum of 5.0 percent at the contact to the granitic gneiss complex. The zoning is generally parallel to the basal contact of the Irruptive, even where it forms embayments or projects back into the hanging-wall. The individual ore lenses do not have a single characteristic nickel value and there is no zoning with respect to depth alone.

The bulk of the deep zone is not strongly zoned and the nickel values vary from 4.0 to 4.5 percent. Ore lenses towards the footwall of the deep zone are strongly zoned and reach 6 percent maximum at the base. The deep zone and main zone do not show a continuous trend of nickel values, however. The former has a mean of 4.4 percent and the latter, 3.6 percent. Two suggestions were made (Cowan, 1968) on the origin of the zoning. One was that the zoning is produced by fractionation of a sulfide melt moving down a thermal gradient. The other was that it is produced by diffusion of the metal through an aqueous phase associated with the sulfide melt.

3-4-2. Distribution of Copper

Copper is almost exclusively contained in chalcopyrite, so that the distribution of copper is also the distribution of chalcopyrite. Copper distribution is erratic but there is a definite trend of increasing copper towards the footwall.

Hanging-wall sulfides contain less than 1 percent copper, while those of the main and deep zone contain 1 to 3 percent with local highs averaging up to 4 percent due to chalcopyrite-rich stringers. The average Cu/Ni ratio in both the hanging-wall and the main zone is 1/2 while in the deep zone it averages 1/1.

3-4-3. Distribution of Cobalt

Cobalt is contained exclusively in pentlandite. The average Ni/Co ratios are 15.7 in the hanging-wall, 21.6 in the main zone, and 43.5 in the deep zone. The average Ni/Co ratios for pentlandite in the main zone and the deep zone are approximately equal, 28.4 and 30.5 respectively. It is only 15.8 in the hanging-wall zone.

3-4-4. Distribution of Hexagonal and Monoclinic Pyrrhotite

Two types of pyrrhotite exist in the Strathcona mine including a high-magnetic susceptible monoclinic pyrrhotite and a low-magnetic susceptible hexagonal pyrrhotite. The two species vary in chemical composition. Hexagonal pyrrhotite has a composition $(Fe, Ni)_9S_{10}$ with Ni 0.68-1.01 weight percent while monoclinic pyrrhotite has a composition $(Fe, Ni)_7S_8$ with Ni 0.35-0.50 weight percent (Vaughan et al., 1971).

The distribution of the two types in the three ore zones is shown in figure 3-5, reproduced from Cowan (1968). The distribution of the hexagonal pyrrhotite is locally quite variable which makes contouring impossible, but when grouped, a clear zoning appears throughout the orebody. Hexagonal pyrrhotite forms a small percentage in the main zone, but is high in the hanging-wall and the deep zones.

In ore containing significant proportions of hexagonal pyrrhotite, the pyrrhotite grains are coarse and the ore contains a higher proportion of magnetite. The pattern of distribution of these two types of pyrrhotite may suggest a variation in original bulk composition of a sulfide melt (Vaughan et al., 1971).

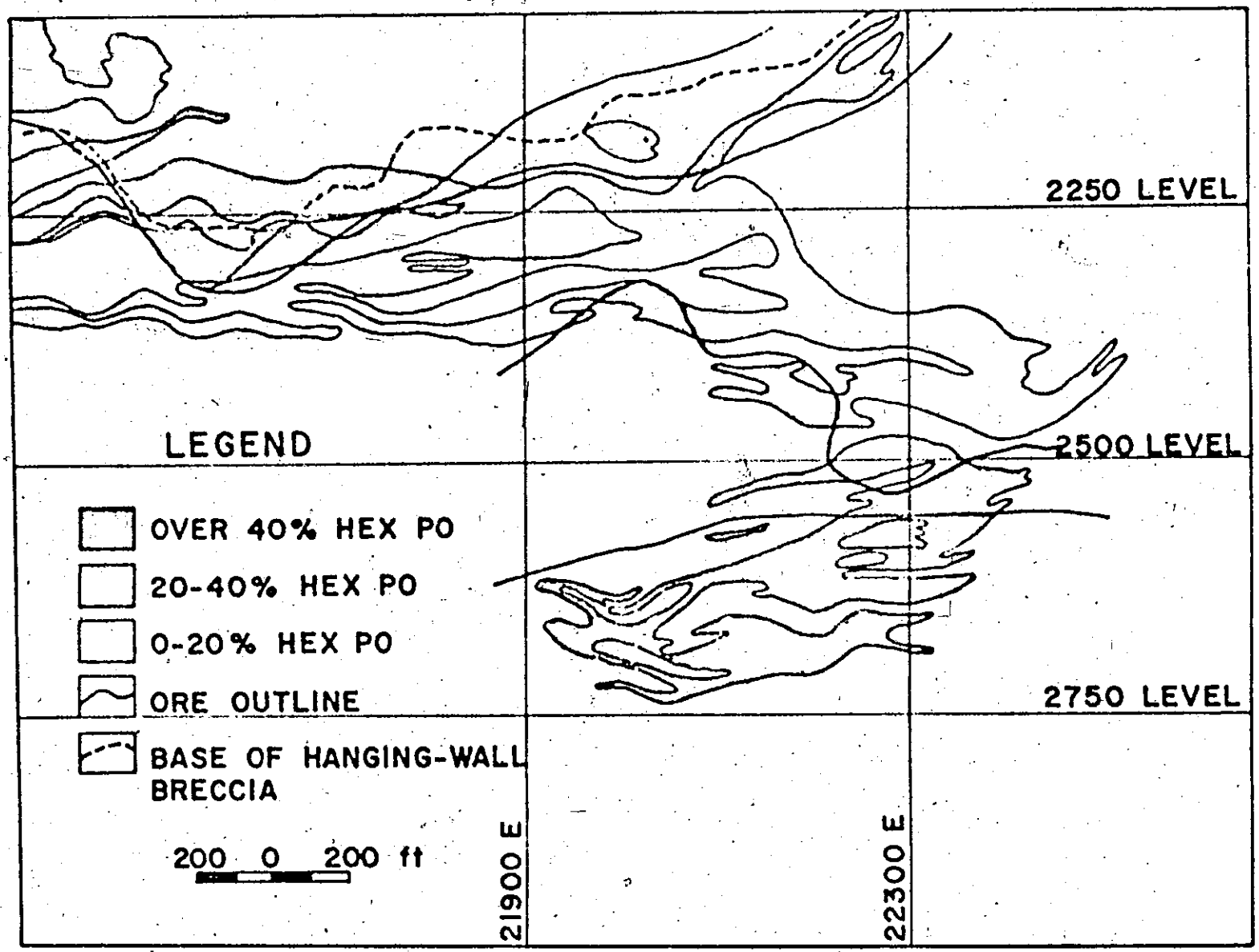

Figure 3-5. The Distribution and Percentage of Hexagonal Pyrrhotite of 10560N E-W Vertical Section (after Cowan, 1968).

CHAPTER 4

EXPERIMENTAL

4-1. Sample Preparation

Two groups of samples were analyzed in this research. They include massive sulfide ores from the deep zone ore to provide mineral separates for study of noble metal partition and composite chip samples from the 2750 level cross-cut to study noble metal variation in the major rock types of the Strathcona mine.

4-1-1. Mineral Separation

The locations of the samples collected from the deep ore zone are shown in figure 4-1. They belong to the same ore lense situated between section 22200E and 22100E and at a depth of approximately 2750 feet. The deep ore zone sulfides, as noted previously, occur dominantly as veinlets injected in footwall gneiss and are extremely heterogeneous. Samples were chosen to provide as uniform mineral assemblages as possible and to avoid obvious cases of two generations of sulfides such as nearly monomineralic chalcopyrite

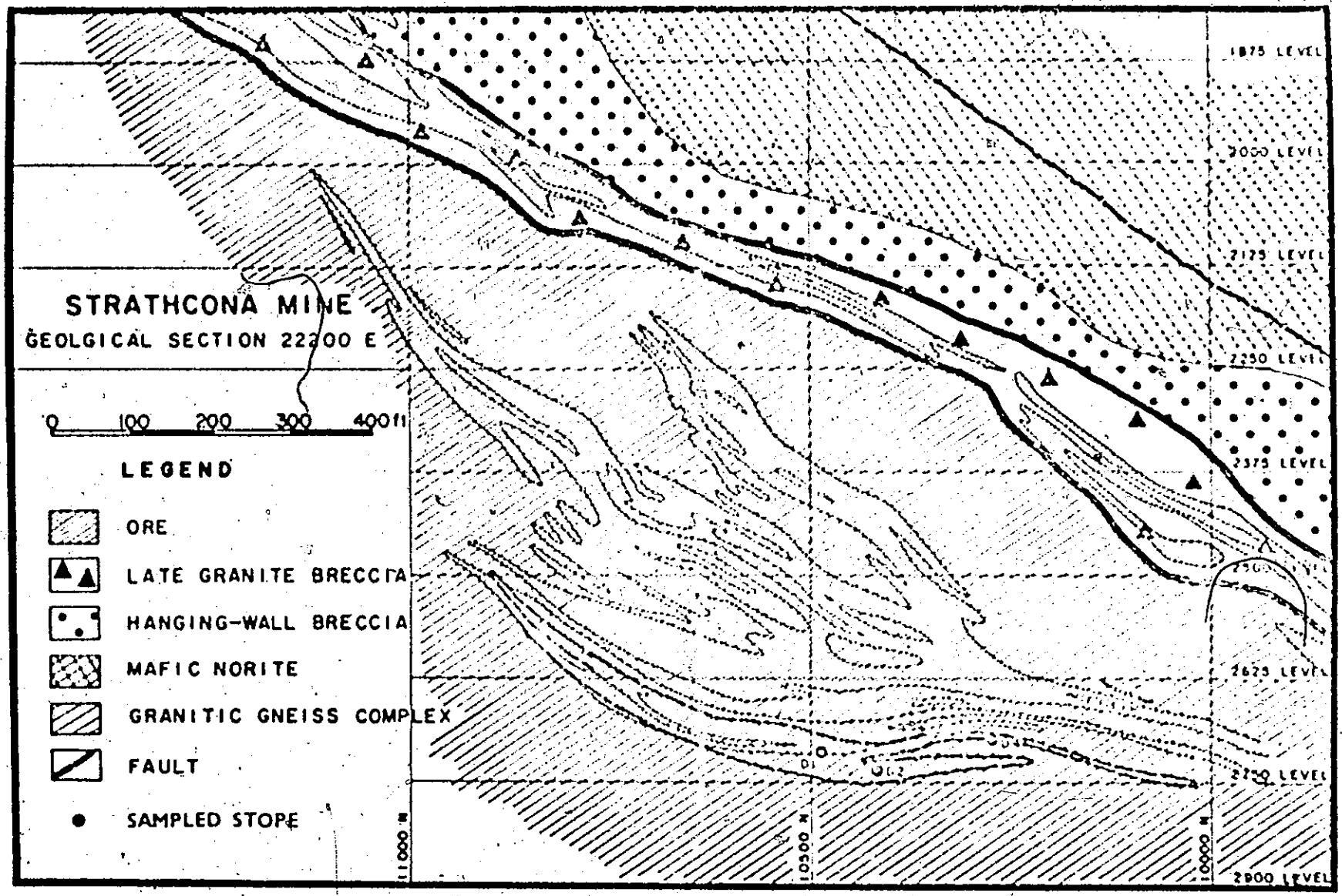

Figure 4-1. Deep Zone Ore Sample Locations (after Cowan, 1968).

veinlets cutting massive pyrrhotite-pentlandite-chalcopyrite. Pieces of about 3"x3"x3" were taken for mineral separation and preparation of polished sections which were used for point counting to estimate modal mineral proportions.

The general textures of the four coexisting minerals, including pyrrhotite, magnetite, chalcopyrite, and pentlandite are shown in plate 4-1. Chalcopyrite and most of pentlandite are granular and are readily separable from pyrrhotite. Some pentlandite, however, occurs as thin rims around pyrrhotite (plate 4-2), or as lamellae along crystallographic planes in pyrrhotite (plate 4-3) and usually presents a problem in separation.

A flow chart for the mineral separation is presented as figure 4-2. Composite grains in the final separates were removed by hand picking under the binocular microscope so that the final mineral separates were nearly 100 percent pure. Because the very fine exsolution pentlandite lamellae in pyrrhotite cannot be removed, a small portion of the pyrrhotite was grain mounted and point counted to determine the modal percentage of lamellar pentlandite. Pyrrhotite noble metal values were then corrected for such pentlandite contribution.

Plate 4-1. General textures of the four coexisting minerals - pyrrhotite (dark golden yellow, upper), magnetite (gray), chalcopyrite (golden yellow, lower), and pentlandite (yellow), X26.

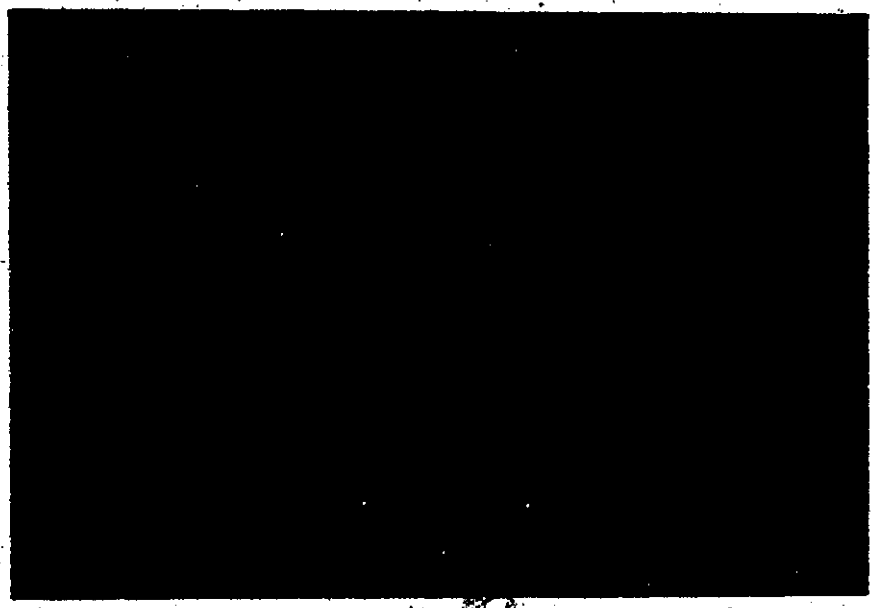

Plate 4-2. Pentlandite (yellow) occurs as thin rims around pyrrhotite (dark golden yellow), X52.

Plate 4-3. Pentlandite (yellow) occurs as lamellae along crystallographic planes in pyrrhotite (dark golden yellow), X52.

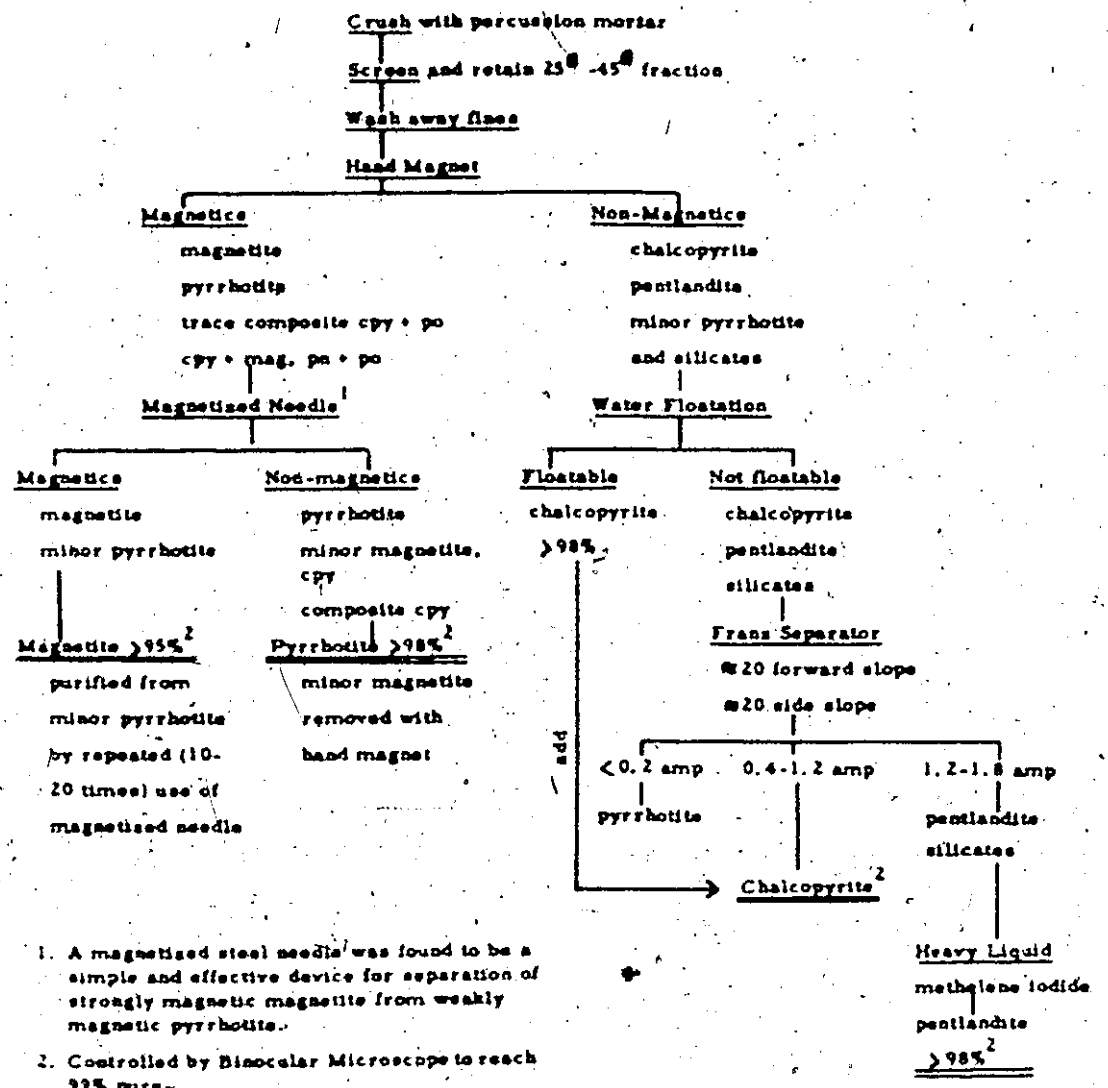

1. A magnetized steel needle was found to be a simple and effective device for separation of strongly magnetic magnetite from weakly magnetic pyrrhotite.
2. Controlled by Binocular Microscope to reach 99% pure.

Fig. 4-2. Flow Sheet for Mineral Separation of Deep Zone Massive Sulfides

4-1-2. Composite Chip Samples

Chip samples consisting of pieces approximately 2"x2" and covering about 50 ft^2 on both sides of the cross-cut were collected systematically at intervals of 50 feet. A shorter interval was taken if warranted by change in rock type along the cross cut. Each sample contained ten to eleven chips which were subsequently crushed and mixed prior to sulfide separation.

The sulfide was first gravitationally concentrated by means of an elutriator (see Keays, 1968 for diagram) to yield a heavy mineral fraction consisting of 40-70 percent sulfide. The rough concentrate was dried under an infra-red lamp and pyrrhotite together with a very small amount of magnetite removed with a hand magnet. By repeatedly picking up pyrrhotite and leaving behind the non-magnetics a pyrrhotite concentrate of 99 percent purity was obtained.

4-2. Neutron Activation Method

4-2-1. General Statement

Neutron activation is a method of elemental analysis based on measuring the decay radiation of a product of an (n, γ) reaction. The activity A in disintegrations/sec induced in the sample from N target nuclei of a given element depends on the flux ϕ in

neutrons/cm^2/sec, the effective cross-section σ of the activation reaction in barns (1 barn=10^{-24} cm^2), and the decay constant λ in sec^{-1} of the newly formed radionuclide. Thus,

$$A = \Phi(E)\sigma(E)N(1-e^{-\lambda t}) \qquad (1)$$

where the neutron flux and effective cross-section are functions of neutron energy.

The nuclear reactor is by far the most important source of neutrons for activation purposes. It produces neutrons of a very wide energy range from 0.001 ev to 15 Mev, including thermal, epithermal, and fast neutrons. Thermal neutrons are those which have reached thermal equilibrium with the medium and have a Maxwell velocity distribution with a peak at 0.025 ev. Epithermal neutrons are those which have been partly moderated but are not yet at thermal equilibrium with the medium. Fast neutrons are those with energies greater than 0.5 Mev.

The effective cross-section σ, according to Westcott's (1962) convention, is given in terms of a thermal cross-section σ_o with correction for an epithermal component given by the relation,

$$\sigma = \sigma_o (g+rs) \qquad (2)$$

where g and s are dimensionless factors (see compilation in CRRP-680 (1957) and AECL (1962) by Westcott) and r is a measure of the proportion of epithermal to thermal neutrons which varies from reactor to reactor and with position in the reactor. In the McMaster Research Reactor the epithermal to thermal ratio is 0.059 according to Tong (1971).

Tong also computed the neutron spectrum of the McMaster Research Reactor for a total flux at 2×10^{13}. The spectrum is shown in figure 4-3. It is pertinent to note that the epithermal part of the spectrum plays a significant role in the irradiation of nuclides with strong epithermal resonance peaks such as ^{197}Au.

4-2-2. Sample and Standard Preparations

Prior to irradiation the sample was ground to powder in an agate mortar under acetone to minimize possible self-shielding effects due to sample inhomogeneity. Powdered samples of 50 to 200 mg were weighed into 3 mm O.D. x 2 mm I.D. quartz ampoules which were sealed with polyethylene plugs.

Standard solutions were prepared from Johnson, Matthey and Mallory "Specpur" gold foil, palladium sponge, platinum sponge, and ammonium chloroiridate. Following the procedure of Crocket et al. (1969), gold, palladium, and iridium were combined into a single solution in 1M HCl while platinum was prepared separately. The final concentrations of the flux monitor standard solutions were 0.02438 mg/ml

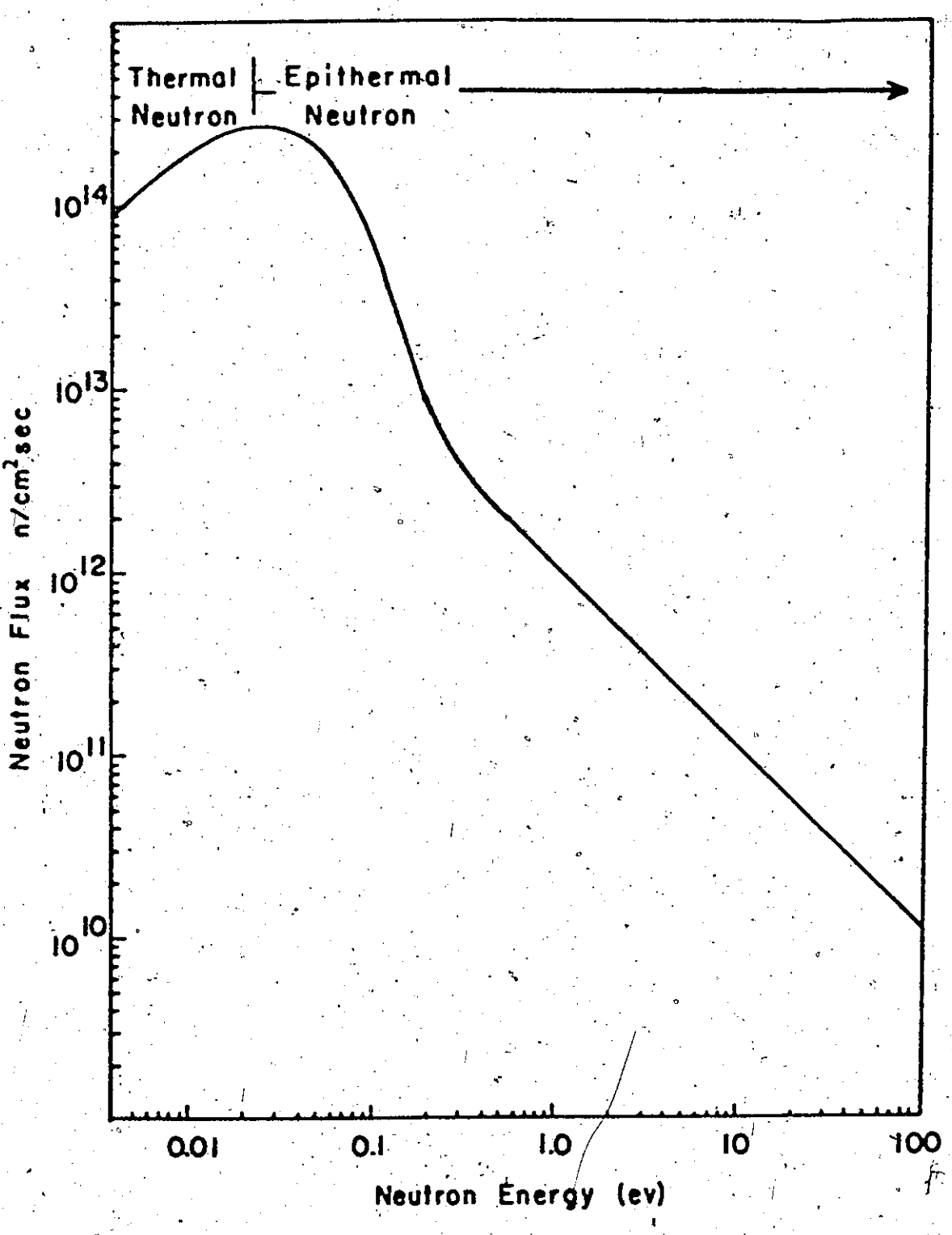

Figure 4-3. The Reactor Neutron Spectrum (after Tong, 1971).

Au, 0.4048 mg/ml Pd, 0.5665 mg/ml Ir, and 26.38 mg/ml Pt. The density of the solution was determined with a pycnometer.

To prepare standards for irradiation the solutions were introduced into weighed ampoules with a capillary polyethylene pipette. After reweighing to obtain the weight of solution, about 50 mg of +200 to -100 mesh quartz powder[1] was added to absorb the solution. The ampoules were then put in a drying oven at 65°-70°C, dried overnight, and sealed with polyethylene plugs.

4-2-3. Irradiation

Table 4-1 presents the nuclear properties and production factors[2] for Pd, Ir, Pt, and Au. As sensitivity is dependent upon induced activity, the nuclide with the highest yield is the best for the

---

[1] The quartz powder was prepared from crushed quartz tubing used for ampoules.

[2] The production factor P.F. is defined as

$$P.F. = \frac{\sigma a}{w} (1-e^{-\lambda_1 t_{ir}}) \quad (3)$$

The production factor of first daughter of species 1 is defined as

$$P.F. = \frac{\sigma a}{w} \left(1+ \frac{\lambda_2}{\lambda_1-\lambda_2} e^{-\lambda_1 t_{ir}} - \frac{\lambda_1}{\lambda_1-\lambda_2} e^{-\lambda_2 t_{ir}}\right) \quad (4)$$

a = fraction abundance of the target nuclide

w = physical atomic weight

λ_1 = 0.693/half-life of the induced radionuclide

λ_2 = 0.693/half-life of the first daughter of species 1

t_{ir} = irradiation time

σ = effective cross-section

Table 4-1. Nuclear Properties and Production Factors of Pd, Ir, Pt, and Au

Element	Stable Isotope	Isotopic Abund. (%)	σ (barns)	Radio-nuclide	Half-Life	Type of Decay	Production Factor 1 week	Production Factor 2 week
Pd	^{102}Pd	0.96	4.8	^{103}Pd	17.0d	E.C.	0.0110	0.0196
	^{108}Pd	26.71	12	^{109}Pd	13.5 hr.	β	2.97	2.97
	^{110}Pd	11.81	0.2	^{111}Pd	22 min	β	0.0215	0.0215
Ir	^{191}Ir	37.3	1050	^{192}Ir	74.0d	β 95.5%, E.C. 4.5%	13.4	25.0
	^{193}Ir	62.7	110	^{194}Ir	19hr.	β	35.7	35.7
Pt	^{190}Pt	0.013	150	^{191}Pt	30d	E.C.	0.00152	0.00283
	^{192}Pt	0.78	2	^{193m}Pt	4.4d	I.T.	0.00542	0.00721
	^{194}Pt	32.9	1.2	^{195m}Pt	4.1d	I.T.	0.141	0.185
	^{196}Pt	25.3	0.9	^{197}Pt	20hr	β	0.116	0.116
	^{198}Pt	7.21	4	$^{199}Pt \xrightarrow{\beta}$	30min	β	0.146	0.146
				^{199}Au	3.15d	β	0.114	0.140
Au	^{197}Au	100	98.8	^{198}Au	2.70d		41.8	48.7

element concerned. For this reason ^{109}Pd, ^{194}Ir, and ^{199}Pt were used for the respective elements. Despite the somewhat higher yield of ^{194}Ir, ^{192}Ir is preferred because of the convenience of the long half life and its distinctive gamma spectrum.

Samples were irradiated for ten to fourteen days to produce sufficient ^{192}Ir and ^{199}Au activities and cooled for four days to reduce matrix activity. They were then re-irradiated for twelve hours to produce ^{109}Pd activity, and then cooled for six hours to reduce short-lived activity. The saturation factors of ^{109}Pd, ^{192}Ir, ^{199}Au, and ^{198}Au following this irradiation scheme allowed simultaneous analysis of Pd, Ir, Pt, and Au (figure 4-4).

4-2-4. Chemical Procedures

A flow chart of the procedures is presented as figure 4-5. It is a modified scheme for Crocket et al. (1969). The purification steps for Au, Pt, and Ir are largely omitted for the application of gamma counting which does not require high radiochemical purity. However, purification with respect to Fe in case of Pd, and Ag in case of Ir is required for the long irradiation period adapted in this research. The procedures which have already been described in detail by Keays (1968) and Crocket et al. (1969), will only be presented in stepwise fashion for continuity.

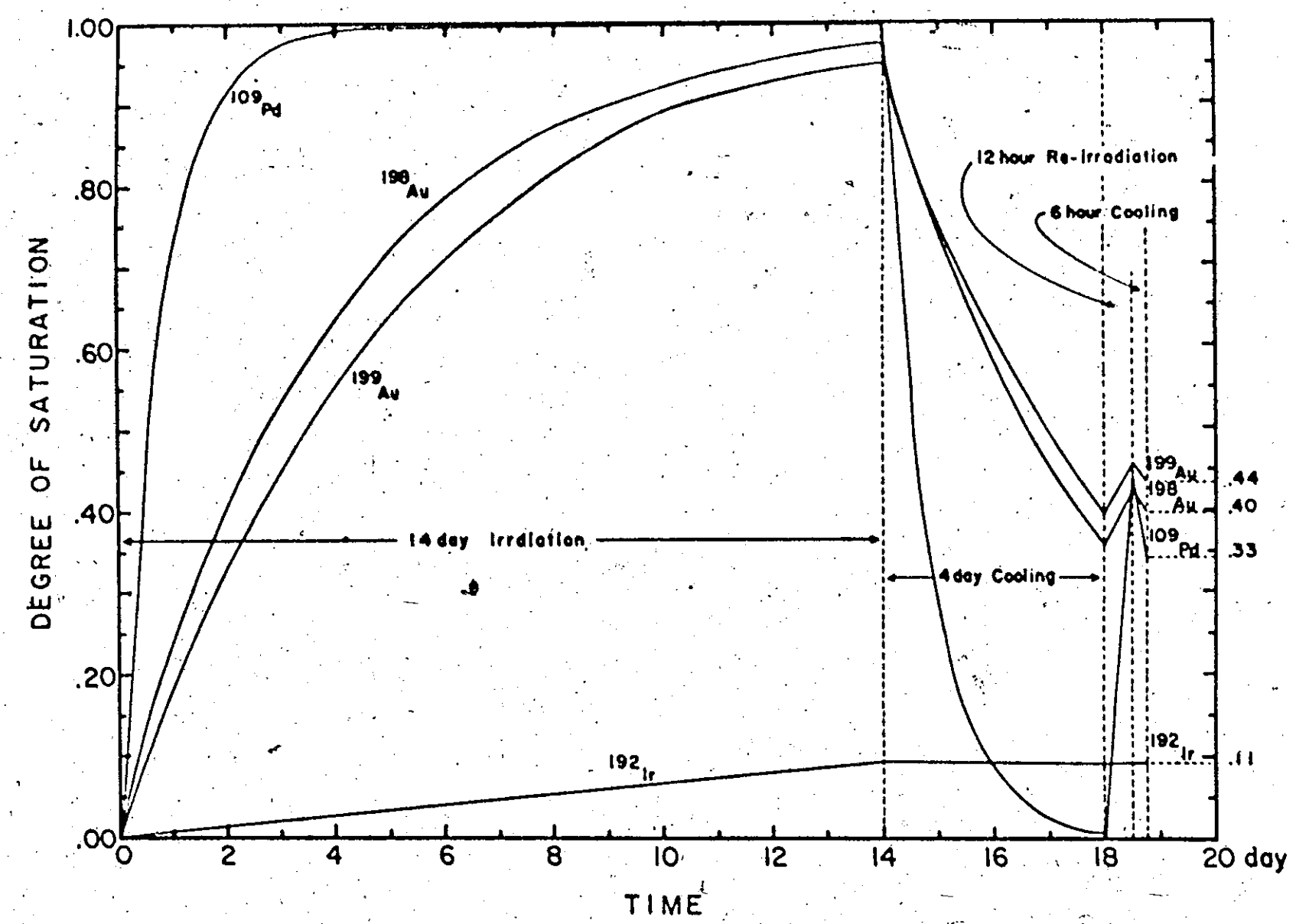

Figure 4-4. Saturation Factors of ^{109}Pd, ^{192}Ir, ^{199}Au, and ^{198}Au for the Present Irradiation Scheme

Figure 4-5. Flow Sheet for Analytical Procedures

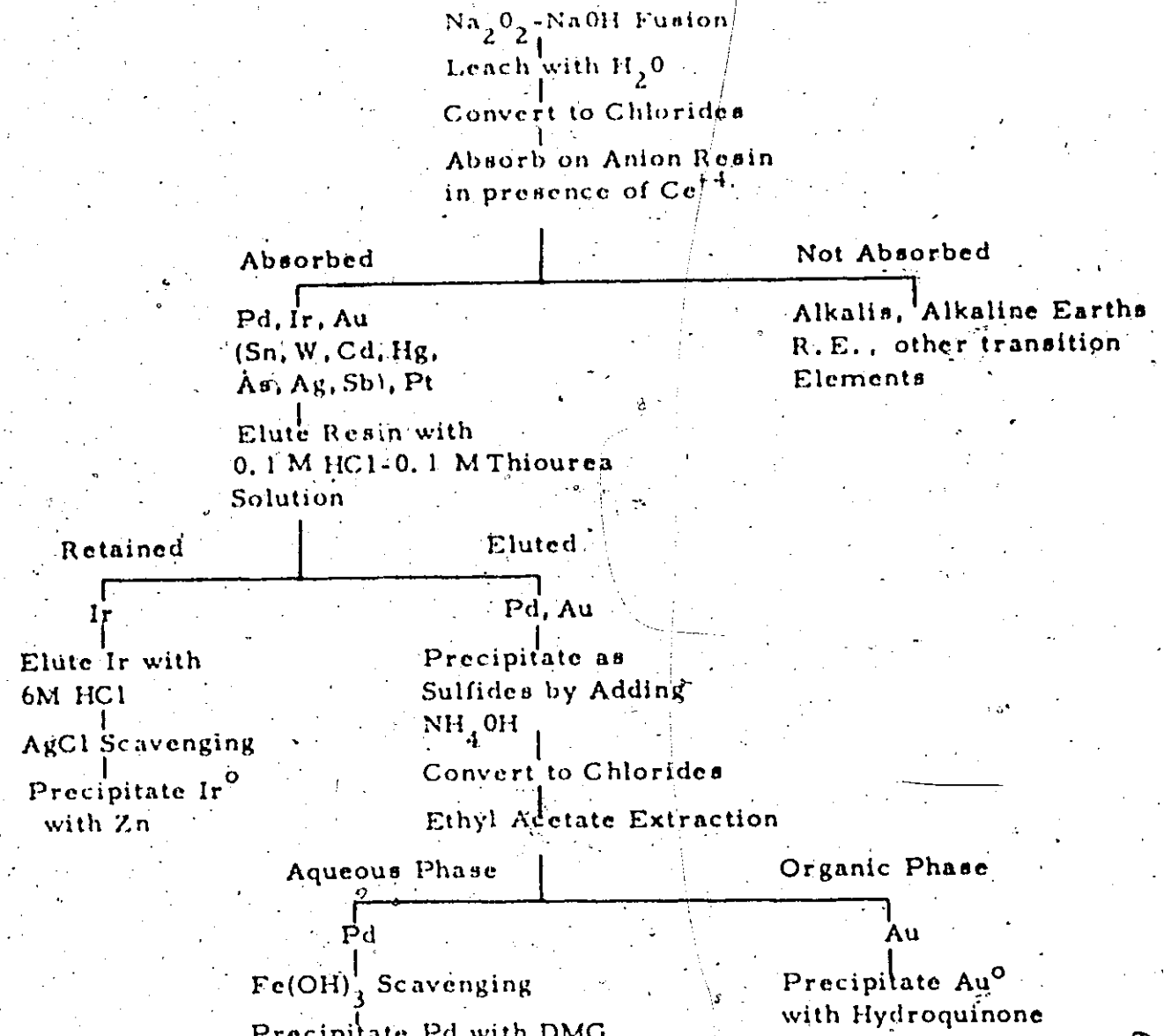

4-2-4-1. Sample Procedures

1. Pipette carrier solutions into a zirconium crucible and carefully evaporate to dryness under an infra-red lamp.
2. Transfer the irradiated sample from the quartz ampoule to the crucible, add 2 gm of Na_2O_2 and 2 gm of NaOH pellets, and fuse on a Meeker burner.
3. Dissolve the fusion cake with distilled H_2O and treat with aqua regia and conc. HCl to convert to chloride complexes.
4. Dissolve the chlorides in 0.5M HCl containing 0.004 moles of ceric ion per ml of solution and feed the solution onto a Rexyn 201 (Cl) anion exchange column.
5. Elute Pd and Au with 120 ml thiourea in 0.1M HCl solution.
6. Add concentrated NH_4OH to destroy thiourea and precipitate Pd and Au as sulfides.
7. Elute Ir with 120 ml of 6M HCl.
8. Convert Pd and Au sulfides to chlorides and separate Au by ethyl acetate extraction.
9. Contact the Au-acetate solution with an equal volume of 2M HCl to transfer Au into the HCl phase and evaporate off ethyl acetate.

10. Add hydroquinone to reduce Au to the metal, wash and transfer into a preweighed vial for counting.

11. Purify the Pd-HCl solution from step 8 by two $Fe(OH)_3$ scavenges to eliminate Fe activity produced in the two week irradiation. The details of the $Fe(OH)_3$ scavenging were described in Chyi's M.Sc. thesis (1968).

12. Take the purified Pd into 1M HCl solution and precipitate Pd with 1.5% dimethylglyoxime in ethanol. Dissolve, reprecipitate, wash and transfer the Pd dimethylglyoximate to an aluminum planchet for counting.

13. Purify Ir from step 7 with two AgCl scavenges to eliminate Ag activity.

14. Take the purified Ir into 2M HCl solution and reduce Ir to the metal with Zn powder. The Ir metal is washed and transferred into a preweighed vial for counting.

4-2-4-2. Procedures for Standard

1. Immerse the ampoule containing standard solution doped quartz powder in aqua regia for 10 minutes, wash it thoroughly with distilled H_2O, and repeat. Break the ampoule and empty the quartz powder into 100 ml beaker containing carrier solution for equilibration. Wash the inside of the ampoule with 6M HCl to ensure the complete removal of the absorbed activity.

2. Purify the standard solution by putting it through ion exchange column following the same procedures as for sample.

3. Au, Pd, and Ir are separated and precipitated by following the same procedures as for sample, but the purification procedures for Pd and Ir are omitted.

4. Pt standard is first equilibrated with carrier and the solution thus obtained is contacted with ethyl acetate to extract Au containing ^{199}Au produced from ^{198}Pt(n, β). Au is precipitated and transferred to preweighed vial for counting as for sample.

4-2-5. Counting and Calculation

4-2-5-1. Instrumentation

For beta counting a gas flow Geiger-Mueller counting tube with coincidence shielding was used. The detector had an average background of 2.0 counts/min. and a window thickness 150 μgm/cm^2. Machine drift was monitored with a uranium standard source. Dead-time corrections were unnecessary for count rates up to 10,000 counts/min.

For gamma counting a Nuclear-Chicago gamma counting system utilizing a well-type 3"x3" NaI(Tl) scintillation detector or a 25 cm^3 Ge(Li) diode, an analog to digital converter, a 1600 channel memory, and a teletype paper print out was used throughout the research.

The NaI(Tl) detector had the higher sensitivity, while the Ge(Li) detector had higher resolution. As sensitivity was the major concern in this research, most of the samples were counted on the NaI(Tl) detector. The Ge(Li) detector was used for samples with significant radiocontaminants, and in particular for low level Ir samples where long lived contaminants, particularly ^{110}Ag, were significant.

4-2-5-2. Evaluation of Photopeaks

In the gamma spectrum obtained from counting a mixture of radionuclides only the highest energy photopeak is free of interference from other nuclides; other photopeaks are superimposed on a Compton continum. In order to measure the peak height of a single photopeak, a line extrapolating the continuous spectrum under the photopeak region is drawn as shown in figure 4-6. To evaluate the area between this base-line and the photopeak curve, Covell's (1959) numerical method was used.

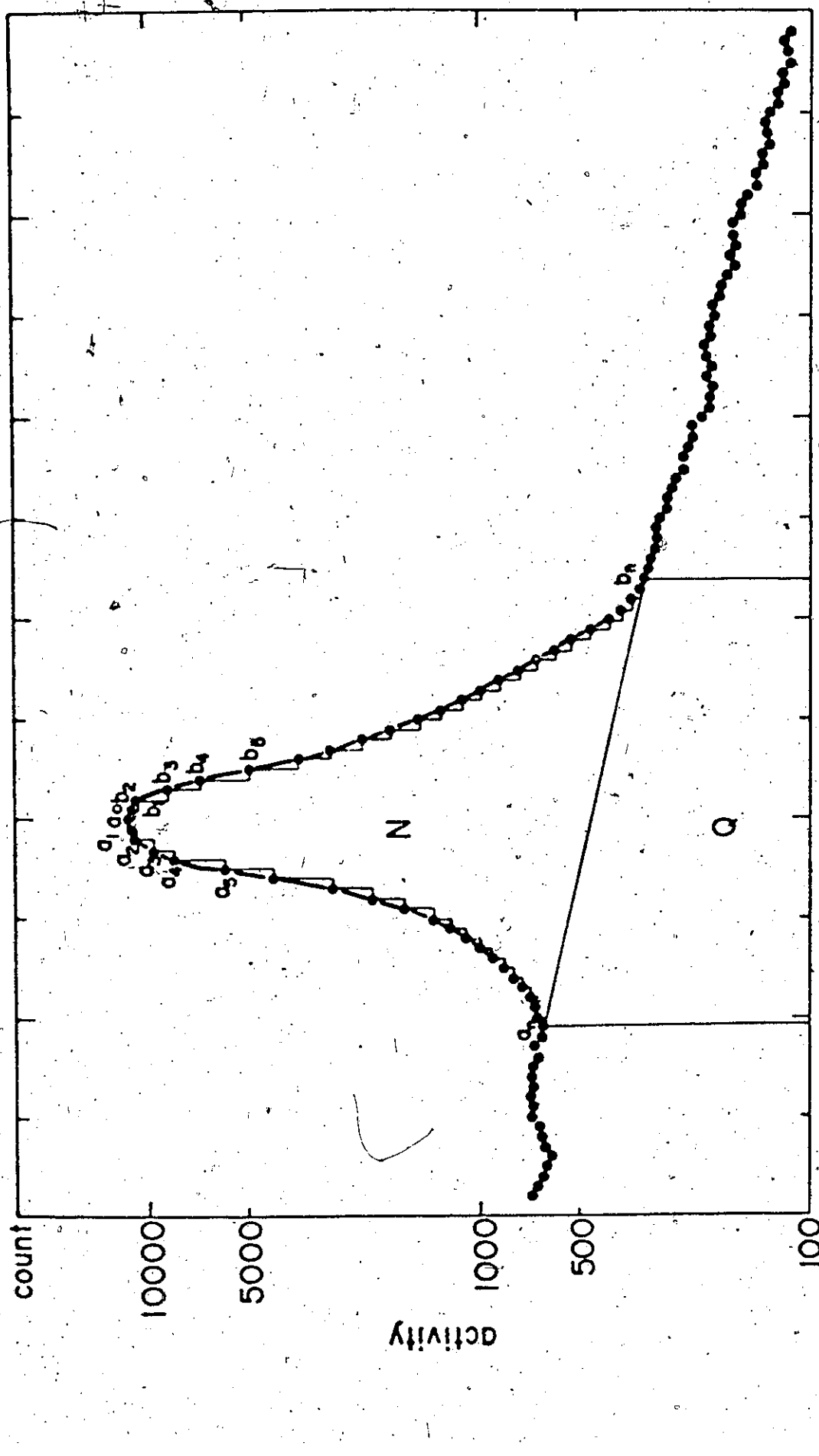

Figure 4-6. Evaluation of Photopeak of a Gamma Spectrum

The background line divides the photopeak into two areas, N and Q as shown in figure 4-6. Let the count rate measured in the channel corresponding to photopeak maximum be a_o, the count rates measured in neighbouring channels to the left of the axis be a_1, a_2, ... a_n and on the right side b_1, b_2, ... b_n, then the area N equals

$$N = a_o + \sum_{i=1}^{n} a_i + \sum_{i=1}^{n} b_i - (n+1/2)(a_n + b_n) \qquad (5)$$

The mean square deviation of this value is

$$\sigma = \sqrt{N + (n-1/2)(n+1/2)(a_n + b_n)} \qquad (6)$$

and usually is less than 1% and thus will not contribute significantly to the analytical error.

The 316 kev and 412 kev photopeaks of ^{192}Ir and ^{198}Au respectively were used for measurement of these elements. The 158 kev radiation from ^{199}Au was used for determination of platinum. However, the 158 kev radiation can be produced not only from ^{199}Pt(n, β) but also by the reaction, ^{197}Au(2n, γ). The procedures for determination of platinum radiation in the 158kev region is illustrated in figure 4-7.

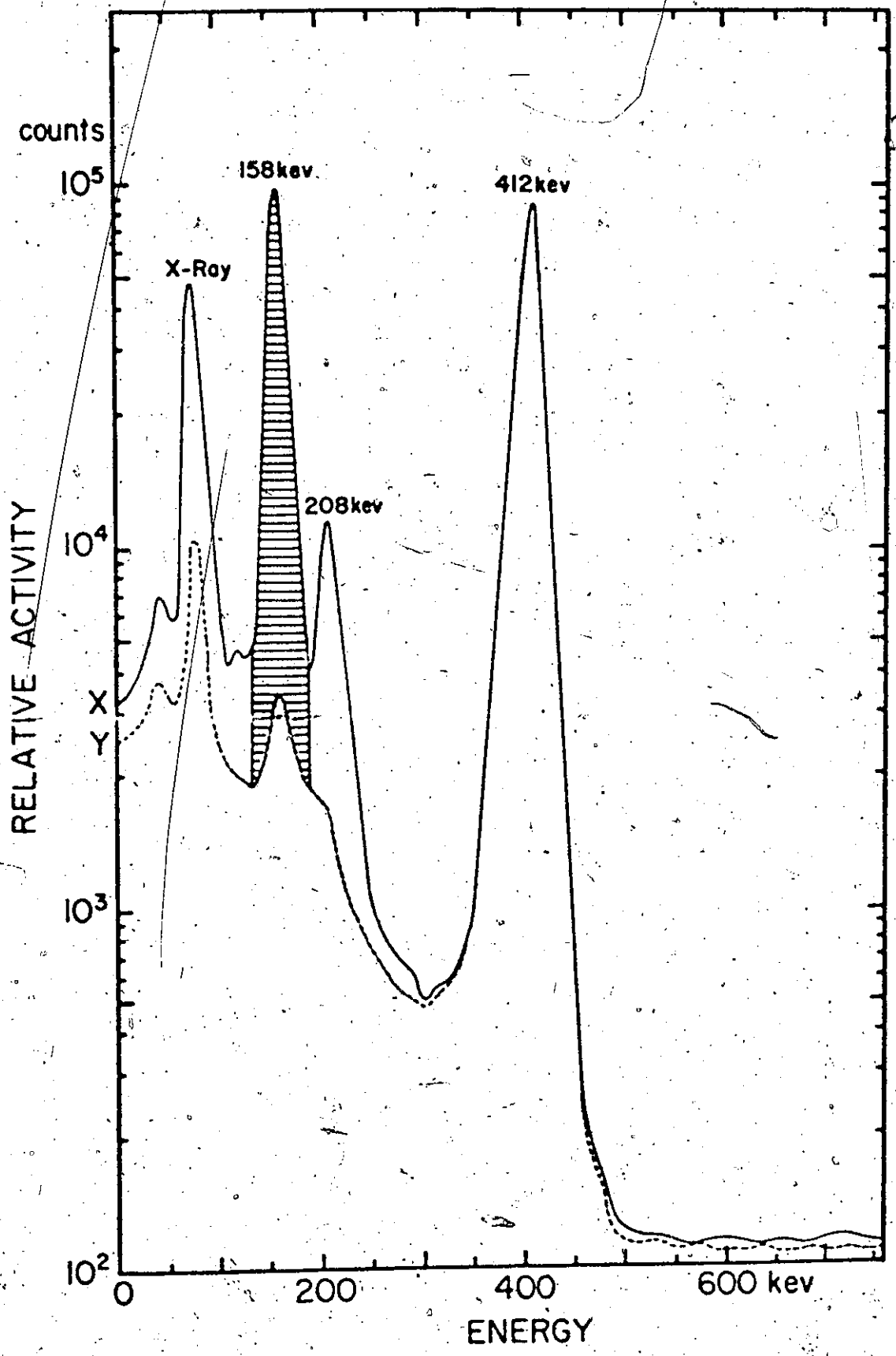

Figure 4-7. Determination of 158 Kev Radiation of ^{199}An Produced from ^{198}Pt (n, β)

X is a sample spectrum with a 412 kev photopeak from ^{198}Au radiation produced from the $^{197}Au(n,\gamma)^{198}Au$ process, and 158 kev and 208 kev photopeaks from ^{199}Au radiation which is produced from both $^{198}Pt(n,\gamma)^{199}Pt \xrightarrow{\beta^-} {}^{199}Au$ and $^{197}Au(2n,\gamma)^{199}Au$ processes. Y is a pure Au standard spectrum with a major 412 kev photopeak from ^{198}Au radiation and minor 158 kev and 208 kev photopeaks from the $^{197}Au(2n,\gamma)^{199}Au$ process only. If the 412 kev photopeaks from both X and Y are set equal, then the 158 kev or 208 kev photopeak due to Pt (that is from the $^{198}Pt(n,\gamma)^{199}Pt \xrightarrow{\beta^-} {}^{199}Au$ process) will be the photopeak area under X minus photopeak area under Y as indicated by the shaded area. As the 208 kev photopeak is rather small, only the 158 kev photopeak is used for platinum measurement.

4-2-5-3. Decay Curve Analysis

Activity from ^{109}Pd beta counting was evaluated by graphical analysis of a decay curve. The main purpose was to subtract any long-lived radiocontaminants.

Pd samples were usually counted about 30 hours after the end of the irradiation. The 22 minute ^{111}Pd activity had already decayed and, in most of the cases, the 13.5 hour ^{109}Pd decay could be followed for four or five half-lives before the activity from long-

lived contaminants become significant. The long-lived activity was followed for one or two weeks and the activity extrapolate back graphically to t_o (time when counting started) and subtracted. The long-lived contaminants were usually less than 5% of the total activity.

There are three other potential sources of error in the Pd determination. The first is ^{109}Pd produced from ^{235}U fission. This interference is not significant in sulfides (Crocket, 1971). The second is 12.9 hour ^{64}Cu. The similar half-lives make it impossible to resolve these nuclides by decay curve analysis. The present analytical scheme has a decontamination factor of at least 5×10^9 for Cu as determined by experiment. The specific cross sections (σ x percent isotope abundance) of ^{64}Cu and ^{109}Pd are similar, so that a 5×10^7 Cu/Pd ratio would introduce a maximum error of 1%. Thus for a maximum Cu/Pd ratio of 10^8 as encountered in chalcopyrite, a maximum error of 2% could arise from this source. The third error involves self adsorption of beta particles in the counting source. A calibration curve for beta adsorption as a function of weight of Pd dimethylglyoximate is presented in Appendix A. For a chemical yield difference between sample and standard of 10% or less, this correction is negligible.

4-2-5-4. Calculation

Knowing the activity of the sample a_o and the standard A_o from either a gamma spectrum or from beta decay curve analysis, the chemical yield of both sample y and standard Y, the weight of sample irradiated m and the weight of metal in the standard M, the metal content C in p.p.b. in the sample can be calculated by the simple relation,

$$C = \frac{Ma_oY}{mA_oy} \times 10^9 \qquad (7)$$

4-2-6. Control of Accuracy

The natural variability of the noble metals is known to be large and sample homogeneity presents a major problem for many materials. In this study two different analytical programs were undertaken. Firstly, for samples from the 2750 cross-cut representative average noble metal values were desired, so that natural variability was a potentially serious problem. Therefore, each sample was collected to be representative of a large area (approximately 50 square feet) by taking a large number of chips over the desired face. An examination of the data in table 5-8 for the 2750 cross-cut indicates that some samples, particularly those characterized by high noble metal values, yielded rather imprecise results. In these cases,

where a significant measure of sample inhomogeneity existed despite the sampling technique used, replicate analyses (3 to 4) were necessary to establish the significance of average values. Secondly, mineral separates were analysed to study noble metal partition. In this work sample preparation variability was a major concern. Composite grains and very fine pentlandite lamellae in pyrrhotite were significant sources of variability. The former were removed by hand picking under a binocular microscope, while the latter were estimated by point counting polished grain mounts. Despite these precautions, up to 1% pentlandite may persist in chalcopyrite. However, as partition of noble metals between pentlandite and chalcopyrite is always less than a factor of 10, errors from this source will not exceed 10%.

The precision obtained over the course of the study is estimated by computation of a pooled variance (see Dixon and Massey, p. 109) using data for those samples for which replicate analyses were carried out. This precision estimate is compared in table 4-2 with that reported by Crocket et al. (1968) for replicate determinations of these metals (except Pt) on the standard rocks G-1 and W-1.

Table 4-2. Comparison of Coefficient of Variation for the Determination of Pd, Ir, Pt, and Au in Strathcona Samples, G-1 and W-1 (%)

Sample	Investigator	Pd	Ir	Pt	Au
Strathcona	This study	21	24	30	16
G-1	Crocket et al.	17	18	--	27
W-1	Crocket et al.	10	19	--	12

The comparison shows that the precision errors for Au and Ir in the Strathcona samples are within the same range as G-1 and W-1, but for Pd are much larger. As a very similar chemical procedure was used, the higher error for Pd in the Strathcona samples is probably related to factors other than chemical procedures. In particular, the fact that fairly large ranges of Pd content are found in these sulfides may give rise to the larger precision errors observed for the Strathcona sulfide analyses.

CHAPTER 5

DISTRIBUTION OF THE NOBLE METALS

5-1. Distribution of the Noble Metals between Coexisting Ore Minerals from the Deep Zone Ore

The deep zone ore was chosen for this type of study because:

1) Four minerals, pyrrhotite-magnetite-chalcopyrite-pentlandite, are commonly found together in typical deep zone ore.

2) The highest Pt, Pd, and Au values are found in the deep zone ore.

3) Pentlandite occurs dominantly as rim pentlandite surrounding pyrrhotite in sufficiently coarse aggregates to allow its separation as a discrete phase.

Further, as compared with the main zone, the deep zone sulfide minerals have an increased grain size and contain more magnetite and chalcopyrite which facilitate mineral separation.

Pyrrhotite, magnetite, chalcopyrite, and pentlandite were separated from six massive sulfide samples, three from stope

D-1, two from stope D-2, and one from stope D-4. They were analyzed for Pd, Ir, Pt, and Au. The samples are located near the lowest portion of the deep zone as shown in figure 4-1.

5-1-1. Modal Analysis of the Deep Zone Ores

The massive sulfide ores from the three stopes were polished and point counted to establish the modal percentage of the ore minerals. The modal data permit an estimate of the proportions of magnetite and pyrrhotite solid solution to be made and thereby to consider noble metal partition at liquidus temperatures. The results are presented as table 5-1. The assay values for Cu, Ni, Fe, and S in the pertinent stopes were kindly provided by Falconbridge Nickel Mines Limited. Comparison of mineral modes determined by point counting and chemical assay are presented as table 5-2. The comparison provides a check on the point counting. The discrepancies of the two independent estimations reflect in part the heterogeneous nature of the ore mineral distribution in the deep zone ore stopes.

5-1-2. Paragenetic History of the Deep Zone Ore

The paragenetic history of the Strathcona sulfide minerals has been deliberated on in great detail by Naldrett and Kullerud (1967). They concluded that all of the Strathcona ores were emplaced as a sulfide magma at a temperature above 1000°C. On cooling pyrrhotite

Table 5-1. Modal Analysis of Deep Zone Ore Stopes Established by Point Counting

	Po.	Mag.	Cpy.	Pn.	Others
D1A*	78.8±1.1	4.9±0.6	8.2±0.7	8.0±0.7	0.1±0.1
	79.4±1.1	4.7±0.6	7.8±0.7	8.1±0.7	-
Av.	79.1±1.1	4.8±0.6	8.0±0.7	8.0±0.7	0.1±0.1
D1B	63.2±1.5	8.9±0.9	19.9±1.3	7.7±0.9	0.3±0.2
	64.9±1.5	8.3±0.9	18.2±1.2	8.2±0.9	0.3±0.2
Av.	64.1±1.5	8.6±0.9	19.1±1.3	7.9±0.9	0.3±0.2
Stope D1 Average					
	71.6±1.8	6.6±1.0	13.6±1.5	8.0±1.1	0.2±0.2
D2A	74.3±1.2	7.9±0.8	8.3±0.8	9.5±0.8	
	73.3±1.3	10.4±0.9	7.9±0.8	8.3±0.8	
Av.	73.8±1.3	9.1±0.9	8.2±0.8	8.9±0.8	
D2B	77.1±1.6	2.9±0.6	8.0±1.0	12.0±1.3	
	77.7±1.6	1.8±0.5	9.3±1.1	11.1±1.2	0.1±0.1
Av.	77.4±1.6	2.3±0.6	8.6±1.1	11.6±1.3	0.1±0.1
Stope D2 Average					
	75.6±2.0	5.7±1.0	8.4±1.4	10.2±1.5	0.1±0.1
D4A	80.9±1.2	6.0±0.8	0.8±0.3	12.3±1.1	
	80.9±1.2	5.9±0.8	0.9±0.3	12.3±1.1	
Av.	80.9±1.2	5.9±0.8	0.9±0.3	12.3±1.1	
D4B	54.5±1.7	15.8±1.2	21.6±1.4	7.1±0.9	0.9±0.3
	56.1±1.7	14.4±1.2	20.1±1.3	8.7±0.9	0.7±0.3
Av.	55.3±1.7	15.1±1.2	20.8±1.4	7.9±0.9	0.8±0.3
Stope D4 Average					
	68.1±2.1	10.5±1.4	10.9±1.4	10.1±1.4	0.4±0.3

* The modal percentage of the same polished section is determined by replicate counts, about 1000 points cover the whole section area.

solid solution and magnetite crystallized initially and persisted to at least 700°C. Minor euhedral pyrite may have formed as the first subsolidus phase by exsolution from pyrrhotite below 675°C. However, in the deep ore zone such pyrite is extremely rare. With further cooling chalcopyrite and pentlandite exsolve from pyrrhotite. The chalcopyrite exsolution may have occurred over a wide temperature range, from at least 700°C to 400°C depending largely upon the copper content of the pyrrhotite solid solution. Pentlandite exsolution occurs at temperatures below 300°C and probably significantly lower, and is dependent largely upon the sulfur content of the melt. The inversion of high temperature hexagonal pyrrhotite to monoclinic pyrrhotite occurs at approximately 300°C.

Most of the chalcopyrite probably exsolved from pyrrhotite solid solution below 450°C and occurs as slivers at the margins of or as lamellae or fine wisps within pyrrhotite. Coarser chalcopyrite masses represent either copper which never was in solid solution with pyrrhotite or remobilized chalcopyrite. Both types of chalcopyrite are believed to exist in the deep zone ores.

If the sulfur and nickel content of the pyrrhotite solid solution allowing for exsolution of chalcopyrite, are estimated by combining pyrrhotite and pentlandite as a single phase; the ore from

stopes D-1, D-2, and D-4 contains 38.8, 38.6, 38.4% sulfur and 3.87, 4.58, 5.28% nickel respectively. A plot of these values on figure 5-1 reproduced from Naldrett and Kullerud (1967) shows that these high sulfur pyrrhotite solid solutions will not exsolve pentlandite above 300°C.

Craig et al. (1967) constructed the succession of mineralogical assemblages which would be produced by crystallization from Cu-Ni-Fe-S melts of various composition as a consequence of decreasing temperature. The concentrations of Cu, S, and Ni in the pertinent deep zone ore stopes can be estimated from the modal data of table 5-2 and the compositions of hexagonal and monoclinic pyrrhotite and pentlandite given by Vaughan et al. (1971). The compositional estimates are presented in table 5-3.

If these values represent the original sulfide melt composition, then crystallization from this melt would produce the mineral assemblage pyrrhotite-cubanite-bornite-magnetite according to Craig et al. (sulfur poor (<37.0%) and copper poor (<5%) melt). However, bornite has never been observed in Strathcona mine. As average Cu is <5% it is very unlikely that chalcopyrite is a primary high temperature phase so that pyrrhotite solid solution plus magnetite represent the assemblage present at high temperature (approximately

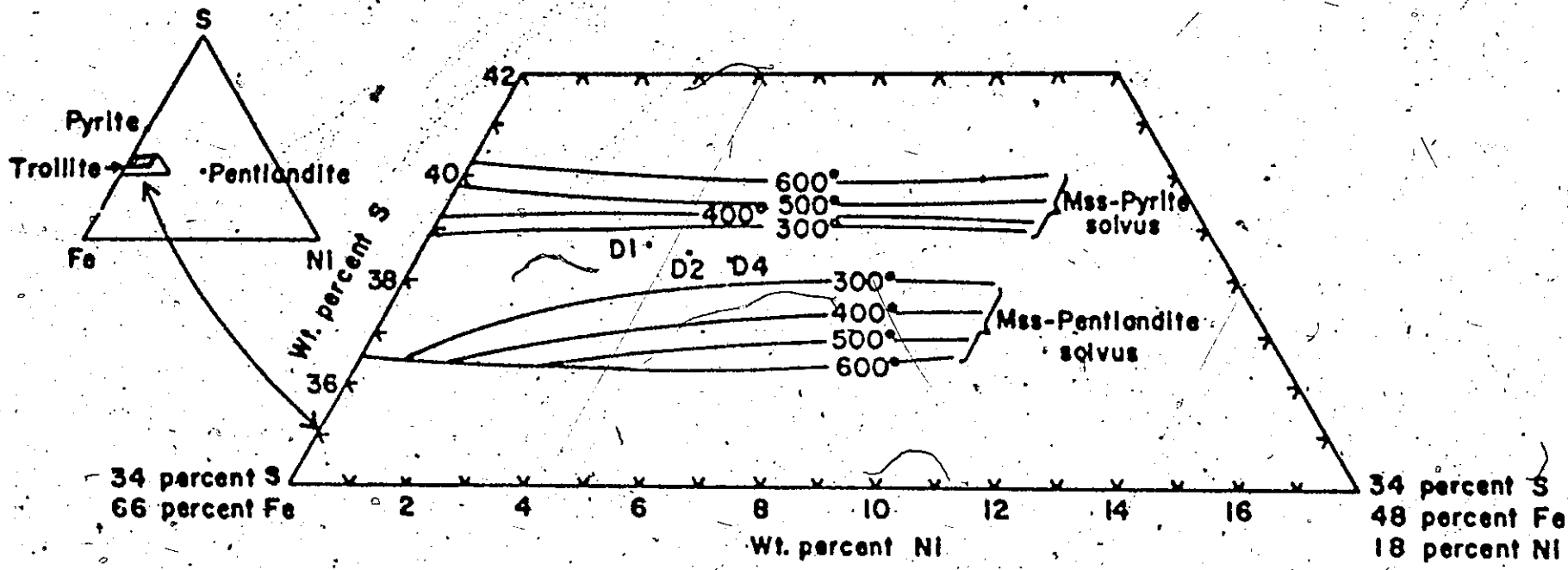

Figure 5-1. Plot of the Composition of Pertinent Deep Zone ore Stopes on a Portion of the Fe-Ni-S System Illustrating the Limits of the $Fe_{1-x}S$-$Ni_{1-x}S$ Solid Solution from the Fe-S Join to 10 wt. Percent Nickel at 600°, 500°, 400°, and 300°C (after Naldrett and Kullerud, 1967).

Table 5-2. Comparison of Mineral Modes Determined by Point Counting and Chemical Assay (in weight %)

Stope	Pyrrhotite		Magnetite		Chalcopyrite		Pentlandite	
	Point Count	Assay	Point Count	Assay	Point Count	Assay	Point Count	Assay
D1	72	71	6	9	15	11	7.5	9
D2	76	72	5	8.5	9	11	10	9
D4	69	70	10	10	12	11	9.5	9

Table 5-3. Concentrations of Cu, S, and Ni in Pertinent Deep Zone Ore Stopes

	Percent Cu	Percent S	Percent Ni
Stope D-1	5.3	36.4	3.4
Stope D-2	3.1	36.8	4.1
Stope D-4	4.2	35.2	4.2
Average	4.2	36.1	3.9

700°C). These criteria require that the original sulfur concentration must have been between 37.0 and 38.5% (with copper less than 5%). The lower sulfur contents of these stopes as indicated in table 5-3, therefore, cannot represent their original values. A possible explanation of the lower sulfur content is that sulfur was lost to the footwall granitic gneiss complex after emplacement of the sulfide melt. This is compatible with the increasing trend of sulfur-poor hexagonal pyrrhotite with respect to the sulfur-rich monoclinic pyrrhotite towards the lowest portion of the deep zone ore (Vaughan et al., 1971). A simplified mineral assemblage succession from Craig et al. (1967) applicable to the deep zone ore compositions is presented as figure 5-2.

Based on these considerations, the distribution of the noble metals can be considered in terms of an initial high temperature event where fractionation between pyrrhotite solid solution and magnetite has been of importance, and in terms of subsolidus events where partition between pyrrhotite solid solution and exsolved chalcopyrite and pentlandite below 450°C has occurred. For convenience of presentation, the subsolidus partition processes will be considered first.

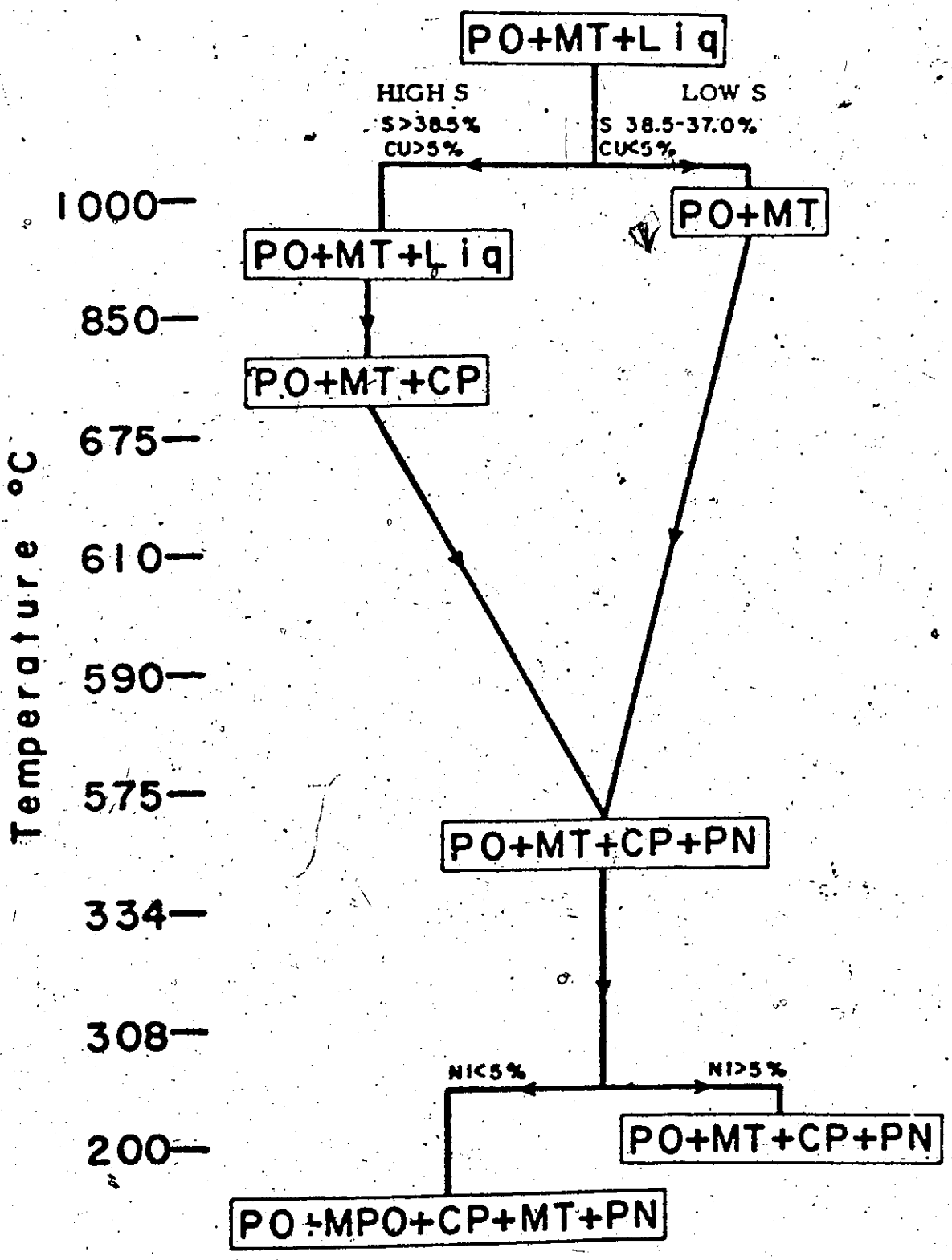

Figure 5-2. A Simplified Mineral Assemblage Succession Applicable to the Deep Zone Ores (after Craig et al., 1967).

5-1-3. Evidence for the Occurrence of Noble Metal Partition at Subsolidus Temperatures

Table 5-4 gives the abundances of the noble metals in co-existing mineral phases. Table 5-5 gives the average noble metal contents of the stopes and figure 5-3 is a schematic presentation of the data from table 5-5.

There is an enrichment of Pd in pentlandite with respect to chalcopyrite, magnetite, and pyrrhotite by factors of 6, 140, and 13 respectively. In particular, the Pd enrichment in pentlandite relative to pyrrhotite is found in every sample analyzed. Pt is enriched in chalcopyrite with respect to pentlandite, magnetite, and pyrrhotite by factors of 9, 18, and 9 respectively. A much weaker enrichment of Ir in chalcopyrite with respect to pentlandite, magnetite, and pyrrhotite by factors of 3.5, 5.7, and 5.3 respectively is observed. Finally, Au is enriched in pentlandite with respect to chalcopyrite, magnetite, and pyrrhotite by factors of 8, 28, and 11 respectively.

Of these partitions the Pd enrichment in pentlandite relative to pyrrhotite is perhaps most significant. As there is no doubt that all pentlandite originates by exsolution from pyrrhotite, and as the highest possible temperature at which this exsolution could

Table 5.4 Abundances of the Noble Metals in Coexisting Minerals

Sample*	Pyrrhotite	Magnetite	Chalcopyrite	Pentlandite
D1A	6.70± 0.67(3)**	4.17± 0.19(2)	9.98± 0.82(2)	59.1± 4.8(2)
D1C	4.28± 1.18(4)	2.44± 0.83(2)	7.04± 1.22(2)	106 ±40(2)
D1E	3.67± 1.34(4)	2.66± 0.20(2)	9.14± 1.62(2)	130 ±17(2)
D2A	6.80± 1.21(4)	1.71± 0.58(2)	16.9 ± 3.5(3)	37.1± 0.25(2)
D2C	14.3 ± 4.7(4)	3.86± 0.02(2)	13.0 ± 0.65(2)	39.7± 6.16(3)
D4	27.7 ±18.1(2)	11.0 ± 1.7(3)	35.1 ±23.2(2)	333 ±39(2)
D1A	192 ± 7(2)	22.9 ± 1.3(2)	242 ± 5(2)	1860 ±125(2)
D1C	195 ± 9(2)	7.5 ± 1.7(2)	451 ±61(2)	2640 ±400(2)
D1E	216 ±10(2)	13.2 ± 1.6(2)	372 ±55(2)	1410 ±50(2)
D2A	202 ±41(3)	20.1 ± 8.1(2)	245 ±75(2)	2265 ±215(2)
D2C	243 ± 2(2)	5.3 (1)	639 ±130(2)	2251 ±157(3)
D4	78 ±37(3)	17.6 ± 5.4(2)	250 ±113(2)	1965 ±275(2)
D1A	1.93± 0.47(3)	0.46± 0.01(2)	6.01± 0.89(2)	1.63± 0.50(2)
D1C	1.25± 0.34(3)	3.77± 0.33(2)	2.36± 1.14(2)	2.36± 0.04(2)
D1E	2.19± 0.12(3)	1.42± 0.41(2)	6.41± 0.74(2)	2.78± 0.31(2)
D2A	1.60± 0.16(2)	1.67± 0.12(2)	3.98± 0.68(3)	1.11± 0.02(2)
D2C	1.06± 0.25(3)	0.58± 0.16(2)	15.0 ± 3.9(2)	2.17± 0.45(2)
D4	9.67± 0.15(3)	0.57± 0.20(2)	6.27± 0.01(2)	2.04± 0.34(2)
D1A	346 ± 1(2)	413 ±35(2)	1110 (1)	575 (1)
D1C	373 ±69(2)	387 ±79(2)	-	963 ±132(2)
D1E	551 ±216(2)	317 ±54(2)	3070 (1)	1465 (1)
D2A	1042 ±205(2)	455 ±88(2)	3340 (1)	723 ±142(2)
D2C	973 ±406(2)	858 ±67(2)	1195 ±65(2)	1450 (1)
D4	1059 ±406(2)	244 (1)	18600 ±2650(2)	675 ±31(2)

* D1, D2 and D4 refer to the stopes from which samples were taken while the letters A, B and C indicate different samples from each of the stopes.

** The figures in brackets ind. ate the number of analyses.

Table 5-5. Average Noble Metal Content of Deep Zone Ore Stopes (p. p. b.).

		Po.	Mag.	Cpy.	Pn.
Au	D1	4.85	3.09	9.42	98.4
	D2	10.05	2.80	15.0	38.4
	D4	27.7	11.0	35.1	333
Pd	D1	171	14.5	348	1970
	D2	243	12.7	442	2260
	D4	78	17.6	250	1970
Ir	D1	1.79	1.89	4.93	2.26
	D2	1.33	1.13	9.49	1.64
	D4	0.67	0.57	6.27	2.04
Pt	D1	437	372	2090	801
	D2	1020	657	2270	1090
	D4	1059	244	18600	675

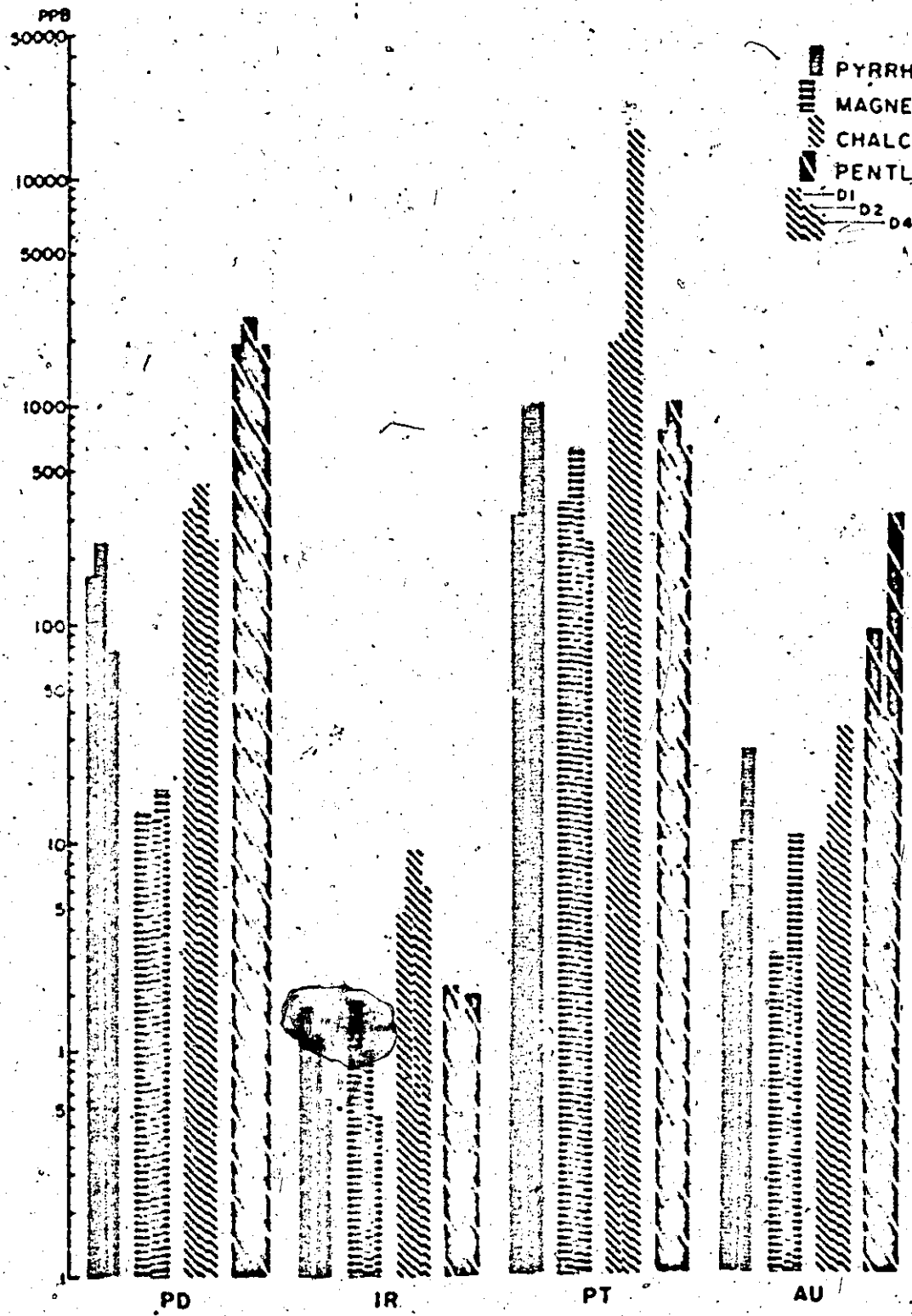

Figure 5-3. Schematic Presentation of the Average Noble Metal Contents of the Deep Zone Ore Stopes

have occurred is well below the liquidus temperature of this system, it seems inescapable that the 13-fold enrichment of Pd in pentlandite occurs by diffusion of the metal in a system containing only solid phases. Likewise subsolidus diffusion appears to be a very important process in redistributing other noble metals, particularly Au and Pt.

5-1-4. Noble Metal Partition at Magmatic Temperatures

The noble metal content of pyrrhotite solid solution at magmatic temperatures can be estimated if it is assumed that all pentlandite and chalcopyrite were initially in solid solution in pyrrhotite. Thus by adding to the noble metal content of pyrrhotite the contribution from chalcopyrite and pentlandite, weighted for their respective modal portions in the ore, the noble metal content of pyrrhotite solid solution may be estimated. We can then compare this estimated noble metal value for pyrrhotite solid solution with the measured noble metal concentration in magnetite to evaluate partition between pyrrhotite solid solution and magnetite at magmatic temperatures. The results are shown in table 5-6 and schematically presented in figure 5-4.

All four noble metals are seen to fractionate rather strongly into pyrrhotite; Pd by 26; Pt by 6, Au by 5, and Ir by 2.

Table 5-6. Partition of Noble Metals between Pyrrhotite Solid Solution and Magnetite

Stope	D1			D2			D4		
	Po. SS	Mag.	Po. SS/Mag.	Po. SS	Mag.	Po. SS/Mag.	Po. SS	Mag.	Po. SS/Mag.
Au	13.1	3.09	4.24	13.4	2.80	4.79	60.7	11.0	5.52
Pd	343	14.5	23.6	466	12.7	36.7	299	17.6	17.0
Ir	2.33	1.89	1.23	2.15	1.13	1.90	1.55	0.57	2.72
Pt	729	372	1.96	1150	657	1.75	3330	244	13.6

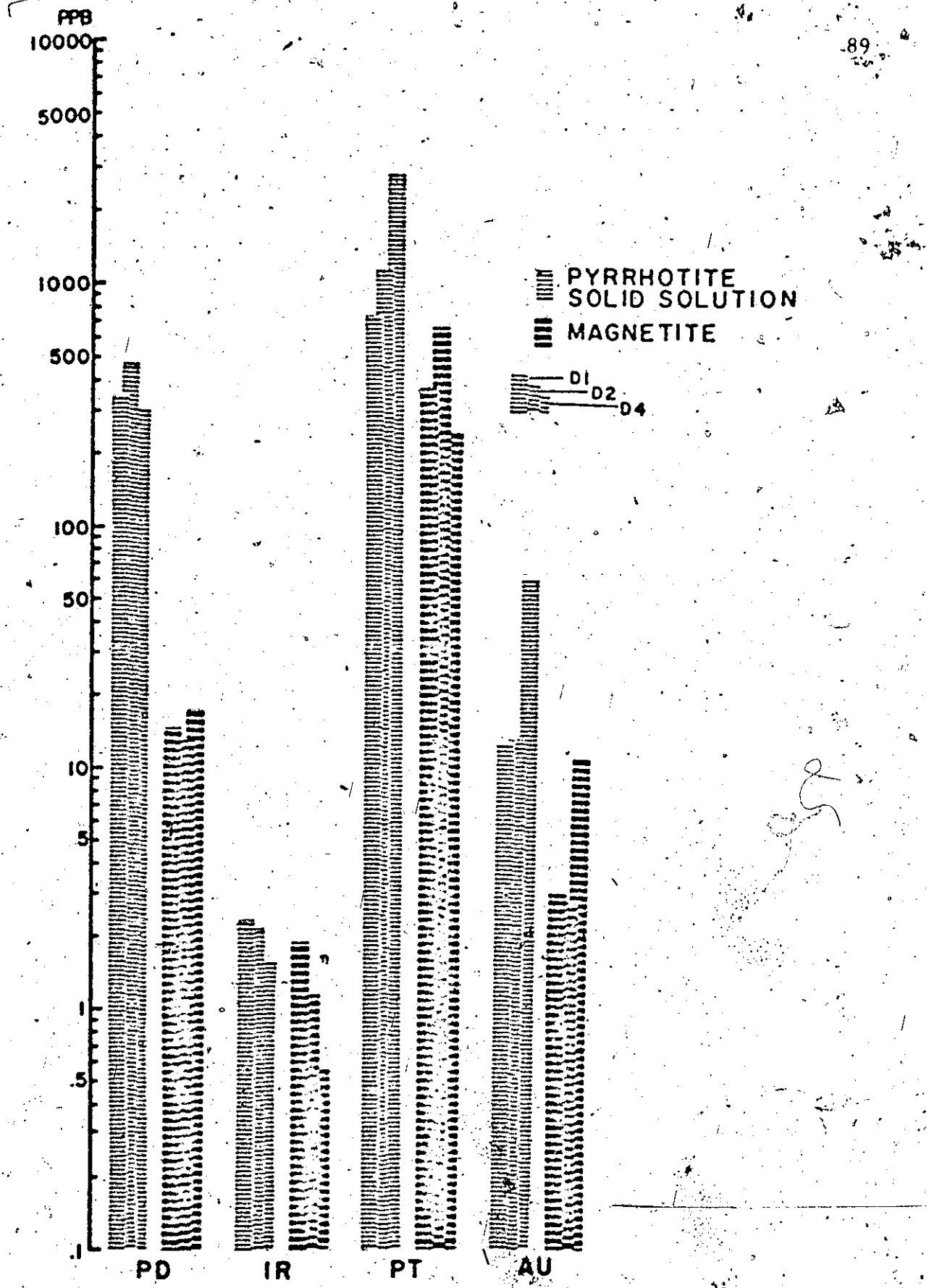

Figure 5-4. Schematic Presentation of Noble Metal Distribution between Pyrrhotite Solid Solution and Magnetite at Magmatic Temperature.

5-1-5. Correlation of the Noble Metals in Coexisting Mineral Pairs

Correlation coefficients for noble metal partition between mineral pairs were calculated for all the deep zone ore samples using the data from table 5-4. The coefficients are presented in table 5-7.

The strongest correlations are for Au between pyrrhotite and magnetite, Au between magnetite and chalcopyrite, and Au between pentlandite and magnetite; the correlations are significant at the 95% level. The next strongest correlations are for Au between pentlandite and chalcopyrite, and Pt between pentlandite and magnetite; these correlations are significant at the 90% level. Pd between chalcopyrite and magnetite is strongly correlated negatively at the 95% significant level. The interpretation of these correlations is discussed in chapter 6.

5-2. Distribution of Noble Metals in Disseminated Sulfides from the Main Rock Types of the Strathcona Mine

Disseminated sulfide is widely distributed in the Irruptive and the sub-layer and varies from less than one percent in the Irruptive to more than five percent in the sub-layer rock units. In felsic norite pyrite is the major sulfide component while in mafic norite and the underlying sub-layer rocks pyrrhotite with less than 1% pentlandite is the major sulfide component. Small amounts of magnetite are occasionally present.

Table 5-7. Correlation Coefficients for Noble Metals in Coexisting Mineral Pairs

	Au in po.	Au in mag.	Au in cpy.	Au in pn.
Au in po.	1.000	0.935	0.532	0.760
Au in mag.		1.000	0.888	0.889
Au in cpy.			1.000	0.823
Au in pn.				1.000

	Pd in po.	Pd in mag.	Pd in cpy.	Pd in pn.
Pd in po.	1.000	0.727	0.807	0.217
Pd in mag.		1.000	-0.920	0.389
Pd in cpy.			1.000	0.295
Pd in pn.				1.000

	Ir in po.	Ir in mag.	Ir in cpy.	Ir in pn.
Ir in po.	1.000	0.030	0.241	0.059
Ir in mag.		1.000	0.612	0.217
Ir in cpy.			1.000	0.179
Ir in pn.				1.000

	Pt in po.	Pt in mag.	Pt in cpy.	Pt in pn.
Pt in po.	1.000	0.256	0.479	0.284
Pt in mag.		1.000	0.568	0.836
Pt in cpy.			1.000	0.333
Pt in pn.				1.000

To study the disseminated sulfide, a cross-cut on the 2750 level which cuts all of the major rock units from the felsic norite of the Irruptive to the deep zone ore in the footwall granitic gneiss complex was chosen. A total of 21 chip samples were collected along the length of the 2750 cross-cut. The sulfide was separated from the silicate material and concentrated magnetically to yield a pyrrhotite concentrate of 99% purity. The analytical results for Pd, Ir and Au are presented in table 5-8 and figure 5-5. Pt was too low to be measured in these samples.

As indicated in figure 5-5, there is a very large variation in noble metal concentrations through the profile. Pd varies by a factor of up to 30, Ir by a factor of 13, and Au by 30.

However, if we group the rock units according to the major intrusive events which they represent (after Greenman, 1970 and Hewins, 1971) then the average noble metal concentrations can be usefully compared. Three main rock units recognized include (1) the Irruptive with the mafic norite regarded as the "chilled" border group, (2) the xenolithic norite and hanging-wall breccia which represent a post-Irruptive intrusion, and(3) the footwall gray breccia and sulfide in the granitic gneiss complex which represent a separate intrusion regarded as post-sub-layer.

Table 5-4. Noble Metal Concentrations in Pyrrhotite from the 2750 Level Cross Cut

	Sample No.	Pd	Ir	Au	in p.p.b.
Felsic Norite	S-27-15	48.6±30.8(2)*	20.9	1.9	
Mafic Norite	S-27-16	6.4	10.4	0.9	
	S-27-17	6.3	3.7	5.3	
	S-27-18	159.3±56.4(4)	12.6	1.9	
	S-27-19	46.2±6.2(6)	14.1	6.6±0.1(2)	
	S-27-20	16.2	6.3	3.9	
	S-27-21	15.5	4.2	1.7	
Nepheline Norite	S-27-22	10.4	26.4±1.9(2)	6.8±0.8(3)	
	S-27-23	77.2	3.4	1.2	
	S-27-24	48.8±10.1(6)	29.0	1.4	
Hanging-wall Breccia	S-27-25	30.1	21.2	8.7	
	S-27-26	15.1±4.2(2)	48.3	2.5	
	S-27-27	27.3±3.4(3)	30.8	0.7	
	S-27-28	31.1±7.1(3)	35.6	0.7	
	S-27-29	35.8±4.7(2)	16.8	1.8	
Footwall Gray Breccia	S-27-30	35.9±7.5(2)	5.5	9.3±1.4(2)	
Granitic Gneiss	S-27-31	42.4±9.6(2)	13.1	8.5	
	S-27-32	78.5	8.0	4.8	
	S-27-33	30.0	32.0	5.8	
	S-27-34	14.1±1.8(2)	11.3	4.2	
	S-27-35	188.0±25(2)	8.0	21.1	

* Number of analyses is indicated in parentheses

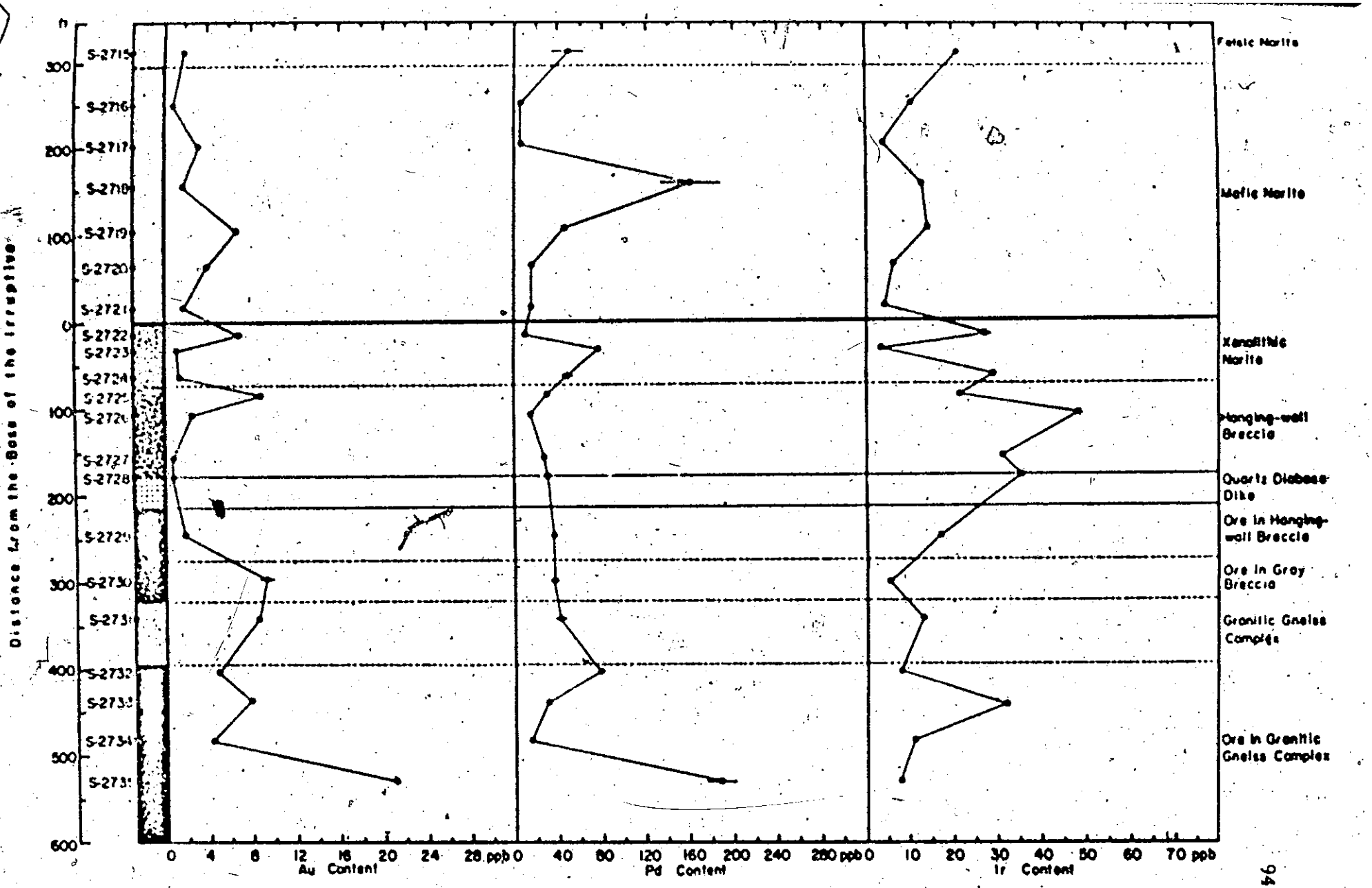

Figure 5-5. Concentration Profiles of Au, Pd, and Ir along 2750 Level Cross-cut

On calculating the average value and standard deviation for Pd, Ir and Au in these units, it is found that only Ir is characterized by statistically different average values: 8.6±4.4 p.p.b. in mafic norite, 26.3±13.2 p.p.b. in the mafic sub-layer, and 12.3±9.1 p.p.b. in the footwall gray breccia and the associated sulfide in the granitic gneiss complex. In the case of Pd and Au average values for these units were found not to differ significantly when tested by an F test. These calculations indicate that the Ir concentration profile in the mafic sub-layer can be differentiated from that of the Irruptive and footwall gray breccia and sulfide in a statistically significant manner.

Positive evidence that Au is sensitive to secondary mobilization is the distribution pattern formed at the boundaries of a quartz diabase dike intrusion. The intrusion tends to disperse Au away from the dike forming a low in the concentration profile at the dike margins (see Figure 5-5).

CHAPTER 6

DISCUSSION

6-1. Occurrence of the Noble Metals

The noble metals may occur as discrete minerals of their own or as impurities in other minerals. Owing to the fact that no individual noble metal mineral has yet been identified in the primary pyrrhotite-magnetite-chalcopyrite-pentlandite assemblage (Cowan, 1967) in Strathcona mine, it is concluded that most of the noble metals occur as impurities of the major sulfide minerals. It is generally recognized that impurities may be incorporated into minerals in three ways including solid solution, solid or liquid inclusions, and adsorbed films (Bethke and Barton, 1971). The occurrence of noble metals in solid solution in Sudbury copper-nickel sulfides was suggested by Hawley (1962), and Cowan (1967). Razin et al. (1965) appealed to solid solution or adsorbed films of the platinum metals as the dominant mode of occurrence in the Merensky Reef of the Bushveld Complex.

6-1-1. Solid Solution

Krauskopf (1967) defined a solid solution as one in which the solid resembles a liquid solution in that it remains homogeneous when its

components are varied over a certain range of composition. It is therefore theoretically possible that the homogeneity of distribution of a trace constituent in a host mineral will provide a test of solid solution. In order to make this test a mineral concentrate of very high purity has to be prepared. It was shown in 4-2-6 that some error always results from impurities in mineral concentrates and from analytical error. Therefore, to test the homogeneity of a metal distribution by means of direct analysis is impractical.

6-1-1-1. Lattice Substitution

An alternative is to test whether the distribution of a minor constituent between two coexisting phases obeys Henry's dilute solution law.

Kretz (1961) has shown that the substitution of trace element A for a common major component B of two coexisting phases α of (A, B)M type and β of (A, B)N type can be expressed as:

$$\frac{X_A^{\alpha}(1-X_A^{\beta})}{(1-X_A^{\alpha})X_A^{\beta}} = \frac{\gamma_B^{\alpha}\gamma_A^{\beta}\lambda_B^{BM}\lambda_A^{AN}}{\gamma_A^{\alpha}\gamma_B^{\beta}\lambda_A^{AM}\lambda_B^{BN}} \qquad (1)$$

where X_A and X_B are the mole fractions of A in phases α and β respectively, λ_A^{α} etc. are activity coefficients, and λ_A^{AM} etc. are absolute activities. If we let A represent a trace element, K_{λ} denotes the term containing absolute activities and K_{γ} the activity coefficients

where both K terms depend on P and T when the standard state is specified, then equation (1) can be simplified to:

$$\frac{X_A^\alpha}{X_A^\beta} \gamma \frac{X_A^\alpha(1-X_A^\beta)}{(1-X_A^\alpha)X_A^\beta} = K_\gamma K_\lambda(P,T) \qquad (2)$$

If Henry's Law is obeyed, K_γ is constant, and $\frac{X_A^\alpha}{X_B^\beta}$ is a function of pressure and temperature only. Usually this applies when the concentration of A is very low. As all the measured noble metal concentrations are at the p.p.m. level or lower, it is quite likely that they exhibit Henry's Law behaviour. Furthermore, as all six samples were collected from the same ore lense within 30' of each other vertically, it is highly probable that all were subjected to a nearly identical temperature and pressure regime. Thus, if it follows that a plot of the concentration of an element in each of two coexisting phases should yield a straight line which extrapolates to the origin if Henry's Law behaviour applies. If this is the case then we infer that the element is held in solid solution by lattice substitution in each of the two phases.

The partition of four elements between four coexisting phases gives 24 partition coefficients. The statistical test for the correlation of each pair was given in table 5-7, and the test for whether the regression line passes through the origin is given in Appendix C.

Six of the 24 distribution coefficients are significant at the 90% probability level, and of these five have regression lines which pass through the origin with 99% probability. They include Au between pyrrhotite and magnetite, Au between chalcopyrite and magnetite, Au between pentlandite and magnetite, and Au between pentlandite and chalcopyrite as well as Pt between pentlandite and magnetite. The plots are shown in figure 6-1, 6-2, and 6-3, and suggest that Au is in solid solution in all four minerals studied.

For the mineral assemblage under consideration it seems that simple lattice substitution may not be the only mechanism whereby noble metal trace constituents are incorporated into solids. Two of the minerals, pyrrhotite and chalcopyrite, are known to form defect structures characterized by lattice vacancies, and therefore it is necessary to consider models in which lattice vacancies are taken into account. Also, simple lattice substitution would not lead to negative linear correlation as displayed by the partition of Pd between chalcopyrite and magnetite. Therefore, it is suspected that certain other mechanisms have caused a departure from the constraints of Henry's Law.

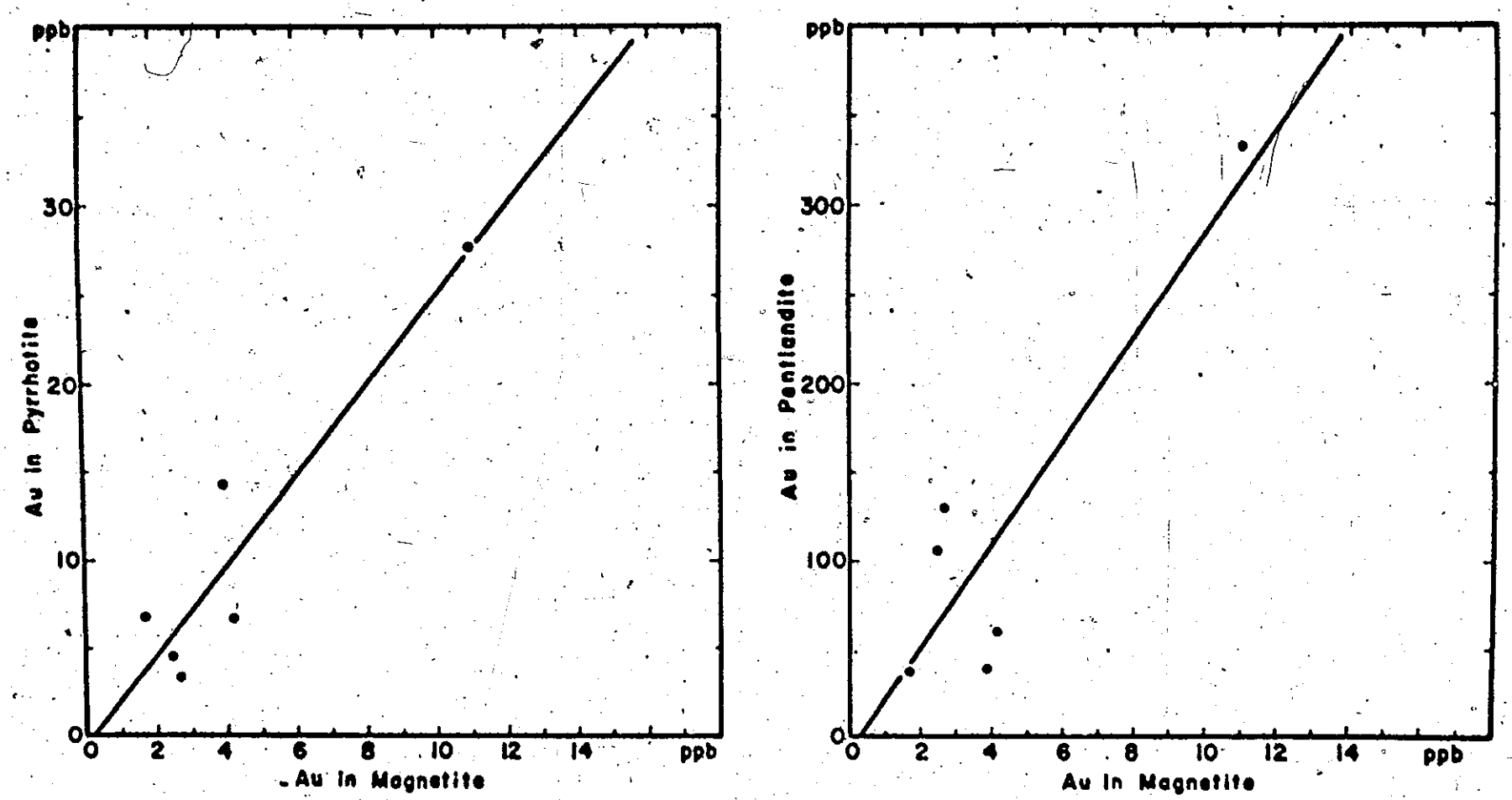

Figure 6-1. Au Partition between Pyrrhotite and Magnetite (left);
Au Partition between Pentlandite and Magnetite (right).

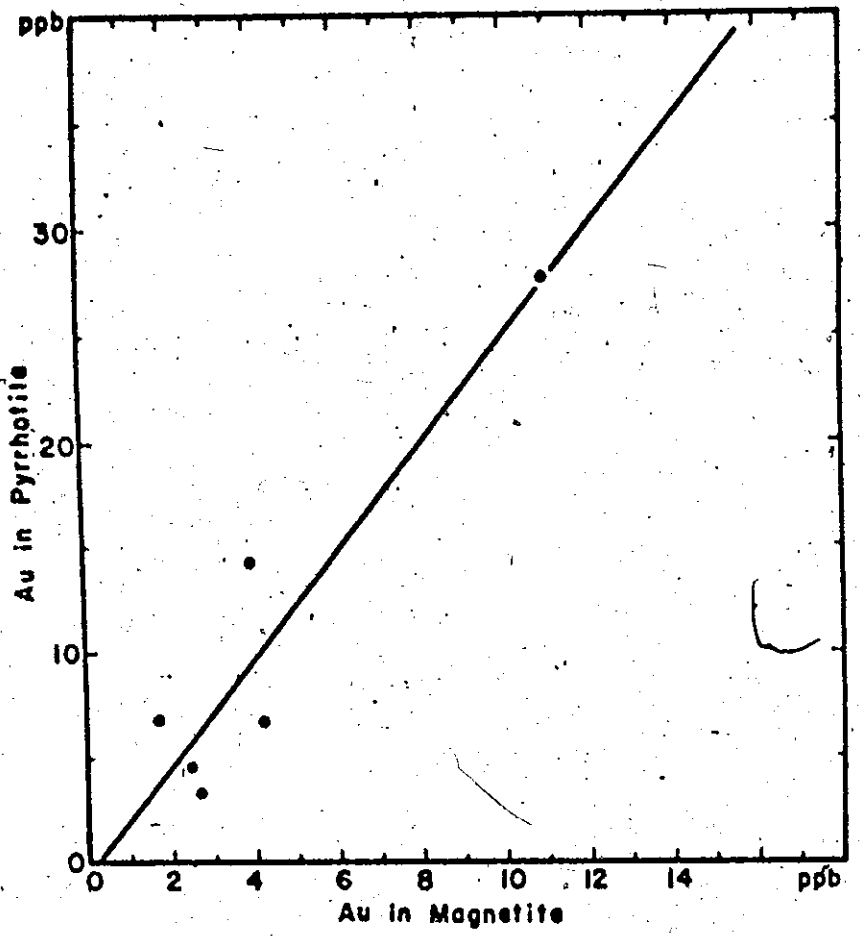

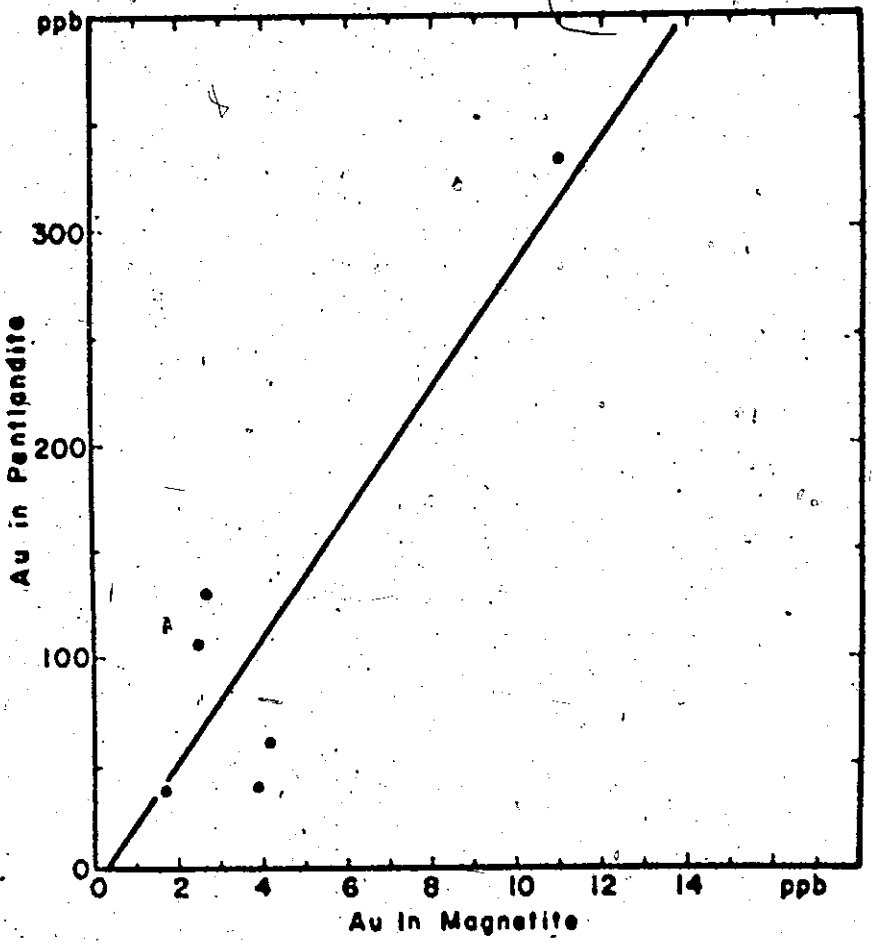

Figure 6-2. Au Partition between Chalcopyrite and Magnetite (left):
Au Partition between Pentlandite and Chalcopyrite (right).

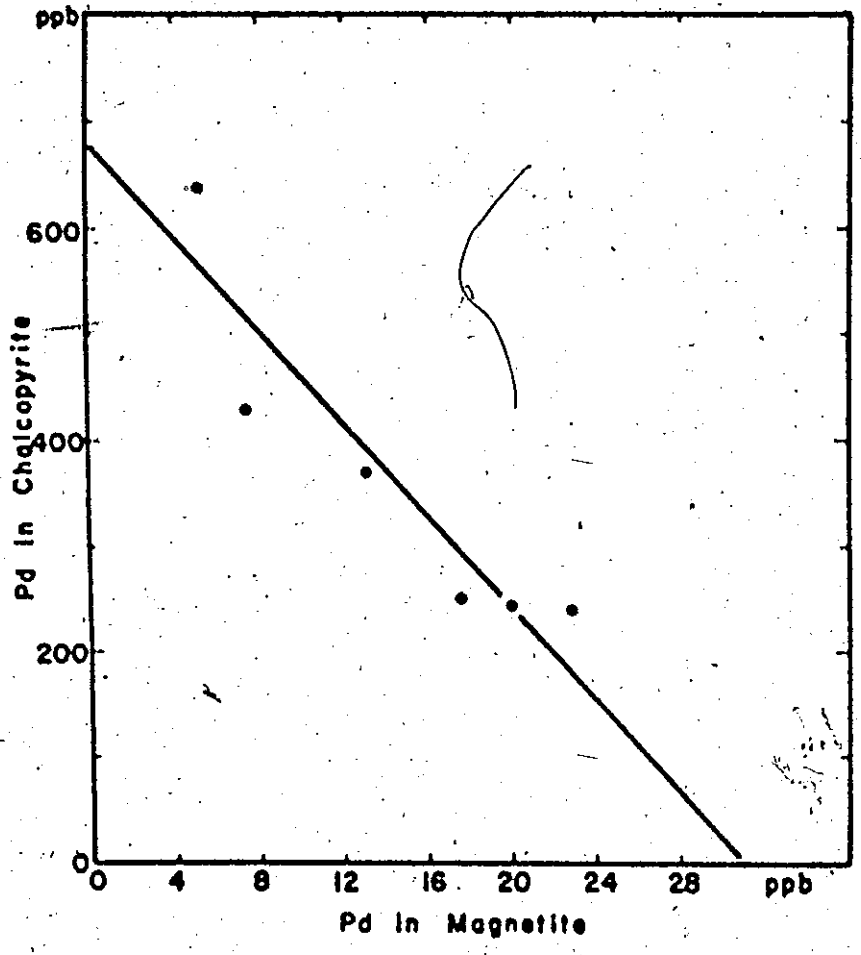

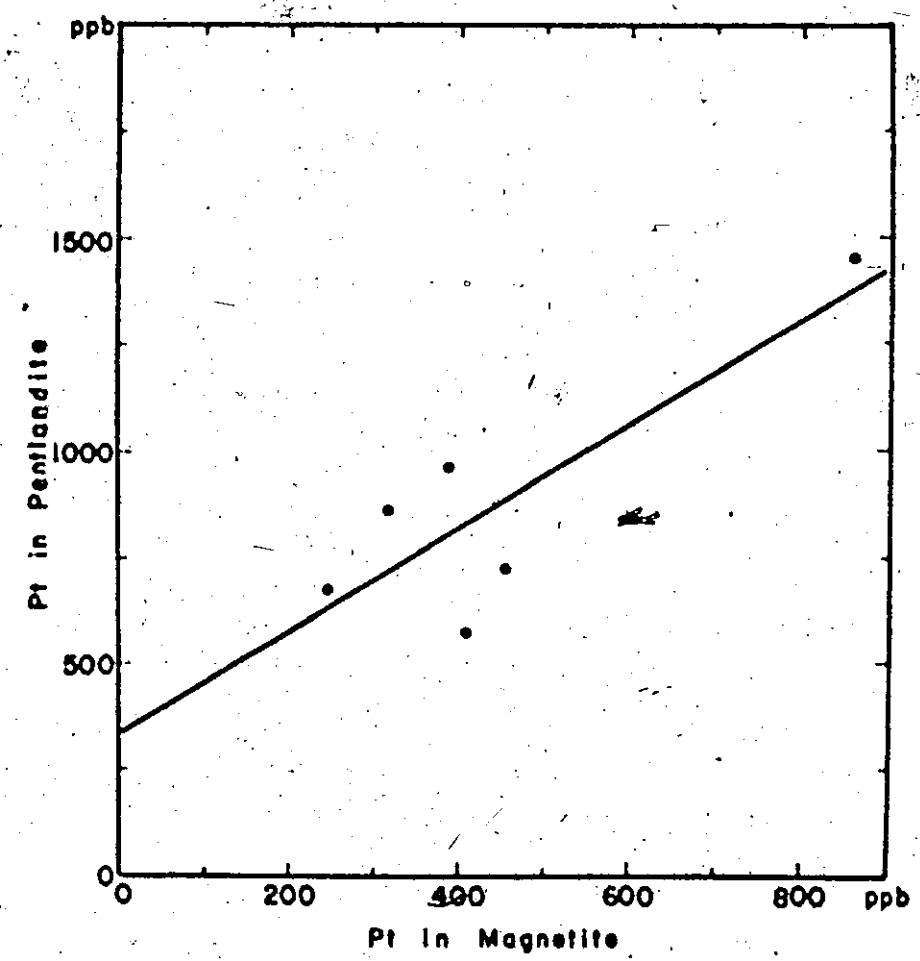

Figure 6-3. Pd Partition between Chalcopyrite and Magnetite (left);
Pt Partition between Pentlandite and Magnetite (right)

6-1-1-2. Induced Lattice Vacancies

McIntire (1958, 1963) has shown that if substitution of an element in a structure necessitates the formation of vacancies, the partition coefficient will not follow Henry's Law. The formation of vacancies in a solid phase is required to neutralize the charge disparity caused by the substitution of an altervalent element, or by the interstitial substitution of any element. Vacancies are known to form in sulfides due to trace element substitution and their effects have been shown to be similar irrespective of type of bonding (Kroger, 1964; and Wagner, 1952).

McIntire's theoretical development is summarized as follows:

Assume that a bivalent ionic microcomponent A_3 substitutes in a normal A_1 site and forms a substitutional defect in a univalent crystalline solid S of type A_1A_2. Electrical neutrality is maintained by

$$n^{S}_{3(1)} + n^{S}_{2\square} = n^{S}_{1\square} \qquad (3)$$

where $n^{S}_{3(1)}$ is the number of A_3 ions substituting in the A_1 position in S and $n^{S}_{1\square}$ and $n^{S}_{2\square}$ are the numbers of A_1 and A_2 vacancies in S.

Based on these assumptions, McIntire has shown that

$$\frac{X_{3(1)}^{S} X_{1\square}^{S}}{X_3^{L}} = K_4(P, T) \text{ or } \frac{X_{3(1)}^{S}}{X_3^{L}} = \frac{K_4}{X_{1\square}^{S}} \qquad (4)$$

and $$X_{1\square}^{S} X_{2\square}^{S} = K_5(P, T) \qquad (5)$$

where $X_{3(1)}^{S}$ is the mole fraction of A_3 ions substituting at the A_1 site in S and X_3^{L} is the mole fraction of A_3 ions in a liquid (L) coexisting with S. $X_{1\square}^{S}$ and $X_{2\square}^{S}$ are the mole fractions of vacant A_1 and A_2 sites, respectively.

Let $$X_{3(1)}^{S} + X_{2\square}^{S} = X_{1\square}^{S} \qquad (6)$$

By combining equation (4), (5), and (6), we get

$$\frac{X_{3(1)}^{S}}{X_3^{L}} = \frac{K_4}{(K_5 + K_4 X_3^{L})^{1/2}} \qquad (7)$$

Assume that the expression for the distribution of elements between a solid and a liquid, as derived by McIntire, is also valid for element "i" distributing between two solid phases α and β. Then equation (7) becomes

$$\frac{X_i^{\beta}}{X_i^{\alpha}} = \frac{K_4}{(K_5 + K_4 X_i^{\alpha})^{1/2}} \qquad (8)$$

Rearrange equation (8) to the form:

$$\left(\frac{X_i^{\alpha}}{X_i^{\beta}}\right)^2 = \frac{1}{K_4}\left(X_i^{\alpha} + \frac{K_5}{K_4}\right) = \frac{X_i^{\alpha}}{X_i^{\beta} X_{1\alpha}^{\beta}}\left(X_i^{\alpha} + \frac{K_5}{K_4}\right) \tag{9}$$

or

$$\frac{X_i^{\alpha}}{X_i^{\beta}} = \frac{1}{X_{1\alpha}^{\beta}} X_i^{\alpha} + \frac{X_{2\alpha}^{\beta}}{K_4} \tag{10}$$

Thus, if a phase contains induced vacancies, the ratio of X_i^{α}/X_i^{β} will increase as X_i^{α} increases. If $X_{1\alpha}^{\beta}$ remains constant then the plot will result in a straight line whereas if $X_{1\alpha}^{\beta}$ varies a culvilinear trend will be produced. The equation assumes that the charge is balanced only by induced vacancies, and that coupled substitution is insignificant. Further, the distribution of one element is assumed not to be affected by another.

The correlation coefficients of X_i^{α}/X_i^{β} versus X_i^{α}, where α and β can be any of the four coexisting phases, have been calculated. The improvement of the correlation coefficients for this solid solution model as compared to those calculated according to the lattice substitution model may be seen in table 6-1. Those significant at the 90% probability level or higher are underlined.

The table shows that none of the correlation coefficients of Au is significantly improved by the induced vacancy model, whereas those of Ir, Pt, and Pd are much higher. In case of Ir, increase in

Table 6-1. Comparison of Noble Metal Correlation Coefficients for Different Solid Solution Models

	Lattice Substitution	Po. Contains Vacancies	Cpy. Contains Vacancies
Au between po. and mag.	0.935*	-0.144	
Au between po. and cpy.	0.532	-0.356	0.604
Au between po. and pn.	0.769	-0.062	
Au between mag. and cpy.	0.884		0.386
Au between cpy. and pn.	0.823		0.493
Pd between po. and mag.	0.727	0.830	
Pd between po. and cpy.	0.607	0.021	0.430
Pd between po. and pn.	0.217	0.685	
Pd between mag. and cpy.	-0.920		0.979
Pd between cpy. and pn.	0.295		0.261
Ir between po. and mag.	0.030	0.961	
Ir between po. and cpy.	0.241	0.884	0.508
Ir between po. and pn.	0.059	0.421	
Ir between mag. and cpy.	0.612		0.934
Ir between cpy. and pn.	0.179		0.397
Pt between po. and mag.	0.256	0.041	
Pt between po. and cpy.	0.429	0.977	0.100
Pt between po. and pn.	0.284	0.326	
Pt between mag. and cpy.	0.568		0.938
Pt between cpy. and pn.	0.333		0.992

* Significant at the 90% level or higher are underlined.

coefficients are seen in all five pairs including pyrrhotite or chalcopyrite: in case of Pt only four pairs are higher; in case of Pd, three pairs are higher while two pairs are lower, but the negative correlation of Pd between magnetite and chalcopyrite as interpreted by lattice substitution model becomes positive and significant at over 90% level as interpreted by assuming that chalcopyrite contains induced vacancies.

The comparison of the noble metal correlation coefficients for simple lattice substitution model and induced vacancy model with pyrrhotite or chalcopyrite containing vacancies allow us to envisage their state of existence. The high coefficients of Au in lattice substitution model and decreasing coefficient in induced vacancy model suggests that simple lattice substitution is the most feasible solid solution model for Au. The low coefficients of Ir in lattice substitution model, improved coefficients in induced vacancy model with either pyrrhotite or chalcopyrite containing vacancies, and the most common +4 oxidation state support that induced vacancy is the most feasible model for Ir. The rather variable behaviour of Pt and Pd may be the results of either their high concentrations which allow the interference of other cations to become significant, or alternatively their formation of bonds with Se, Te, or As isomorphously held in pyrrhotite or chalcopyrite.

6-1-2. Mineralogy

The compounds of these four noble metals found in nature can be grouped into metallic and non-metallic minerals (Parthé, 1971). The native platinum metals and their alloys are usually found as disseminations in ultramafic rocks as represented by Urals of the U.S.S.R. or placers derived from them such as in the Tulameen River district, Canada, and the Choco area of Columbia. Metallic gold is widely distributed and generally found in placers, hydrothermal deposits associated with acidic igneous intrusions, or in greenstone belts.

Non-metallic noble metal minerals are usually found in nature as chalcogenides and pnictides usually associated with copper-nickel sulfides such as in the Rustenberg district of South Africa, the Noril'sk-Talnakh area of the U.S.S.R., and the Sudbury district of Ontario, Canada.

In the Sudbury area, three platinum minerals have been confirmed. They are froodite, $PdBi_2$; michenerite (Pd, Pt)Te(Bi, Sb); and sperrylite, $PtAs_2$. All of them come from off-set deposits. Froodite and michenerite are found associated with nickel arsenides in the siliceous mineral zone of the lower levels of the Frood mine. Sperrylite was first discovered at Vermilion mine, but the most common

association is at the Frood mine with nickel arsenides. The association of arsenides and platinum minerals with secondary silicates, quartz, and carbonates in the off-set environment contrasts rather sharply with the more common pyrrhotite-magnetite-chalcopyrite-pentlandite assemblage of the north and south range environment where discrete platinum metal minerals are apparently absent. Arsenides are most abundant in the off-set environment and to a lesser extent are present along the south range environment, but never have been reported in the north range deposits (Hawley, 1962).

Millerite stringers occur in the footwall granitic gneiss complex of Strathcona mine. They usually have a wide alteration band (Cowan, 1967), and according to Graham (1964), crystallized at a temperature above 380°C from a relatively iron-poor, sulfur-rich fluid containing high proportions of copper and nickel. Graham believed that they represented a late stage mineralization related to the formation of the main zone ore. Cowan (1967) reported that these stringers contained minute unidentified minerals rich in Pt, Pd, Bi, Te, and Se.

Keays (1968) analyzed some Strathcona sulfides for arsenic. His data are reproduced in table 6-2.

Table 6-2. Arsenic Content of Strathcona Sulfides

	No. of Analyses	Range (p.p.m.)	Average (p.p.m.)
Pyrrhotite	5	2.3-46	19.8
Chalcopyrite	5	3.6-530	127

The data indicate that arsenic is enriched in chalcopyrite relative to pyrrhotite by a factor of 6. Pd, Ir, and Au contents for these samples were also determined and the results indicated a strong correlation of As with Pd. The arsenic content is pentlandite, unfortunately it was not determined.

On the basis of mineralogy, natural association, and laboratory information, it appears that the noble metals in Strathcona are associated primarily with S, Se, Te, As, Sb, and Bi.

6-2. Factors Affecting Noble Metal Distribution Coefficients.

The partition of noble metals between the major ore minerals will be affected mainly by temperature, pressure, migration of anions and the bond character of the host minerals.

6-2-1. Temperature and Pressure

From equation (2), we know that temperature and pressure affect the distribution coefficient by determining the value K_λ. As all

the samples were collected from one ore lense, the temperature and pressure effects on the distribution coefficient are considered negligible.

6-2-2. Anion Concentrations

Platinum chalcogenides occur in nature as braggite, (Pd, Pd)S; cooperite, PtS; and moncheite, $PtTe_2$. Palladium chalcogenides occur in nature as vysotskite, PdS; oosterboschite, $(Pd, Cu)_7Se_5$; merenskyite, $PdTe_2$; and kotulskite, PdTe. Iridium does not form a chalcogenide of its own. Usually it occurs in other platinum metal chalcogenides as a solid solution such as in erlichmanite, $(Os, Ir, Rh, Ru, Pd)S_2$ and laurite, $(Ru, Ir, Os)S_2$. Thus it is inferred from mineral occurrences that the most stable valence states of Pt, Pd, and Ir under typical natural conditions are +2, +2, and +4 respectively.

Gold does not form a stable sulfide in nature (Krauskopf, 1967), but does form stable intermetallic compounds with tellurium such as krennerite, Au_3Te_5 and calaverite, $AuTe_2$.

6-2-2-1. Sulfur

The stability of the sulfide species can be related to a reaction of the kind.

$$2Pt(s)+S_2 = 2PtS(s) \quad (11)$$

where the equilibrium constant K is a function of temperature and pressure. As the effect of pressure is negligible at Strathcona,

$$K_T = \frac{(PtS)^2}{(Pt)^2 P_{S_2}} \approx \frac{1}{P_{S_2}} \quad (12)$$

where K_T is the equilibrium constant at temperature T and unit solid phase activities are assumed. Free energies of the reaction PtS and Ir_2S_3 at various temperatures can be computed from

$$\Delta G_T = A+BT\log T+CT \quad (13)$$

where ΔG_T is the free energy of the reaction at temperature T. The coefficients A, B, and C for these reactions are given in Kubaschewski et al. (1967). These values are not available for the reaction of PdS. They are therefore roughly estimated by using ΔH and ΔS at 25°C from McDonald and Cobble (1962) and Kubaschewski et al. (1967) from the equation

$$\Delta G_T = \Delta H - T\Delta S \quad (14)$$

that is, assuming neither ΔH nor ΔS vary with temperature.

The equilibrium constant can be related to the free energy of the reaction by

$$\Delta G_T = -RT\ln K_T \quad (15)$$

Combining equations (12) and (15), we have

$$\Delta G_T = -RT\ln\frac{1}{S_2} = RT\ln f_{S_2} \qquad (16)$$

and

$$\log f_{S_2} = \frac{\Delta G_T}{2.3RT} \qquad (17)$$

Univariant equilibria for the reaction of sulfur vapor with a metal to produce a sulfide are computed from (17) and presented as figure 6-4.

The magnitude of f_{S_2} values in equilibrium with the deep zone ore can be estimated from the sulfur fugacity data of Naldrett (1969) for liquids in the Fe-S-O system. The average composition of the deep zone ore, as estimated from table 5-2 taking all copper and nickel as iron, is: Fe=62.6%, S=35.5%, and O=1.9%. The $\log f_{S_2}$ values applicable to the deep zone ore at temperatures of 1,200°, 1,120°, and 1,050°C are -1, -1.8, and -2.3 respectively.

By taking all copper and nickel as iron and thus neglecting the effect of copper and nickel on temperature, Naldrett (1969) suggested 1045°C as the minimum emplacement temperature of average Strathcona sulfide. He stated that nickel has little or no effect on the melting temperature while 2 wt% copper will reduce the temperature by up to 20°C. The deep zone ore contains an average of 4.1 wt% copper so that this temperature should be subject to a modification of up to 40°C. A minimum emplacement temperature for the

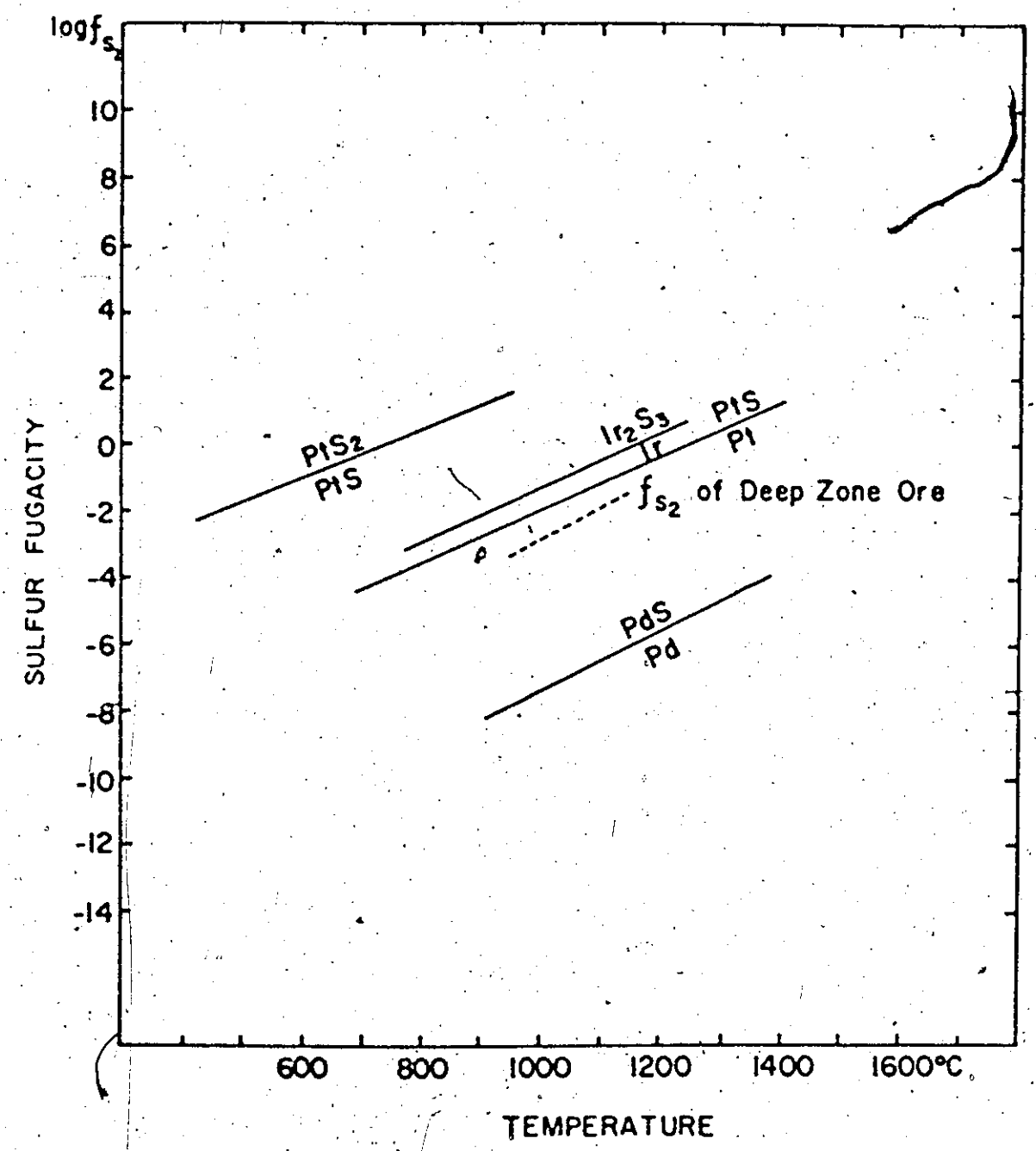

Figure 6-4. Stability of Pd, Ir, and Pt Sulfides as Function of logf_{S_2} and Temperature

deep zone ore is thus put at 1005°C. The trend of sulfur vapor in equilibrium with the deep zone ore is extrapolated 50°C above and below this temperature to allow for uncertainties and variation of copper content in the ore.

The plot indicates that f_{S_2} in equilibrium with the deep zone ore is not in excess of that required to stabilize Pt as PtS and Ir as Ir_2S_3, but can stabilize Pd as PdS.

Gold sulfide is not stable in nature and there is no available thermodynamic information on AuS. Gold may be stabilized in sulfides by bonding with Te which itself is isomorphously substituted for sulfur.

6-2-2-2. Possible Relevance of Se, Te, As, Sb, and Bi to Noble Metal Partitions

Since selenium and tellurium are similar to sulfur, their behaviour in mineral formation processes is determined largely by sulfur (Chizhikov and Shchastlivyi, 1966). The three elements have the same structure of the outer electron shells:

sulfur	$1s^2 2s^2 p^6 3s^2 p^4$
selenium	$1s^2 2s^2 p^6 3s^2 p^6 d^{10} 4s^2 p^4$
tellurium	$1s^2 2s^2 p^6 3s^2 p^6 d^{10} 4s^2 p^6 d^{10} f^{14} 5s^2 p^4$

However, the polarizability will increase with the number of electron shells from sulfur to tellurium. Table 6-3 gives some of their physical properties.

Table 6-3. Physical Properties of the Chalcogens

Element	Radius in Å			Ionization Potential(ev)	Electro-negativity
	Atomic	Ionic	Covalent		
Sulfur	1.04	1.82	1.05	8.75	2.5
Selenium	1.16	1.93	1.14	8.19	2.3
Tellurium	1.33	2.11	1.36	7.19	2.1

In the series sulfur-selenium-tellurium there is a regular increase in the atomic, ionic, and covalent radii and a decrease in ionization potential and electronegativity.

Selenium is isomorphously incorporated in sulfide minerals but unlike sulfur it combines only with heavy elements. Selenium, in general, does not form ore of commercial grade and is recovered as a by-product from many sulfide ores (e.g. Sudbury). When combined with heavy elements, it displays an affinity for the elements Fe-Zn-Co-Ni-Cu-Hg-Bi-Ag-Pb increasing from Fe to Pb according to Sindeeva (1959).

The selenium contents of some sulfide minerals from four copper-nickel sulfide deposits are summarized in table 6-4. It is clear that the geochemical affinities suggested by Sindeeva are followed. In order of increasing Se enrichment, the mineral sequence is pyrrhotite, pentlandite, and chalcopyrite. Hawley (1962) found that among the common Sudbury sulfide minerals chalcopyrite is the best host for Se and that as a general trend, the south range sulfides tend to be higher in selenium content than north range sulfides.

Of the four noble metals, Pt and Ir follow the selenium enrichment trend closely with increasing concentration in pyrrhotite-pentlandite-chalcopyrite. Possible explanations of this correlation are that:

1) Pt and Ir form bonds preferentially with Se relative to S.

2) Pt and Ir may substitute preferentially for Cu (relative to Ni or Fe) while Se bonds more strongly with Cu than does S.

The atomic radii of tellurium, as shown in table 6-3, are much larger than sulfur so that tellurium tends to substitute isomorphously into the sulfide lattice only at high temperature, and of course will exsolve with decreasing temperature.

In copper-nickel sulfide deposits tellurium shows a trend of enrichment in the following mineral sequence (table 6-5): pyrrhotite-chalcopyrite-pentlandite.

Shcherbina (1937) established the following metal series of increasing affinity for tellurium Cu-Pb-Ni-Bi-Hg-Ag-Au. We therefore expect that the phase most enriched in tellurium, pentlandite, should also be enriched in Au. This is observed for the Strathcona data. The enrichment of Au in pentlandite may be due in part to the strong bonding between Au and Te.

Finally, the occurrence of froodite $PdBi_2$, michenerite (Pd, Pt)Te(Bi, Sb) and sperrylite $PtAs_2$ in Sudbury sulfides indicates that the noble metals are strongly correlated with the pnigogen elements. As pointed out by Cabri (1972), in michenerite Pd>Pt, Te>Bi+Sb, and Bi≫Sb. This observation suggests that Pd and Pt correlate with Te, Bi, and Sb in the decreasing order Te>Bi≫Sb, and that Pd has a stronger affinity for these elements than Pt. Pt is strongly correlated with As which is indicated by the occurrence of sperrylite $PtAs_2$.

Table 6-4. Content of Selenium (p. p. m.) in Ore Minerals of Certain Copper-Nickel Sulfide Deposits

Deposit	Pyrrhotite	Chalcopyrite	Pentlandite	Magnetite
Monchegorsk	10-36	20-105	22-24	---
Pechenga	7-89	12-100	12-90	---
Noril'sk	40-82	32-136	35-60	3
Sudbury	12-63	40-97	85	---

After Yushko-Zakharova (1963)

Table 6-5. Content of Tellurium (p. p. m.) in Ore Minerals of Certain Copper-Nickel Sulfide Deposits

Deposit	Pyrrhotite	Chalcopyrite	Pentlandite	Magnetite
Monchegorsk	trace-4 (2)	1-8 (3)	not detected -26(8)	---
Pechenga	trace-34 (5)	trace-15 (8)	trace-50 (11)	---
Noril'sk	10-28 (17)	10-36 (21)	8-60 (33)	trace

After Yushko-Zakharrova (1963)
Average contents of tellurium in minerals are given in parentheses

6-2-3. Metal-ligand Bonding

An important property of the noble metals is their strong tendency to form covalent bonds as reflected in their occurrence as chalcogenides and pnictides. Noble metal oxides, fluorides, and silicates never occur in nature. This tendency is inherent in their electronic configurations which provide increased stability in combination with the 'metalloid' elements (Burns, 1970). In order to understand this behaviour, a brief discussion of molecular orbital theory follows.

6-2-3-1. Molecular Orbitals

The energy levels of the five nd, one (n+1)s, and three p orbitals are very similar. In forming a compound with octahedral coordination the single (n+1)s, three (n+1)p, and two e_g orbitals of a transition metal are vacated and hybridize to form six d^2sp^3 hybrid orbitals which project along the cartesian axes. These orbitals overlap with filled orbitals belonging to six ligands in octahedral coordination to form bonding σ molecular orbitals and six antibonding σ molecular orbitals. The bonding molecular orbitals represent the maximum positive overlap between symmetric wave functions and are more stable than uncombined individual metal and

ligand atomic orbitals. The t_{2g} group orbitals projecting between the ligand atoms may either remain non-bonding or form π-molecular orbitals with the ligand. The energy relations of Fe^{+2} in an octahedral site with six ligands which do not form π bonds are shown in figure 6-5. The molecular orbital has much more of the character of the atomic orbital nearest in energy. The diagram indicates that six σ molecular orbitals have more of the character of ligand orbitals than of metal orbitals. Thus electrons occupying these orbitals will be mainly ligand electrons, but electrons occupying the anti-bonding molecular orbitals will be predominantly metal electrons. Electrons in t_{2g} orbitals will be all metal electrons if there is no π molecular orbitals.

6-2-3-2. Formation of π Bonds

The non-bonding electron pairs of the t_{2g} orbitals of the metal ion in octahedral sites tend to overlap with certain p or d orbitals of the ligands to form π molecular bonds. Formation of π bonds modifies the energy level diagram of figure 6-5. The effect depends on the energy of the ligand π orbitals relative to the metal orbitals and whether the ligand π orbitals are filled or empty.

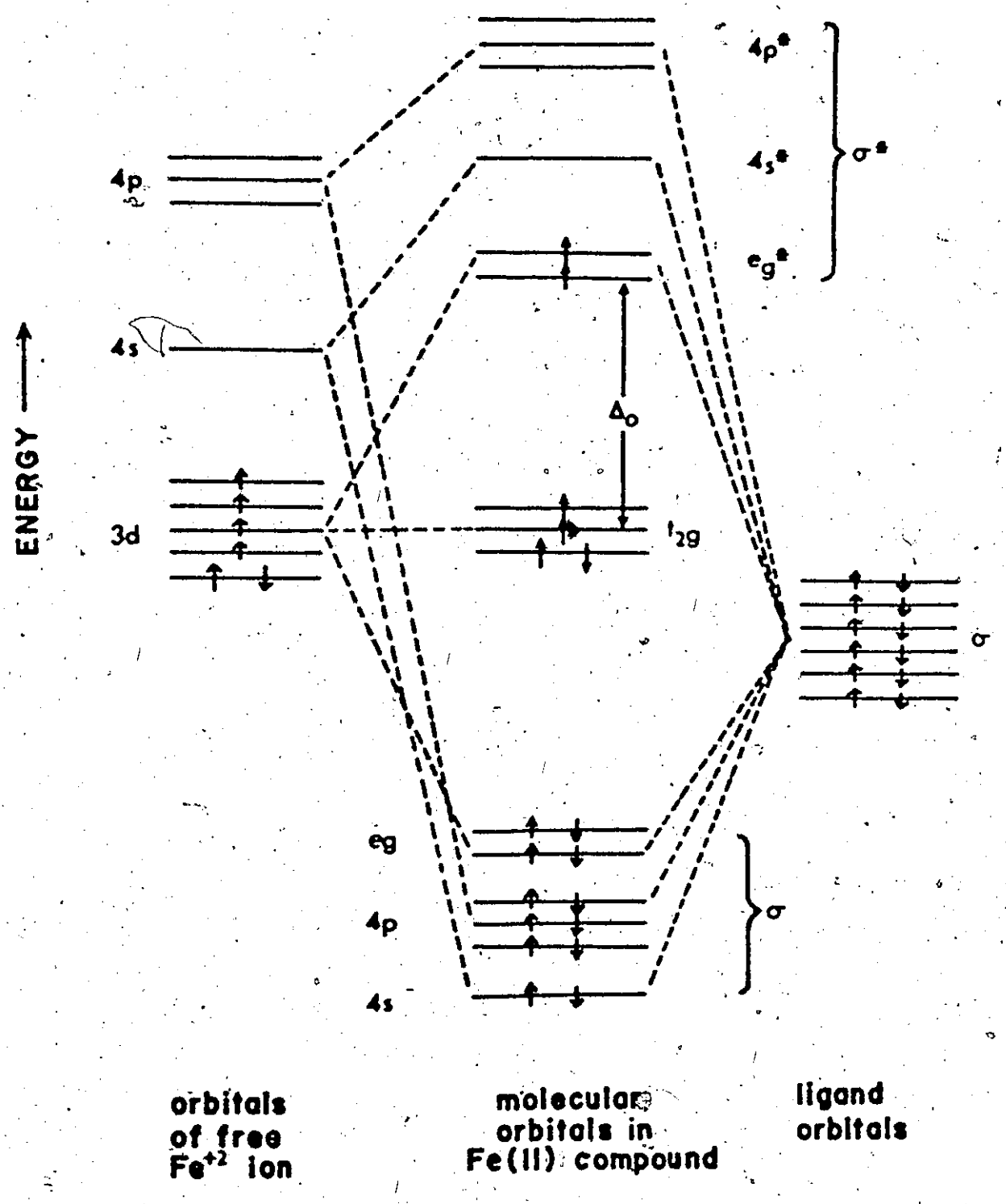

Figure 6-5. Molecular Orbital Energy Level Diagram for the Fe^{+2} Ion in Octahedral Coordination (after Burns, 1970)

The energy separation or split between non-bonding t_{2g} group orbitals and the antibonding e_g group orbitals is called Δ_o in octahedral coordination.

When ligand π orbitals are less stable than the metal t_{2g} orbitals and are unoccupied, electrons in the metal t_{2g} orbitals will overlap with the ligand π orbitals to form π bonds, increase the Δ_o and thus stabilize the metal t_{2g} orbitals. This situation happens when transition metals encounter S, Se, Te, P, As, and Sb. When ligand π orbitals are more stable than the metal t_{2g} orbitals and are filled, the overlapping between the metal t_{2g} orbitals with the ligand π orbitals will decrease Δ_o, unstabilize the metal t_{2g} orbitals, and thus no π bonds can form. This happens when the transition elements encounter O and F.

Bond strength may be increased by the formation of π bonds between the metal t_{2g} electron pairs and vacant π orbitals in acceptor ligands such as S, Se, Te, P, As, and Sb (Burns and Fyfe, 1967). The result is an increase in Δ_o and was illustrated by the data for the +2 state of transition metal sulfides and oxides (George and McClure, 1959). The number of π bonds which can form depends on the number of electron pairs in the t_{2g} non-bonding group available. The iron, nickel, copper, and noble metal species concerned which possess the necessary electronic configuration to form π bonds, are listed in table 6-6.

Table 6-6. Electronic Configuration Necessary to Form π Bonds in an Octahedral Site

Species	Configuration	Number of Bonds
High-spin Fe^{+2} and Co^{+3}	$(t_{2g})^4(e_g)^2$	1
Low-spin Fe^{+2} and Co^{+3}	$(t_{2g})^6$	3
High-spin Co^{+2} and Ni^{+3}	$(t_{2g})^5(e_g)^2$	2
Low-spin Co^{+2} and Ni^{+3}	$(t_{2g})^6(e_g)^{-1}$ ———	3
Ni^{+2}, Pd^{+2}, Pt^{+2}, Au^{+3} and Cu^{+2}	$(t_{2g})^6(e_g)^2$	3
Low-spin Ir^{+3}	$(t_{2g})^6$	3
Low-spin Ir^{+4}	$(t_{2g})^5$	2

This table will provide a guide to the partition of noble metals between high temperature pyrrhotite solid solution and magnetite.

6-2-3-3. The value of Δ

The value of Δ is a reflection of the bond strength between the metal ion and the surrounding ligands.

According to Gray (1965), the value of Δ depends on a number of variables, the most important being the geometry of the complex, the nature of the ligand, the charge on the central metal ion, and the principal quantum number n of the d valence orbitals.

1) Geometry of the Complex

The total splitting decreases as follows:

Square planar	Octahedral	Tetrahedral
$1.3\ \Delta_o$	$1\ \Delta_o$	$0.45\ \Delta_o$

The tetrahedral splitting is smallest because the d orbitals are not involved in strong π bonding.

2) Nature of the Ligand: the Spectrochemical Series

This series represents the ordering of ligands in terms of their ability to split σ antibond and π bond d molecular orbitals. The series correlates reasonably well with the π-bonding ability of the ligand. The good π-acceptor ligands, which are capable of forming strong metal to ligand π bonding, cause large splitting, whereas the good π-donor ligands, which are capable of forming strong ligand to metal π bonding, cause small splitting. Unfortunately such a series is not available for the discussion of chalcogens and pnigogens.

3) Charge on the Central Metal Ion

In complexes containing ligands that are not good π-acceptors, Δ increases with increasing positive charge on the central metal ion. In complexes containing good π-acceptor ligands, an increase in positive charge on the central metal does not seem to be accompanied by a substantial increase in Δ.

4) Principal Quantum Number of the d Valence Orbitals

In an analogous series of complexes, the value of Δ increases with n in the d orbitals by 30% for each series (Cotton and Wilkinson, 1962).

The value of Δ or ligand field stabilization energy (V_s) can be related to total bond energy (V_T) according to Nockolds (1966) by the relation,

$$V_T = V_c + V_I + V_s \tag{18}$$

where V_c is the covalent contribution and V_I is the ionic contribution. Nickel (1970) has shown that the energies of V_c and V_I decrease slightly through the series FeS_2-CoS_2-NiS_2 whereas the values of V_s increases rather sharply in weak field (crystal field) and decrease sharply in strong field (ligand field), therefore, the relative order of bond strengths are dominated by the V_s term.

Due to the fact that Δ increases with n in the d orbitals by 30% for each series whereas V_c and V_I only change slightly, it is anticipated that the dominancy of V_s term to the bond strength is greatly enhanced in case of the noble metals. There is no information on the value of Δ of the second and third transition metal series with pnictide or chalcogenide as ligand, but as the stabilization has the effect of depressing the energies of the t_{2g} d-electron orbitals and thus results in mixing with the ligand orbitals, it is reflected in the degree of π-bonding (Burns and Vaughan, 1970). An example of this from the present data is demonstrated in section 6-3.

6-3. High Temperature Partition

The deep zone sulfide was emplaced at a temperature above 1005°C. The composition of the sulfide melt is that of point P in figure 6-6 and the variation of log f_{S_2} and log f_{O_2} with the composition of the melt is shown in figure 6-7. It has been argued by Naldrett (1969) that once the sulfide-oxide liquid collected as a large pool, the system was closed to both oxygen and sulfur. On considering the crystallization history of the melt, however, the composition P will not reach the pyrrhotite-magnetite cotectic line unless pyrrhotite with higher than 60.6% Fe can be crystallized. The Fe content of the iron-rich hexagonal pyrrhotite is only 60.1%. It is therefore concluded that

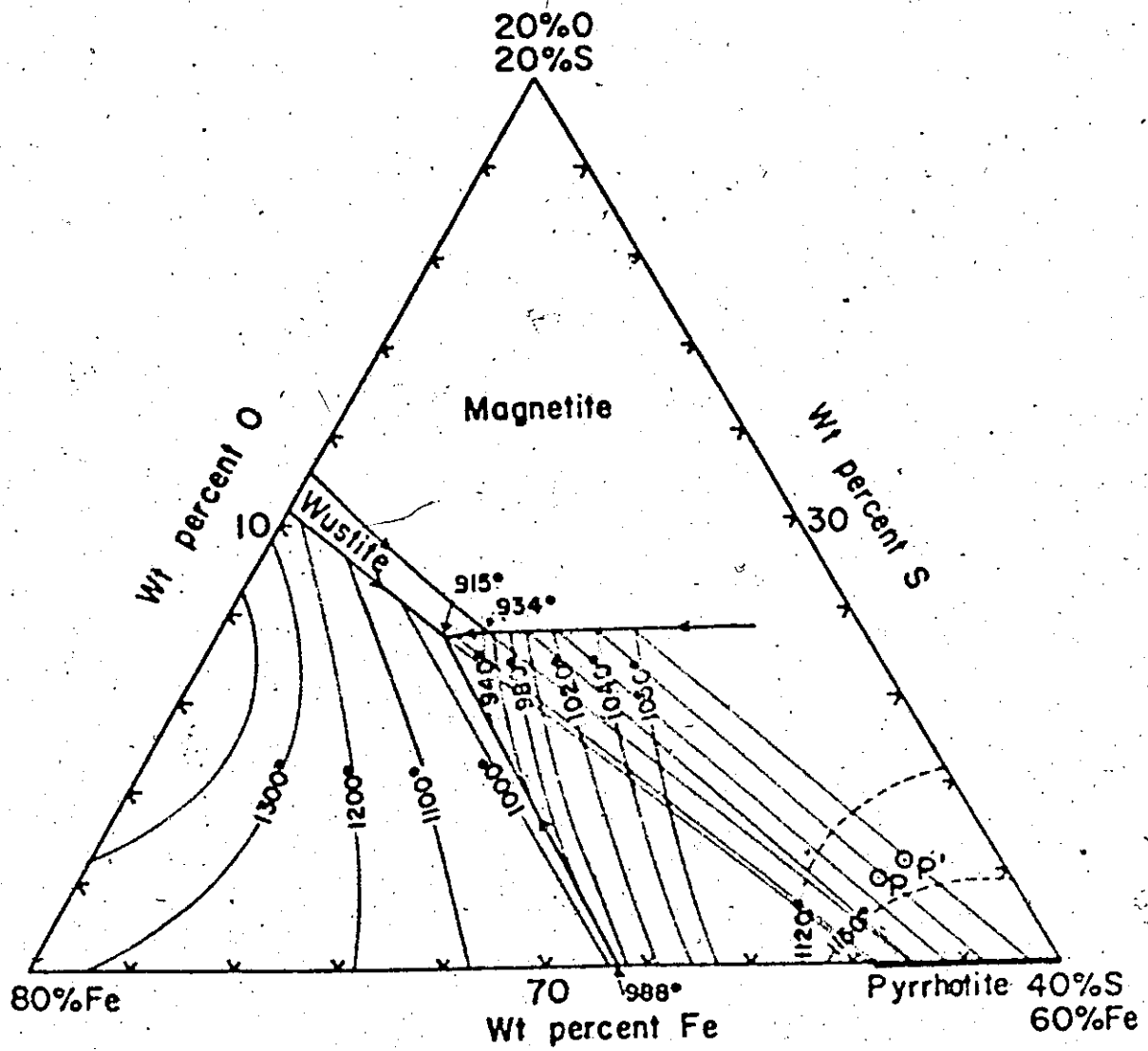

Figure 6-6. Liquidus Relations in a Portion of the Fe-S-O System (after Naldrett, 1969).

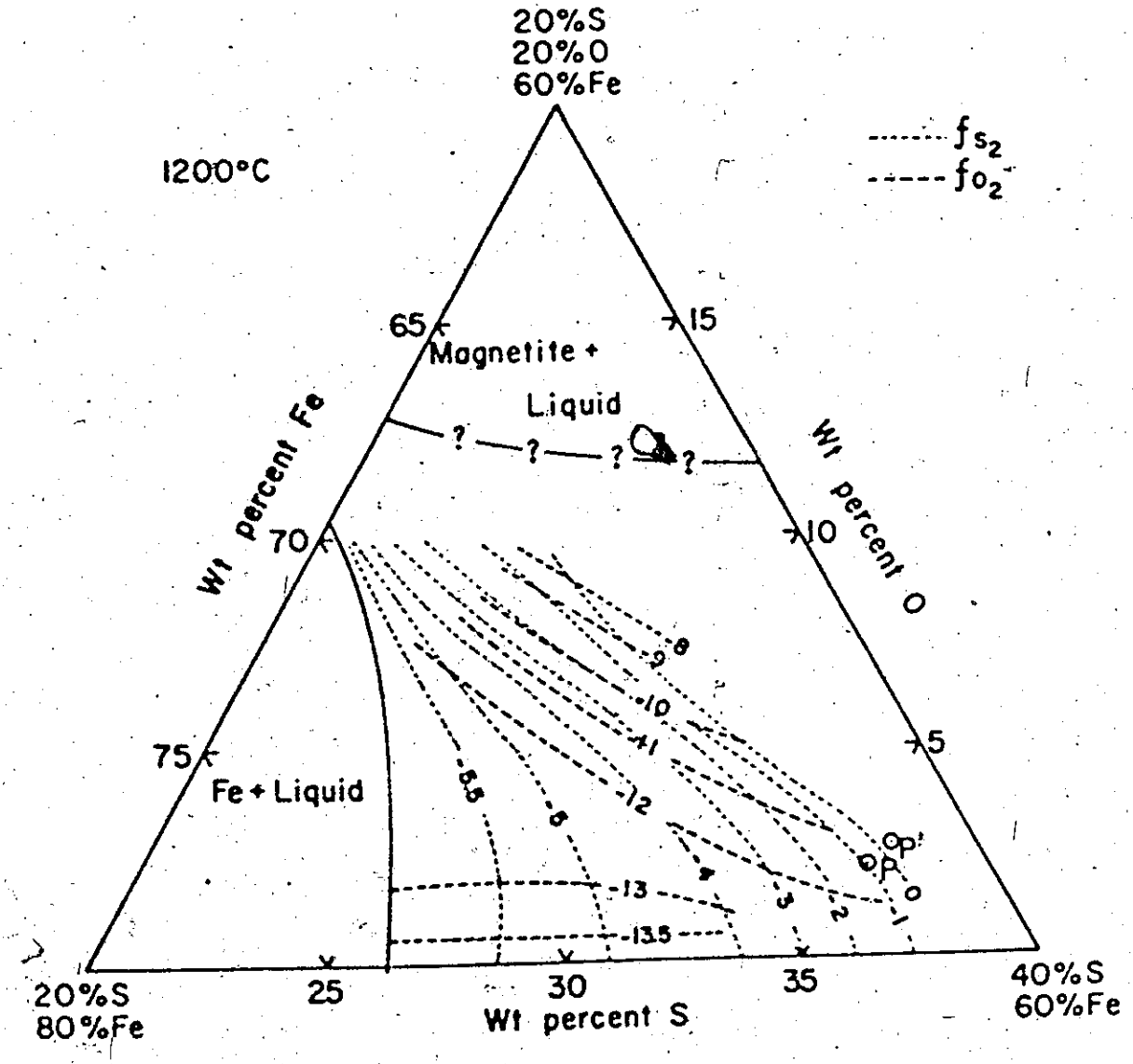

Figure 6-7. Variation in $\log f_{S_2}$ and $\log f_{O_2}$ with Composition of Iron Sulfide-Oxide Liquid at 1200°C (after Naldrett, 1969).

the oxygen and sulfur content of the original melt must be higher than those inferred from the present modal analysis.

Assume a melt with higher oxygen and sulfur content P' is at its liquidus temperature (1140°C). On cooling, pyrrhotite will crystallize and the remaining liquid will become enriched in oxygen until its composition reaches the pyrrhotite-magnetite cotectic line. Magnetite will start to crystallize at this point and the residual liquid will move down the cotectic line towards the ternary peritectic. As the residual liquid moves down the cotectic line and is enriched in iron, it will react with the early formed pyrrhotite causing it also to become enriched in iron. The liquid will have solidified completely when it reaches the point on the cotectic connecting magnetite and point P'.

Therefore, in terms of high temperature process and assuming that the system remained closed to the noble metals, their partition would be between pyrrhotite solid solution and magnetite.

Vaughan et al. (1971) reported the presence of two distinct types of pyrrhotite at Strathcona - monoclinic pyrrhotite (Fe_7S_8) and hexagonal pyrrhotite (Fe_9S_{10}). Monoclinic pyrrhotite is ferrimagnetic between 200° and 205°C. According to phase equilibrium studies of the synthetic pyrrhotite system (Arnold, 1969; Taylor, 1970),

the separation of these phases occurs below 300°C. Above this temperature, according to Ward (1970), a high temperature hexagonal type of continuously variable composition (from FeS to the pyrite solvus) exists in which the iron vacancies are in a state of more or less random disorder, and diffusion of iron vacancies is very rapid. The interlocking texture of monoclinic and hexagonal pyrrhotite as shown in plate 6-1 makes the magnetic separation of these two phases impossible and hence the partition of the noble metal between them was not studied.

Magnetite is octahedral and granular and has a general formula $Fe^{+2}Fe_2^{+3}O_4$. Fe^{+2} is in a tetrahedral site, and Mg, Zn, Mn and less often Ti and Ni may substitute for it. Fe^{+3} is in an octahedral site and Al, Cr, Mn^{+3}, and V may subsitute for it (Mason and Berry, 1968). Hawley (1962) reported the presence of Mn, V, Cr, Ti, Mg, Al, Ni, Co, and Cu in Sudbury magnetite. Among these metals Co and Ag are present only in traces while Ni and Cu may be due to the presence of minute sulfide inclusions.

Diadochic substitution, in which a trace element ion proxies for a major ion in the crystal, is dependent largely upon ionic size and secondly, on electronegativity. Empirically, the substitution is not common between elements whose ionic radii differ

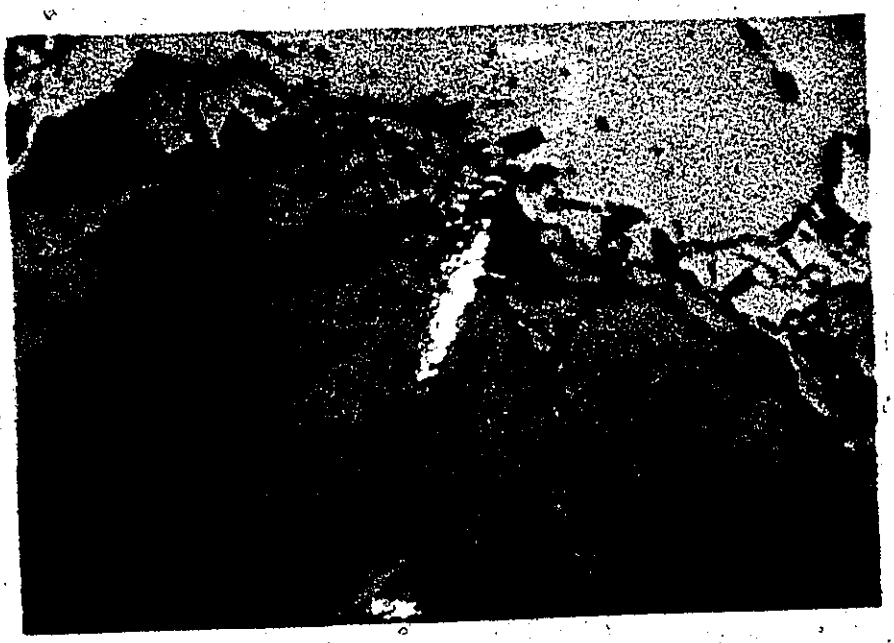

Plate 6-1. The Effect of HI Etch Showing the Interlocking Texture of Monoclinic and Hexagonal pyrrhotite (gray). X52.

by more than 15%. Table 6-7 gives the ionic size and electronegativity of Fe^{+2}, Fe^{+3}, the ions which usually substitute for them, and the pertinent noble metal ions for comparison.

It is possible, from the point of view of ionic radius, that Ir^{+4} replaces Fe^{+3} in six-fold coordination, and that Pd^{+2} replaces Fe^{+2} in four-fold coordination. But from the point of view of electronegativity, we see a trend that all the metal ions (table 6-7) which replace iron in magnetite have electronegativity smaller than iron. This observational trend suggests that the very electronegative noble metals will not be incorporated into the magnetite crystal structure regardless of their suitable ionic sizes.

The Fe-O bond in magnetite has a large ionic component, while the Fe-S bonding in pyrrhotite is predominantly covalent. Table 6-8 gives the character of bonding between anion sulfur and oxygen and cation iron, nickel, copper, and the noble metals computed from the empirical relation (Pauling, 1960)

$$P = 16 (X_A - X_B) + (X_A - X_B)^2 \qquad (19)$$

where P is percentage of ionic character of the bond, and $X_A - X_B$ is the electronegativity difference between ions A and B given by Pauling. Table 6-9 gives the covalent radii of these metals.

Table 6-7. Ionic Size and Electronegativity of Some Pertinent Elements

Ion	Coordination	Ionic Radius Å	Electronegativity (1)
Au^{+}	6	1.37(2)	2.4
Au^{3+}	4 SQ.	0.70(3)	
	6	0.85(2)	
Al^{3+}	6	0.53(3)	1.5
Cr^{3+}	6	0.62(3)	1.6
Fe^{2+}	4	0.63(3)H.S.	1.8
Fe^{3+}	6	0.65(3)H.S.	
Ir^{3+}	6	0.73(3)?	2.2
Ir^{4+}	6	0.63(3)	
Mg^{2+}	4	0.49(3)	1.2
Mn^{3+}	6	0.65(3)H.S.	1.5
Ni^{2+}	4	—	1.8
Pd^{2+}	4 SQ.	0.64(3)	2.2
Pt^{2+}	4	—	2.2
	6	0.80(2)	
V^{3+}	6	0.64(3)	1.6
Zn^{2+}	4	0.53(3)	1.5

(1) Pauling (1960)

(2) Ahrens (1952)

(3) Shannon and Prewitt (1969)

SQ. square planar

H.S. high-spin

Table 6-8. Character of Bonding

Bond Type	$X_A - X_B$	Amount of Ionic Character (%)
Fe-S	0.7	12.9
Ni-S	0.7	12.9
Cu-S	0.6	10.9
Pd-S	0.3	5.1
Ir-S	0.3	5.1
Pt-S	0.3	5.1
Au-S	0.1	1.6
Fe-O	1.7	37.4
Ni-O	1.7	37.4
Cu-O	1.6	34.7
Pd-O	1.3	26.8
Ir-O	1.3	26.8
Pt-O	1.3	26.8
Au-O	1.1	21.8

Table 6-9. Covalent Radii in Å

Tetrahedra

Cu	Au
1.35	1.50

Octahedral

Fe^{+2}	Ni^{+2}	Ni^{+3}	Ir^{+3}	Pd^{+4}	Pt^{+4}	Au^{+4}
1.23	1.39	1.30	1.32	1.31	1.31	1.40

Square Radii

Ni^{+2}	Pd^{+2}	Pt^{+2}	Au^{+3}
1.39	1.31	1.31	1.40

After Evans (1964)

The concept of characteristic covalent radii is subject to a number of qualifications. The first is that the covalent radius of an atom, unlike its ionic radius, cannot be interpreted as implying to a sphere. The covalent radii are suitable for calculation of atomic distances which are joined by covalent bonds. The second is that the bond length depends upon bond number. The bond lengths of Pd-S, Ir-S, Pt-S, and Au-S, if they ever form, are definitely smaller than those predicted from covalent radii because of the possibility of forming two or three π bonds in addition to the σ bonds (table 6-6). The third qualification is that we have to consider resonance not only between covalent bonds of different bond number but also between covalent and ionic bonds. As was previously shown, these metals still have 5-13% ionic character (table 6-8), but usually this effect will result in less than 0.1 Å contraction. The fourth qualification is that the bond length depends also on the state of hybridization although the differences are rather small. Taking into account these qualifications, we can see that the noble metals will not have difficulty in going into the pyrrhotite structure.

The univariant equilibria for the reaction of sulfur vapor with the metal (figure 6-4) indicate that the sulfur fugacity in equilibrium with the present mineral assemblage is not high enough to stabilize Pt and Ir. The observation that Pt and Ir are enriched

in pyrrhotite solid solution with respect to magnetite by factors of 6 and 2 respectively confirms that these two metals are stabilized in pyrrhotite somehow. The explanation is probably twofold: either the sulfur fugacity was much higher at the time of emplacement or the noble metals bond preferentially with Se, Te, or As which are incorporated isomorphously with high efficiency into the pyrrhotite structure.

Two lines of evidence support the first point. Firstly, as discussed in section 5-1-2, the sulfur content to give the present mineral assemblage has to be higher than 37.0% instead of the observed 36.1% which would crystallize bornite at high temperature. Secondly, as just discussed, the original sulfur content in the melt must be higher than the inferred value from the present modal analysis in order to crystallize pyrrhotite with less than 60.6% Fe which is commonly found in the deep zone ore.

It is likely that Pt and Ir bonded more readily with sulfur in the pyrrhotite structure at the higher sulfur fugacity prevailing at high temperature. Preferential bonding with Se, Te, or As isomorphously incorporated in the pyrrhotite structure may also be an important factor in accounting for the observed Pt and Ir concentrations in this mineral. It may be particularly pertinent in the case of Au which forms no stable sulfide.

An element will select that particular crystal structure for which the net cohesion is a maximum. Net cohesion is defined as the difference between the promotion energy of a specific electron configuration needed to combine and the bonding energy released after the combination (Parthé, 1971). As the electronic configuration of the noble metals leads to covalent bonding and a tendency to form a number of π bonds, these metals will go preferentially into the more covalent pyrrhotite crystal structure forming multiple bonds with sulfur, selenium, tellurium or arsenic. The present data indicate that all four noble metals are fractionated rather strongly into pyrrhotite relative to magnetite: Pd by 26, Pt by 6, Au by 5, and Ir by 2. The fractionation ratios of the noble metals between pyrrhotite and magnetite depend on the concentrations of not only sulfur but also selenium, tellurium, and arsenic, and their respective affinity to these anions.

If both Ir and Pt were stabilized as sulfides their usual mineralogic occurrence in nature indicate that Pt prefers +2 state while Ir prefers a +4 state. Table 6-4 shows that Pt^{+2} can form three π bonds while Ir^{+4} forms only two in addition to the six σ bonds. The number of π bond reflects that Pt has a larger Δ than Ir and therefore should enrich in the pyrrhotite phase more strongly than Ir. This prediction is compatible with the present analytical

data where Pt is enriched in pyrrhotite relative to magnetite by a factor of 6 as compared with 2 for Ir. The application of ligand field stabilization energy to predict the partition of the noble metals at high temperatures should be more successful if we have a better knowledge of their stabilization energies and the chemical states in pyrrhotite.

Except for PdTe and IrTe, the noble metal chalcogenides have different crystal structures than pyrrhotite (Hulliger, 1968). At high temperature, however, the iron vacancies in pyrrhotite are in a state of more or less random disorder and diffusion of the vacancies is very rapid. The property that cation vacancies move freely from one interstice to another with a relatively low energy of activation, is likely to absorb the strain induced in the structure by the solution of noble metals, even up to fairly high concentrations. Whether the very large fractionation of Pd into pyrrhotite relative to magnetite is due to the combined effect of bonding with sulfur and the similarity of structure of PdTe and pyrrhotite is presently a matter of speculation.

6-4. Partition in Subsolidus Exsolution

There is less information about the mechanism of the partition of trace elements under subsolidus conditions. The present analytical data strongly indicate that subsolidus processes are very

effective in redistribution of the noble metals. To explain this, we need to understand the interaction of the trace elements with respect to the nucleation, growth, and kinetics of the host phases (Yund and McCallister, 1970). Although the fact that the Strathcona chalcopyrite exsolved from pyrrhotite at 450°C or less and pentlandite at 300°C or less is well established, there is no information about their nucleation, growth, and kinetics. And as a consequence, quantitative evaluation of the noble metal response to these processes is impossible. But from a qualitative point of view, the causes of diffusion are believed to be due to relief of lattice strain, grain boundary diffusion, and transition of spin state.

6-4-1. Relief of Lattice Strain

When pyrrhotite solid solution crystallizes at high temperature, small amounts of Se, Te, and As can dissolve in the pyrrhotite isomorphously. At high temperature pyrrhotite has a disordered lattice in which the rate of vacancy diffusion is high. This property tends to absorb the lattice strain caused by the incorporation of these anions, as well as other cations. But as the temperature lowers, the diffusion rate will decrease according to the general relation

$$D = D_o e^{-\frac{Q}{RT}} \qquad (20)$$

where D is diffusion coefficient, and D_o and Q are constants for fixed temperature T but vary with composition. Condit and Birchenall (1960) found that the iron diffusion coefficient in pyrrhotite between 350° and 697°C increases with increasing iron deficit.

The decrease of the diffusion rate is a reflection of the strengthening of the crystal structure. As the lattice strain caused by the impurities tends to build up, the impurities segregate to grain boundaries because of interaction forces (Lucke and Detert, 1957) and actually diffuse out of the host phase.

The critical strain needed to initiate this type of exsolution may be reached at different temperatures for various elements depending on their respective directional bonding with sulfur or other anions replacing sulfur isomorphously in the structure. An example of how this strain can arise is illustrated in figure 6-8.

Pyrrhotite has a hexagonal lattice at high temperature while PtS is tetragonal. The two lattices are mutually correlative by twisting parallel to the "a" axis. The elongation of the anion octahedron in pyrrhotite is such that the cation is in square-planar coordination while the anion is surrounded by a deformed tetrahedron of four cations which corresponds to the structure of PtS (Jellinek, 1957). Jellinek believed that this type of deformation can be achieved by transition of Fe^{+2} from high- to low-spin state.

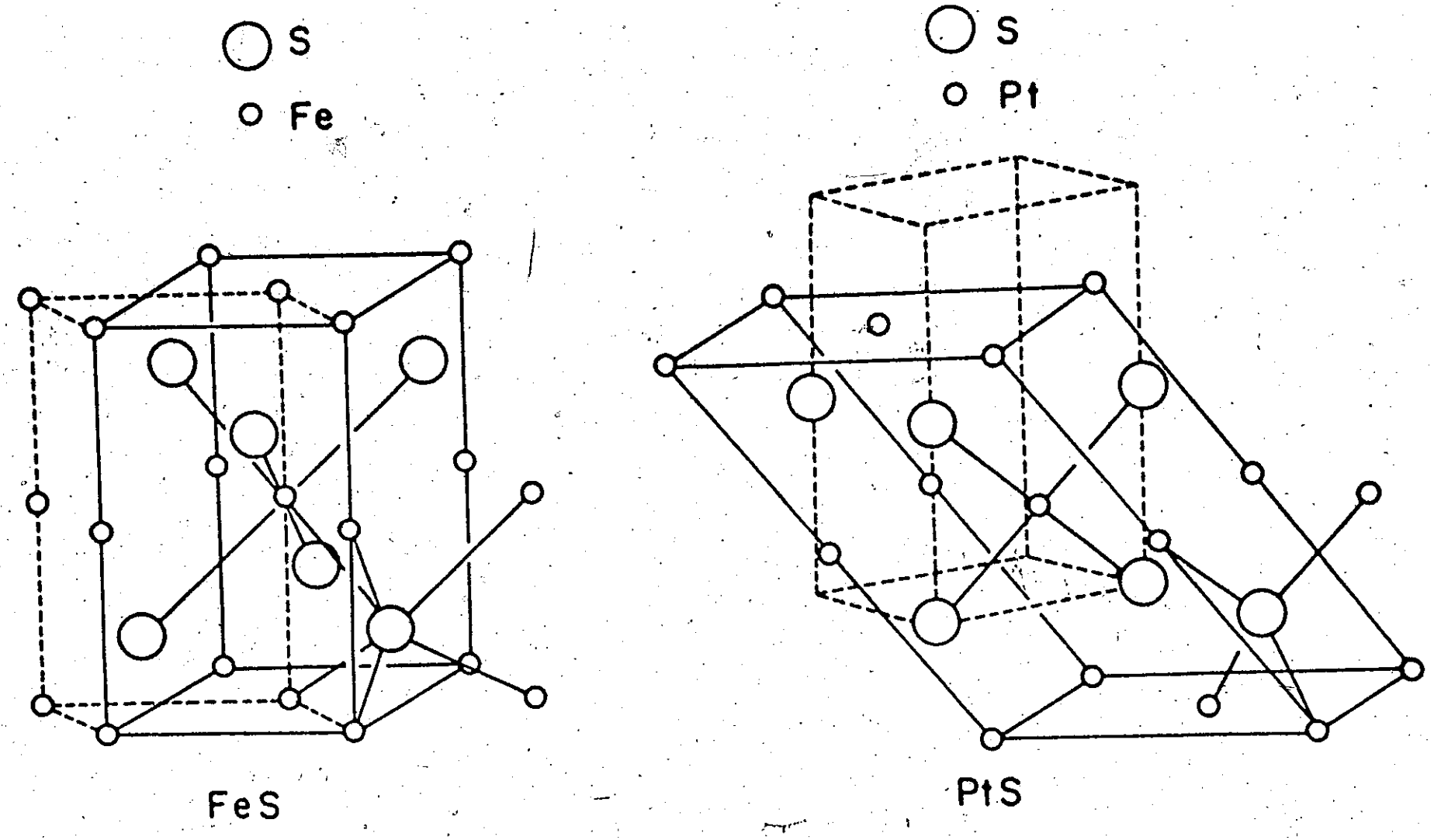

Figure 6-8. Relation between Pyrrhotite and PtS. Crystal Structure (after Jellinek, 1957).

6-4-2. Grain Boundary Diffusion

According to Kubaschewski and Hopkins (1967) diffusion often involves two different mechanisms depending on temperatures. At high temperature the diffusion is dominantly transgranular while at low-temperature it is associated with grain boundary process. The occurrence of pentlandite as rims around pyrrhotite may indicate that the latter mechanism is operative in the exsolution of pentlandite under 300°C. The high concentration of Pd in pentlandite indicates that it is also involved in grain boundary diffusion processes.

6-4-3. Cation Spin-state Transition

Magnetic susceptibility indicates that Fe^{+2} in pyrrhotite is in a high-spin state while Fe^{+2} in pentlandite is at low-spin state. The exsolution of pentlandite from pyrrhotite thus involves a transition of Fe^{+2} from high- to low-spin state. Shannon and Prewitt (1969), gave the ionic radius of Fe^{+2} for high and low-spin states as 0.77Å and 0.61Å respectively. A 20% contraction is thus involved. As pointed out by Jellinek (1957), the transition of Fe^{+2} from high- to low-spin results in the elongation of the anion octahedron in pyrrhotite to such a degree that cations form square-planar coordination. Both Pd^{+2} and Au^{+3} can form electronic configurations of dsp^2 hybridization and thus give square-planar co-

ordination. That is to say, when a phase containing high-spin iron coexists with a phase containing low-spin iron, Pd^{+2} and Au^{+3} tend to go into the phase containing low-spin iron preferentially. The enrichment of these two metals in pentlandite is compatible with this prediction.

6-5. Thermal Effect of Dike Intrusion on Noble Metal Profiles

The concentration profiles of figure 5-5 indicate that the intrusion of a quartz diabase dike disperses Au away from the dike and forms a low in the concentration profile, but at the same time causes no observable effect for Pd and Ir. These effects are probably due to the heat effect of the dike.

Shewmon (1963) noted that when a pure metal containing trace amounts of a solute is annealed in a temperature gradient, the thermal diffusion of the solute up the thermal gradient is opposed by a vacancy concentration gradient down the thermal gradient. In the case of Zn and Fe, the two effects just cancel out and cause no change of the solute concentration while in the case of Au there is a net flux of vacancies from the hotter to the colder region causing the Au concentration to increase in the cooler region. This model is useful for consideration of the present case in that the diffusion medium, essentially pyrrhotite, is a defect structure.

As pyrrhotite contains vacancies which diffuse at high rate at high temperature, it is likely that the intrusion of the diabase dike would reactivate the diffusion of the vacancies in pyrrhotite and cause Au to diffuse down the thermal gradient and thus away from the heat source. The diffusion of Au could be greatly accelerated by a small amount of aqueous fluid derived from both the dike and the hanging-wall breccia.

Pd and Ir are relatively insensitive to the intrusion of the diabase dike. The implication from Shewmon's observations is that these metals resemble Zn and Fe in that the diffusion effects of solute and vacancies have just cancelled out and cause no net concentration change.

6-6. The Origin of the Sulfides

The origin of the Sudbury sulfides has long been a topic of controversy. However, it is clear that the Sudbury ore deposits are always associated with the sub-layer rocks (figure 2-3). Impressed by the intermixed nature of the ore bodies and the sub-layer, Naldrett and Kullerud (1967) thought that they were post-Irruptive injections of magmatic sulfide liquids derived from deep seated ultramafic layers. Dietz (1972), on the other hand, suggested that

they were pre-Irruptive and represented a mixture of sulfides from a shock melted differentiated asteroid and country rocks. These two hypotheses are discussed below on a basis of the noble metal data, particularly the metal profiles across the 2750 cross-cut and a comparison of Sudbury noble metal ratios with those of other rock types and meteorites. Also inferences on the thermal history of the Irruptive are considered in the light of the irreversible lattice expansion of pentlandite.

6-6-1. Concentration Profiles from the 2750 Cross-cut

The concentration profiles shown in figure 5-5 reveal that the variation of Au and Pd within each lithologic group intersected by the 2750 cross-cut is very large. A statistical F test explicitly indicates that none of these groups have average Au or Pd values which are significantly different. Ir, on the other hand, does pass the F test and has significantly different average values for each group: 8.6 p.p.b. for mafic norite; 26.4 p.p.b. for mafic sub-layer and 13.0 p.p.b. for leucocratic sub-layer. The large variations of Au and Pd are due, in part, to subsolidus redistribution as indicated by their strong enrichment in pentlandite, and, in the case of Au, thermally induced migration resulting from intrusion of young diabase dikes.

As Ir has significantly different average values for each lithologic group, and as there is no evidence for redistribution of Ir by subsolidus or other process, it is suggested that these differences are due to different average Ir contents of three different intrusions (mafic norite, mafic sub-layer, and leucocratic sub-layer) as suggested by Greenman and Hewins. The first intrusion was the Irruptive proper whose initially crystallised sulfides, represented by the pyrrhotite of the border member of the mafic norite*, have an average Ir content of 8.6 p.p.b. The second was the main zone sulfides associated with mafic sub-layer with an average Ir content of 26.4 p.p.b., and the third and the last intrusion was the deep zone sulfides associated with leucocratic sub-layer or gray breccia with an average Ir content of 13.0 p.p.b.

---

* According to Hewins (1971), the mafic norite has two members — poikilitic and hypidiomorphic mafic norite. The former is a border member and the latter represents gravitational accumulate. In the section across the 2750 level, the border group is 360 feet thick and only the top 30 feet is hypidiomorphic. All of the analyzed samples were collected from the poikilitic mafic norite.

Greenland (1970) observed that in the differentiated Great Lake Dolerite (Tasmania) Ir decreased systematically from early mafic dolerite (0.25 p.p.b.) to late granophyre (0.006 p.p.b.). If this trend is generally applicable to differentiated, layered gabbroic rocks, a possible explanation of the different Ir values is that they are inherited from a differentiated layered sequence at depth with the earliest or mafic sub-layer being derived from earliest sulfides highest in Ir content.

6-6-2. Implications of Metal Ratios with Special Reference to the Cosmogenic Ore Hypothesis

Assuming that the type I carbonaceous chondrites represent the most primitive material of our solar system (Mason, 1960; Fish et al., 1960; Ringwood, 1961, 1962) and that the earth was formed by accretion and fractionation of this type of material, the fractionation of noble metals in terrestrial rocks and ores can be interpreted by comparing with metal ratios in meteorites. In the primary fractionation of the earth to form the core the noble metals were in a reduced state and largely concentrated as a group in this metallic Fe-Ni core. In the process of forming the crust, two major types of magma are involved including an extremely widespread primordial

basaltic magma and a secondary granitic magma restricted to areas of orogenesis and extensive metamorphism. It is therefore pertinent to compare noble metal ratios of the various lithologic groups of Strathcona with meteorites, taken as the best available representatives of primitive unfractionated material on the one hand and average basic rocks on the other. As Dietz suggested, the Sudbury sulfides could be derived from a differentiated asteroid containing both chalcophyllic phases supplying Cu and S, and a siderophyllic phase supplying the noble metals. It is also interesting to consider whether the Strathcona noble metal ratios are compatible with such a hypothesis. The relevant data are presented in table 6-10.

Table 6-10. Comparison of Noble Metal Ratios for Strathcona Sulfides, Basaltic Rocks and Meteorites

Rock Unit	Ir	Pd	Au	Reference
Mafic Norite	1	4.88	0.320	This work
Mafic Sub-layer	1	4.03	0.124	" "
Leucocratic Sub-layer	1	4.98	0.702	" "
Ultramafics	1	3.29	0.458	Crocket & Chyi (1972)
Basic and Intermediate Rocks	1	15	7	Crocket et al. (1972)
Carbonaceous Chondrites	1	1.03	0.288	" " "
Iron Meteorites	1	1.12	0.325	" " "

It is clear from the table that the average sub-layer noble metal ratios are very similar to those of mafic norite which is considered to be of magmatic origin. The mafic norite and the sub-layer noble metal ratios are much more similar to ultramafics than to carbonaceous chondrites or iron meteorites. If the noble metals must be derived from the siderophyllic phase of a differentiated meteorite, then there must have been a process causing an enrichment of Pd. Volatilization is the most likely process to have changed metal ratios relative to parental material immediately after impact. However, the boiling points of Pd, Ir, and Au, which are 3980°C, 5300°C, and 2970°C, respectively, suggest that differential loss of the metals should increase in the series Au>Pd>Ir. Therefore, one expects Au/Ir and Pd/Ir ratios smaller than in the meteorites, with the effect being larger for the Au/Ir ratio. Obviously, the data do not fit this model. The observed trend indicates that volatilization cannot be responsible for Pd enrichment with respect to Ir in the Strathcona sublayer sulfides.

As required by Dietz's hypothesis of meteoritic parenthood, the distribution of the sub-layer components should reflect inertial or density differences in a gravitational field. Therefore, the material should be arranged with increasing density away from the center of the Sudbury basin with the heaviest material closest to

the footwall. As the concentration effect is proportional to mass we expect that the effect would be larger and nearly equal for Au and Ir and smaller for Pd. The concentration gradients of the three metals are shown in table 6-11 where the concentration of each metal is normalized to the value in mafic norite and where atomic weights are taken relative to Pd. The average concentration for each lithologic unit is computed from the data in table 5-8.

Table 6-11. Concentration gradients of Pd, Ir, and Au in Mafic Norite and the Sub-layer Units

Element	Atomic Wt. Ratio	Mafic Norite	Mafic Sub-layer	Leucocratic Sub-layer
Increasing atomic wt. ↓ Pd	1.00	1.00	0.827	1.55
Ir	1.80	1.00	3.07	1.51
Au	1.91	1.00	1.11	3.37
		Towards the Footwall →		

Firstly, the table shows clearly that only Au increases in concentration towards the footwall. Pd shows a reverse trend in mafic sub-layer while Ir shows a large reverse trend in leucocratic sub-layer.

Secondly, if the concentration effect is proportional to mass, the relative increase in concentration of Au and Ir toward the footwall should be greater than that of Pd which is obviously not the case.

Thus, there do not appear to be any aspects of noble metal ratios for Strathcona sublayer rocks which support the hypothesis of meteoritic hypervelocity emplacement of sulfides derived directly from siderophyllic phases of the meteorite as a feasible model for distribution of the noble metals.

6-6-3. Pentlandite Irreversible Expansion

A very interesting experiment performed by Knop et al. (1965) on the thermal expansion of the pentlandite lattice has significant implications on the thermal history of the sub-layer ores. Knop et al. demonstrated that natural pentlandite when heated will undergo an irreversible lattice expansion of 0.5% at temperatures between 150° and 200°C from 10.043Å to 10.100Å. The expansion of the cell parameter is due to migration of iron from octahedral to tetrahedral sites in pentlandite (Knop et al., 1970) and cannot be prevented by pressures of up to 2 Kb. It was also shown by Knop et al. (1965) that no trace elements incorporated in the pentlandite structure will decrease the cell parameter.

All Sudbury pentlandite analyzed by Naldrett (1961) have cell parameters between 10.036 and 10.054 Å. It is therefore concluded that this low parameter must mean that Sudbury pentlandite was never exposed to temperatures in excess of 150°C so that its exsolution from pyrrhotite probably occurred below this temperature.

Based on this argument, we can see that redistribution of the noble metals must be accomplished by low temperature diffusion or hydrothermal solutions but not remobilization. Furthermore, this argument supports the hypothesis that the copper-nickel sulfides of the sub-layer ores were emplaced after the Irruptive for the thick Irruptive would undoubtedly heat the several hundred feet of underlying sub-layer up to a very high temperature.

6-7. Economic Aspects

The noble metals are recovered as by-products from the smelting of copper-nickel floatation concentrates obtained from the Sudbury ores. This research suggests that the Pt/Pd ratio should closely follow the Cu/Ni ratio if the Pd enrichment in pentlandite and Pt enrichment in chalcopyrite apply to the mine as a whole.

Almost all copper is obtained from chalcopyrite and the bulk of the nickel from pentlandite. Equal amounts of chalcopyrite and pentlandite produce approximately equal amounts of copper and nickel. Taking this approximation and calculating according to the relation

$$\frac{W_{cpy} C_{Pt}^{cpy} + W_{pn} C_{pt}^{pn}}{W_{cpy} + W_{pn}} \sim C_{Pt}^{Cu-Ni} \qquad (21)$$

we have that the concentration of Pt in copper-nickel concentrate C_{Pt}^{Cu-Ni} approximately equals the weight of chalcopyrite W_{cpy} times concentration of Pt in chalcopyrite C_{pt}^{cpy} plus weight of pentlandite W_{pn} times concentration of Pt in pentlandite C_{pt}^{pn}. Based on the data of table 5-4, the average Pt concentration in chalcopyrite (deleting the 18600 p.p.b. sample as it cannot represent an overall average) and pentlandite are computed as 2180 p.p.b. and 880 p.p.b. respectively, and average Pd concentrations in pentlandite and chalcopyrite are computed as 2070 p.p.b. and 360 p.p.b. respectively.

Taking the Cu/Ni weight ratio as 1:1 and using equation (21), the Pt concentration in copper-nickel concentrate can be calculated as,

$$\frac{1 \times 2180 + 1 \times 880}{1+1} = \frac{3060}{2} = 1530 \text{ p.p.b.}$$

Pd concentations and Pt concentrations for other Cu/Ni ratios can similarly be calculated and the results are presented in table 6-12.

Table 6-12. Pt and Pd concentrations in Cu-Ni concentrate predicted from Cu/Ni Ratios (p.p.b.)

Cu/Ni	Pd	Pt	Pt/Pd
1/3	1640	1200	0.73
1/2	1500	1310	0.87
1/1	1210	1530	1.26
2/1	930	1850	1.88
3/1	790	1850	2.34

According to Hawley (1962) production from all of the Sudbury ores, averaged over from 1947-1957 gives 46% Pt, 41% Pd, and 13% combined Rh, Ru, and Ir. This corresponds to a Pt/Pd ratio of 1.12. The Cu/Ni ratio for the same period was estimated at 0.926. The present analyses, if assumed to represent overall average Sudbury ore, would give a Pt/Pd ratio of 1.18 for a Cu/Ni ratio of 0.926. This close agreement with actual production data indicates that the suggestion that the Pt/Pd ratio should closely follow the Cu/Ni ratio in a copper-nickel concentrate is, in general, valid.

CHAPTER 7

CONCLUSIONS

Pd, Ir, Pt, and Au are present in copper-nickel sulfides in very small quantities and do not form primary crystalline phases in the Strathcona mine. They may occur in solid solution, as inclusions or adsorbed films.

To prove that the noble metals are in solid solution in the principal mineral phases - pyrrhotite, magnetite, chalcopyrite, and pentlandite - their partition between coexisting phases was tested to determine if Henry's dilute solution Law was obeyed or if the observed partitions could be explained by induced vacancies due to altervalent substitution or interstitial-substitution. Although conclusions are tentative and need to be substantiated by further analytical data, the present data suggests that solid solution in host sulfides accounts for the dominant mode of occurrence of these trace metals in the Strathcona ores.

Sulfur fugacity in equilibrium with the ore which is inferred from the present mineral modal analysis, and the thermo-

dynamic data of some Pd, Pt, and Ir sulfides were used to evaluate whether the sulfides were stabilized by the prevailing sulfur fugacity. The computation indicated that Pd could be stabilized as sulfide but Pt and Ir could only be stabilized as sulfide if the sulfur fugacity were somewhat higher than the present inferred value.

The geochemical affinities of the noble metals for Se, Te, As, Sb, and Bi and the Sudbury platinoid mineralogy were considered to aid in a qualitative interpretation of noble metal partition. Pt and Ir follow the selenium enrichment trend closely with increasing concentration in the order pyrrhotite-pentlandite-chalcopyrite. Because of the strong bonding between Au and Te, pentlandite shows enrichment in both Te and Au. The platinoid mineralogy of Sudbury suggests that 1) Pd and Pt correlate with Te, Bi, and Sb in the decreasing order Te > Bi ≫ Sb and that Pd has a stronger affinity for these elements than Pt, and 2) Pt strongly correlates with As.

Molecular orbital theory indicates that strong multiple σ and π bonds can form between noble metal cations and chalcogen or pnigogen anions. This explains why these metals are enriched in chalcogenides and pnictides. In an ideal case, the order of enrichment can be related to the total number of σ and π bonds when their bonding character is of the same covalency.

At high temperature, the noble metals fractionate rather strongly into pyrrhotite solid solution relative to magnetite: Pd by 26, Pt by 6, Au by 5, and Ir by 2. Upon cooling below liquidus temperatures the geochemical history of the noble metals appears to be closely related to phase transformations and other processes affecting pyrrhotite. In particular, some chalcopyrite and all pentlandite exsolve from pyrrhotite solid solution at temperatures below 450° and 300°C respectively. Because of the strong preference of Pt for chalcopyrite and Pd and Au for pentlandite, it is concluded that these metals diffuse from pyrrhotite at temperatures similar to those at which Ni and Cu exsolved. Grain boundary diffusion processes which would prevail at these low temperatures are probably dominant. The enrichment of Pd and Au in pentlandite is also probably related to the transition of ferrous iron from a high-spin to a low-spin state. There can be little doubt that the present noble metal partitions between sulfides were established by diffusion at relatively low temperatures, probably in the range 450° to 150°C.

Concentration profiles for Pd, Ir and Au taken along the 2750 cross-cut included the border group of the Irruptive (mafic norite), the mafic sub-layer including part of the main zone ore, and leucocratic sub-layer. Pd and Au are highly variable and their average values

for the three major units are not statistically different. Some secondary migration of Au due to intrusion of diabase dikes is also evident. The concentration profile of Ir gave averages for the three major units which were statistically different suggesting that the Irruptive proper, the main zone ore, and the deep zone ore represent three different intrusions. This conclusion is supported by the nickel zoning and distribution of hexagonal and monoclinic pyrrhotite.

The noble metal data from 2750 cross-cut do not support a cosmogenic origin of the Sudbury copper-nickel sulfides for two reasons: 1) the noble metals are not arranged in a density sequence away from the center of the Irruptive as required by the meteorite impact hypothesis, 2) the noble metal ratios of the sub-layer sulfides do not indicate that the noble metals were derived from the siderophyllic phase of a differentiated meteorite directly. It is also noted that the irreversible expansion of pentlandite cell parameter indicates that the sub-layer must be post-Irruptive.

The noble metals in Sudbury are recovered as by-products from copper-nickel flotation concentrate smelting. The present research suggests that the Pt/Pd ratios should closely follow the Cu/Ni ratio due to the fact that Pd and Pt are enriched in pentlandite and chalcopyrite respectively.

REFERENCES CITED

ARNOLD, R.G. (1969): Pyrrhotite Phase Relations below 304±6°C at < 1 atm. Total Pressure, Econ. Geol., 64, pp. 405-419.

BATEMAN, A.M. (1917): Magmatic Ore Deposits, Sudbury, Ontario, Ecgn. Geol., 12, pp. 391-426.

BELL, R. (1891): On the Sudbury Mining District, Rept. Geol. Surv. Can., 5, Pt. F.

BETHKE, P.M. and BARTON, P.B. Jr. (1971): Distribution of Some Minor Elements between Coexisting Sulfide Minerals, Econ. Geol., 66, pp. 140-163.

BOUMA, A.H. (1962): Sedimentology of Some Flysch Deposits, A Graphic Approach to Facies Interpretation, Elsevier, Amsterdam, 168 p.

BUNCH, T.E. (1968): Some Characteristics of Selected Minerals from Craters, in French, B.M. and Short, N. (eds.), Shock Metamorphism of Natural Materials, Mono Book Corp., Baltimore, pp. 413-432.

BURNS, R.G. and FYFE, W.S. (1967): Crystal-Field Theory and the Geochemistry of Transition Elements, in Researches in Geochemistry, vol. II, John Wiley and Sons, New York, pp. 259-285.

_____ (1970): Mineralogical Applications of Crystal Field Theory, Cambridge University Press, 224 p.

_____ and VAUGHAN, D.J. (1970): Interpretation of the Reflectivity Behaviour of Minerals, Am. Mineral., 55, pp. 1576-1586.

CABRI, L.J. (1972): The Mineralogy of the Platinum Group Metals, Journal of Minerals, Science and Engineering (in press).

CARD, K.D. and HUTCHINSON, R.W. (1972): The Sudbury Structure: Its Regional Geological Settings, in Guy-Bray, J.V. (ed.), New Developments in Sudbury Geology, The Geol. Assoc. of Can. Special Paper 10, pp. 67-91.

CHIZHIKOV, D.M. and SHCHASTLIVYI, V.P. (1966): Tellurium and Tellurides, English Ed., Collet's, London and Wellingborough, 297 p.

_____ and _____ (1968): Selenium and Selenides, English Ed., Collet's, London and Wellingborough, 403 p.

CHYI, L.L. (1968): The Geochemistry of Precious-Metals in the Mt. Albert Ultramafic Pluton, Quebec, Unpub. Master's Thesis, McMaster University.

COLEMAN, A. P. (1905): The Sudbury Nickel Field, Ontario Bur. Mines Ann. Rept., 14, Pt. 3.

_____ (1913): The Nickel Industry, Dept. of Mines, Can., 170.

COLLINS, W. H., MOORE, E. S. and WALKER, T. L. (1929): The Sudbury Nickel Intrusive, Univ. of Toronto Stud. Geol. Ser. 28, pp. 1-54.

_____ (1934): Life History of the Sudbury Nickel Irruptive (I), Roy. Soc. Can. Trans., 28, pp. 123-177.

_____ (1935): Life History of the Sudbury Nickel Irruptive (II), Roy. Soc. Can. Trans., 29, pp. 27-47.

_____ (1936): Life History of the Sudbury Nickel Irruptive (III), Roy. Soc. Can. Trans., 30, pp. 29-53.

_____ (1937): Life History of the Sudbury Nickel Irruptive (IV), Roy. Soc. Can. Trans., 31, pp. 15-43.

COTTON, F. A. and WILKINSON, G. (1962): Advanced Inorganic Chemistry, Interscience Pub. 959 p.

COVELL, D. F. (1959): Determination of γ-ray Abundance Directly from the Total Absorption Peak, Anal. Chem. 31, pp. 1785-1790.

COWAN, J. C. (1968): Geology of the Strathcona Ore Deposit, Sudbury District, Ontario, Can. Min. Metall. Bull., 61, pp. 38-54.

CRAIG, J.R., NALDRETT, A.J., and KULLERUD, G. (1967): Succession of Mineral Assemblages in Pyrrhotite-rich Ni-Cu Ores, Carnegie Geophys. Lab., Ann. Rept. 1966-67, pp. 431-434.

CROCKET, J.H., KEAYS, R.R., and HSIEH, S.S. (1968): Determination of Some Precious Metals by Neutron Activation Analysis, J. Radioanal. Chem., 1, pp. 487-507.

_____ (1969): Platinum Metals, in Wedepohl, K. (ed.), Geochemistry II-1, Chap. 78, Springer-Verlag, Berlin.

_____ (1970): Neutron Activation Analysis for Noble Metals in Geochemistry, in Brunfelt, A.O. and Steinnes, E. (eds.), Proc. N.A.T.O. Advanced Study Institute-Activation Analysis in Geochemistry and Cosmochemistry, Kjeller, Norway, pp. 339-351.

_____ and CHYI, L.L. (1972): Abundances of Pd, Ir, Os and Au in an Alpine Ultramafic Pluton, Proc. Sec. 10 (Geochemistry), 24th Internat. Geol. Congr., 1972 (in press).

_____, MacDOUGALL, J.D. and HARRISS, R.C. (1972): Gold, Palladium and Iridium in Marine Sediments (in preparation).

DICKSON, C.W. (1904): The Ore Deposits of Sudbury, Trans. Am. Inst. Min. Eng. 34, pp. 1-67.

DIETZ, R.S. (1964): Sudbury Structure as an Astrobleme, Jour. Geol. 72, pp. 412-434.

_____ (1972): Sudbury Astrobleme, Splash Emplaced Sub-layer and Possible Cosmogenic Ores, in Guy-Bray, J.V. (ed.), New Developments in Sudbury Geology, The Geol. Assoc. of Can. Special Paper 10, pp. 29-40.

DIXON, W.J. and MASSEY, F.J. Jr. (1957): Introduction to Statistical Analysis, McGraw-Hill, 2nd Ed., New York, 488 p.

EVANS, R.C. (1964): An Introduction to Crystal Chemistry, Cambridge University Press, 2nd Ed., 410 p.

FAIRBAIRN, H.W., HURLEY, P.M., and PINSON, W.H. Jr. (1960): Mineral and Rock Ages at Sudbury-Blind River, Ontario, Geol. Assoc. Can. Proc., 12, pp. 41-46.

_____, _____ and _____ (1965): Re-examination of Rb-Sr Whole Rock Ages at Sudbury, Ontario, Geol. Assoc. Can. Proc., 16, pp. 95-101.

FRENCH, B.M. (1967): Sudbury Structure, Ontario. Some Petrographic Evidence for an Origin by Meteorite Impact, Goddard Space Flight Centre, Maryland, Publication X-641-67-67, pp. 1-56.

FRENCH, B.M. (1968): Sudbury Structure, Ontario. Some Petrographic Evidence for an Origin by Meteorite Impact, in French, B.M. and Short, N. (eds.), Shock Metamorphism of Natural Materials, Mono Book Corp., Baltimore, pp. 383-412.

FULLIGAR, P.D., BOTTINO, M.L., and FRENCH, B.M. (1971): Rb-Sr Study of Shock-metamorphosed Inclusions from the Onaping Formation, Sudbury, Ontario, Can. J. Earth Sci., 8, pp. 435-443.

GEORGE, P. and McCLURE, D.S. (1959): The Effect of Inner Orbital Splitting on the Thermodynamic Properties of Transition Metal Compounds and Coordination Complexes, Progr. Inorg. Chem. I, pp. 382-463.

GIBBINS, W. and McNUTT, R.H. (1972): Rubidium-Strontium Studies on the Sudbury Irruptive (personal communication).

GRAHAM, A.R., RUCHAN, R. and LEE, C.R. (1964): Millerite at Strathcona Mine, Sudbury District, Can. Mineralogist 8, p. 135.

GRAY, H.B. (1965): Electrons and Chemical Bonding, W.A. Benjamin Inc., New York, 223 p.

GREENMAN, L. (1970): Petrology of the Footwall Breccias in the Vicinity of the Strathcona Mine, Levack, Ontario, Unpub. Ph.D. Thesis, University of Toronto.

GRIFFITHS, J.C. (1967): Scientific Method in Analysis of Sediments, McGraw-Hill, New York and London, 508 p.

GUY-BRAY, J. and GEOLOGICAL STAFF (1966): Shatter Cones at Sudbury, J. of Geol., 74, pp. 243-245.

HAWLEY, J.E. and BERRY, L.G. (1958): Michenerite and Froodite, Palladium Bismuthide Minerals, Can. Mineralogist 6, pp. 200-209.

_____ (1962): The Sudbury Ores, Their Mineralogy and Origin, Can. Mineralogist, 7, Pt. 1, 207 p.

HEWINS, R.H. (1971): The Petrology of Some Marginal Rocks along the North Range of the Sudbury Irruptive, Unpub. Ph.D. Thesis, University of Toronto.

HOWE, E. (1914): Petrographic Notes on the Sudbury Nickel Deposits, Econ. Geol., 9, pp. 505-522.

HSIEH, S.S. (1967): Analysis of Ruthenium and Osmium Abundances in Sulfide Minerals from the Sudbury Ores, Ontario, Unpub. Master's thesis, McMaster University.

HULLIGAR, H. (1968): Crystal Chemistry of the Chalcogenides and Pnictides of the Transition Elements, Structure and Bonding, 4, pp. 83-229.

JELLINEK, F. (1957): The Structure of the Chromium Sulphides, Acta Cryst., 10, pp. 620-628.

KEAYS, R.R. (1968): A Neutron Activation Analysis Technique for Determination of the Precious Metals and its Application to a Study of their Geochemistry, Unpub. Ph. D. Thesis, McMaster University.

_____ and CROCKET, J.H. (1970): A Study of Precious Metals in the Sudbury Nickel Irruptive Ores, Econ. Geol., 65, pp. 438-450.

KNIGHT, C.W. (1917): Report of the Royal Ontario Nickel Commission, Toronto, pp. 105-211.

_____ (1923): The Chemical Composition of the Norite-Micropegmatite, Sudbury, Ontario, Econ. Geol., 18, pp. 592-594.

KRETZ, R. (1961): Some Application of Thermodynamics to Coexisting Minerals of Variable Composition, Examples: Orthopyroxene-Clinopyroxene and Orthopyroxene-Garnet, J. Geol., 69, pp. 361-387.

KROGER, F.A. (1964): The Chemistry of Imperfect Crystals, North Holland Pub. Co., Amsterdam.

KUBASCHEWSKI, O. and HOPKINS, B.E. (1967): Oxidation of Metals and Alloys, 2nd Ed., Butterworths, London, 319 p.

_____, EVANS, E.L. and ALCOCK, C.B. (1967): Metallurgical Thermochemistry, 4th ed., Pergamon Press, New York and London, 495 p.

MASON, B. and BERRY, L.G. (1968): Elements of Mineralogy, W.H. Freeman and Co., San Francisco and London, 550 p.

McDONALD, J.E. and COBBLE, J.W. (1962): The Heats of Combustion of ReS_2 and Re_2S_7 and the Thermodynamic Functions of Transition Metal Sulfides, J. Phys. Chem., 66, pp. 791-794.

McINTIRE, W.L. (1958): A Thermodynamic Treatment of Trace Element Distribution in Geologic Systems with Application to Geologic Thermometry, Unpub. Ph.D. Thesis, M.I.T.

_____ (1963): Trace Element Partition Coefficients - A Review of Theory and Application to Geology, Geochim. Cosmochim. Acta, 27, pp. 1209-1264.

MERTIE, J.B. Jr. (1969): Economic Geology of the Platinum Metals, U.S. Geol. Surv. Prof. Paper 630, 120 p.

NALDRETT, A.J. and KULLERUD, G. (1967): A Study of the Strathcona Mine and its Bearings on the Origin of the Ni-Cu Ores of the Sudbury District, Ontario, J. Petrology, 8, pp. 453-531.

_____, BRAY, J.G., GASPARRINI, E.L., PODOLSKY, T., and RUCKLIDGE, J.C. (1970): Cryptic Variation and the Petrology of the Sudbury Nickel Irruptive, Econ. Geol., 65, pp. 122-155.

_____, ARMSTRONG, T., HEWINS, R.H., PATTISON, E.F. and PHIPPS, D. (1971): Field Guide to the Sudbury Nickel Irruptive, G.A.C., M.A.C. Meeting, May 12-15, 1971.

PARTHÉ, E. (1971): Platinum, in Wedepohl, K. (ed.), Handbook of Geochemistry, II-1, Chap. 78, Springer-Verlag, Berlin.

PAULING, L. (1960): The Nature of the Chemical Bond, 3rd Ed., Cornell University Press, Ithaca, N.Y.

PERKIN-ELMER (1971): Analytical Methods for Atomic Absorption Spectrometry.

PHEMISTER, T.C. (1925): Igneous Rocks of Sudbury and their Relation to the Ore Deposits, Ont. Dept. Mines Ann. Rept., 34, Pt. 8.

_____ (1956): The Copper Cliff Rhyolite in McKim Township, District of Sudbury, Ont. Dept. Mines Ann. Rept., 65, Pt. 3, pp. 91-116.

RAKOVIC, MILOSLAV (1970): Activation Analysis, Academia, Prague, English Ed., The Chemical Rubber Co., Cleveland, Ohio.

RAZIN, L.V., KHVOSTOV, V., and NOVIKOV, V. (1965): Platinum Metals in the Essential and Accessory Minerals in Ultramafic Rocks, Geochem. Int., 2, pp. 118-131.

SHANNON, R.D. and PREWITT, C.T. (1969): Effective Ionic Radii in Oxides and Fluorides, Acta Cryst., B25, pp. 925-946.

SHEWMON, P.G. (1963): Diffusion in Solids, McGraw-Hill Series in Material Science and Engineering, 203 p.

SOUCH, B.E., PODOLSKY, T. and MEMBERS OF THE GEOLOGICAL STAFF, INTERNATIONAL NICKEL CO. OF CANADA LTD. (1969): The Sulfide Ores of Sudbury, their Particular Relation to a Distinctive Inclusion-bearing Facies of the Nickel Irruptive, in Wilson, H.D.B. (ed.), Econ. Geol.,

Mono. 4, Magmatic Ore Deposits, pp. 252-261.

STEVENSON, J.S. (1972): The Onaping Ash-flow Sheet, Sudbury, Ontario, in Guy-Bray, J.V. (ed.), New Developments in Sudbury Geology. The Geol. Assoc. of Can., Special Paper 10, pp. 41-48.

TAYLOR, L.A. (1970) Low Temperature Phase Relations in the Fe-S System, Carnegie Inst. Wash. Yb., 68, pp. 259-270.

THOMSON, J.E. (1956): Geology of the Sudbury Basin, Ont. Dept. Mines Ann. Rept., 65, Pt. 3, pp. 1-56.

_____ (1969): Discussion of Sudbury Geology and Sulfide Deposits, Ont. Dept. Mines Misc. Pub. 30, 22 p.

TONG, S.L. (1971): Mass-yield variations in the Thermal and Epi-Thermal Fission of ^{239}Pu, Unpub. Ph.D. Thesis, McMaster University.

VAUGHAN, D.J., SCHWARZ, E.J., and OWENS, D.R. (1971): Pyrrhotite from the Strathcona Mine, Sudbury, Canada, A Thermomagnetic and Mineralogical Study, Econ. Geol., 66, pp. 1131-1144.

WAGNER, C. (1952): Thermodynamics of Alloys, Addison Wesley Pub. Co., Inc. 161 p.

WALKER, T. L. (1897): Geological and Petrographical Studies of the Sudbury Nickel District, Canada, Geol. Soc. London, 53, pp. 40-66.

WANDKE, A. and HOFFMAN, R. (1924): A Study of the Sudbury Ore Deposits, Econ. Geol., 19, pp. 169-204.

WARD, J.C. (1970): The Structure and Properties of Some Iron Sulfides, Rev. Pure and Appl. Chem., 20, pp. 175-206.

WELLS, H. L. (1889): Sperrylite, A New Mineral, Am. J. Sci., 37, pp. 67-70.

WESTCOTT, C. H. (1957): CRRP-680.

_____ (1962): AECL-1101.

WILLIAMS, Howell (1956): Glowing Avalanche Deposits of the Sudbury Basin, Ont. Dept. Mines Ann. Rept., 65, Pt. 3, pp. 57-89.

WILSON, H. D. B. (1956): Structure of Lopoliths, Geol. Soc. Am. Bull., 67, pp. 289-300.

YATES, A. B. (1938): The Sudbury Irruptive, Roy. Soc. Can. Trans., 32, (VI) pp. 151-172.

_____ (1948): Properties of the International Nickel Company of Canada, in Structural Geology of Canadian Ore Deposits, 2(Congress Volume), Montreal, Can. Inst. Min. Metall.

APPENDIX A

SELF-ABSORPTION OF ^{109}Pd BETA RADIATION

Self-absorption is proportional to the thickness of the source and consequently a sample with higher chemical yield may be expected to have an apparently lower specific activity due to this effect. A calibration curve is determined by using radioactive ^{109}Pd as tracer and is used to correct for this effect. The procedure for preparation of the sources is as follows:

Irradiate about 30mg of Pd standard solution containing 4.048mg Pd/ml. for 24 hours and cool for 12 hours. Wash the irradiated solution out of the ampoule into a 100ml beaker with 1M HCl and dilute to 50ml. Pipette 1ml of this solution into each of several Pd carrier solutions containing different weights of Pd. Warm on a hot plate to homogenize. Precipitate Pd with 5 to 10ml of 1.5% dimethylglyoxime in ethanol, dissolve the precipitate with aqua regia, convert to chloride, and repeat the precipitation. Transfer the Pd dimethylglyoximate into 50ml centrifuge tubes, wash twice with ethanol.

Plate the precipitate out carefully with the aid of a capillary pipette on a preweighed Al-planchet to ensure uniformity of the Pd dimethylglyoximate layer. Dry the salt slowly with an infra-red heat lamp and weigh to determine the chemical yield.

Figure A-1 shows the percentage of activity with respect to a carrier-free source (i.e. a carrier-free source set at 100%), plotted as a function of weight of Pd. In the present research, about 5mg Pd was usually taken for the carrier. Therefore, a 20% chemical yield difference between sample and standard would produce about 2% error if no correction for self-absorption was applied.

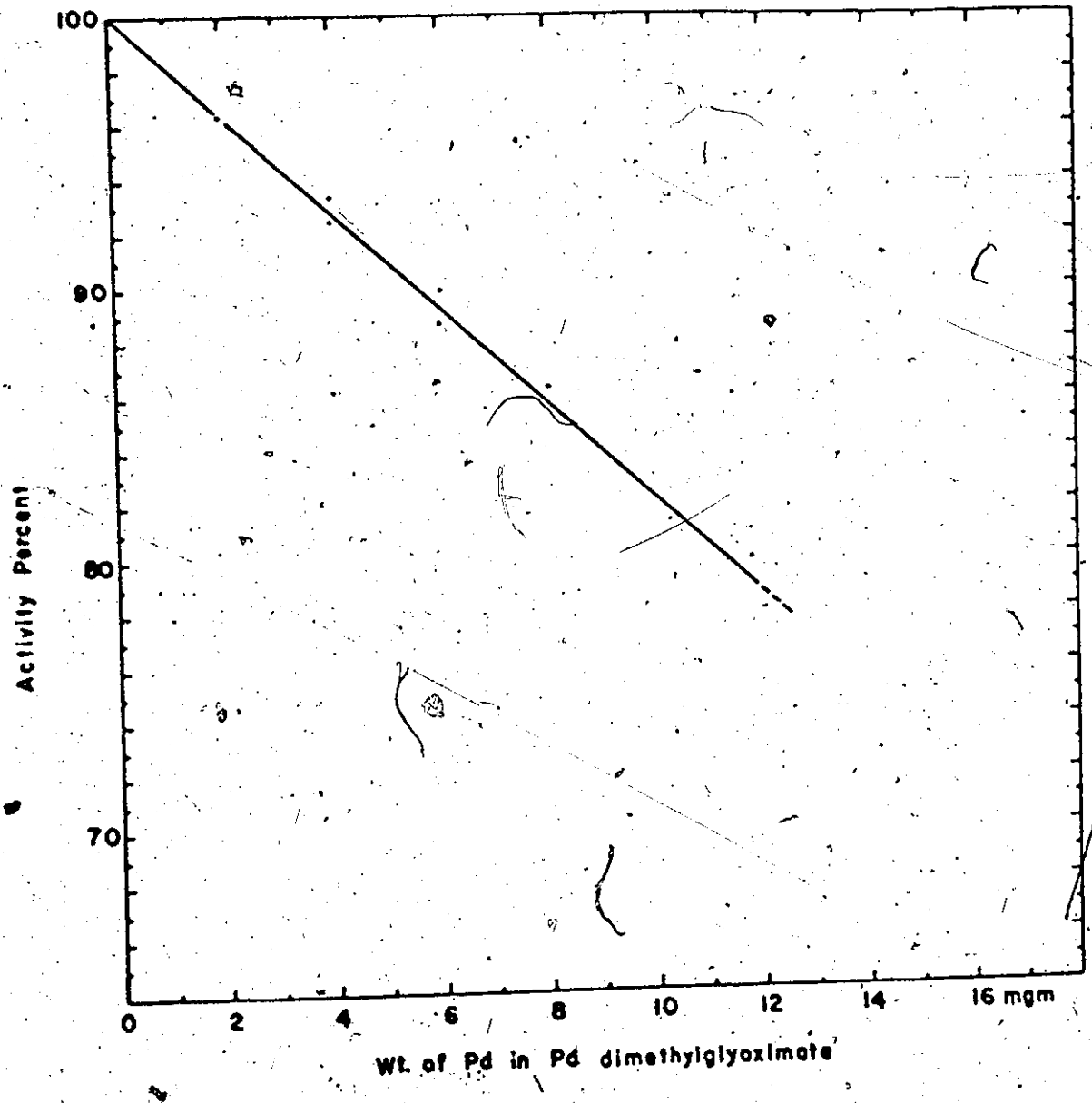

Figure A-1. Self-absorption of ^{109}Pd as a Function of Pd Weight in Pd Dimethylglyoximate.

APPENDIX B

NEUTRON FLUX ATTENUATION

Neutron activation is based on the assumption that both sample and standard are irradiated by the same neutron flux. This is nearly justified when the sample size is small or contains insignificant amounts of elements having large absorption cross sections. Considerable error can be introduced if the sample and standard are not irradiated by the same energy spectrum of neutrons.

Two important factors cause changes of the energy spectrum of the neutrons on penetrating the material - self-absorption and hardening of the neutron flux. The distortion of the spectrum is largely caused by the former.

Self-absorption increases with the mass of sample material irradiated and with the proportion of elements with high absorption cross sections in the material being irradiated. There are two ways to reduce the error introduced by this effect (Rokovic, 1970): 1) Preparing sample and standard in such a manner so that the self-absorption

effect is the same for both standard and sample, and 2) using an internal standard method.

If the neutron flux is coming from only one direction through a layered sample with thickness X, the neutron flux after passing through the sample Φ is related to the original flux Φ_o by the relation (Rokovic, 1970):

$$\Phi/\Phi_o = e^{-X \sum_i N_i (\sigma_a)_i} \quad (1)$$

where N_i is number of target nuclei of the i-th nuclide in 1 cm^3 of sample and $(\sigma_a)_i$ is its absorption cross section. This simple equation cannot be used to correct for self-absorption of a non-layered sample, and for the case of a neutron flux from more than one direction. Equation (1), however, does give an estimate of the maximum neutron absorption by samples contained in quartz ampoule and irradiated by an isotropic neutron flux.

Among the four minerals analysed, the largest absorption of the neutron flux occurs in case of chalcopyrite due to ^{63}Cu (the mineral contains 34.6% Cu which is 69.2% ^{63}Cu; the nuclide has an absorption cross section, σ_a = 4.7 barns). As 1 cm^3 of chalcopyrite weighs 4.4gm,

$$N_i = \frac{4.4 \times 0.346 \times 0.692 \times 6.02 \times 10^{23}}{63.54} = 9.98 \times 10^{21}$$

where the atomic weight of Cu = 63.54gm/mole, the Avogrado Number = 6.02×10^{23} atoms/mole.

For a quartz ampoule with an inner diameter of 2 mm, the ratio Φ/Φ_o calculated from (1) is,

$$\Phi/\Phi_o = e^{-0.2 \times 9.98 \times 10^{21} \times 4.7 \times 10^{-24}} = e^{-9.38 \times 10^{-3}} = e^{-0.00938}$$

$$= 0.9914$$

giving a maximum absorption of about 1%. This type of error due to self-absorption of the matrix material is much smaller in case of pyrrhotite, magnetite, and pentlandite. These minerals do not contain significant amounts of elements with high-absorption cross sections.

APPENDIX C

TEST FOR WHETHER THE REGRESSION LINE PASSES THROUGH THE ORIGIN

This test is described in "Scientific Method in Analysis of Sediments" by Griffiths (1967), pp. 446-447. Assume Y determinations are normally and independently distributed around their respective mean in the range of X values used for regression and can be defined by the linear equation

$$Y = \hat{\alpha} + \hat{\beta} X \tag{1}$$

$$\text{Variance } (\hat{\alpha}) = \frac{\hat{\sigma}^2_{YX}}{n-2} \tag{2}$$

$$\sigma^2_{YX} = \frac{\Sigma Y_i^2 - \hat{\alpha}\Sigma Y_i - \hat{\beta}\Sigma X_i Y_i}{n-2} \tag{3}$$

$$\hat{\beta} = \frac{N\Sigma X_i Y_i - \Sigma X_i \Sigma Y_i}{N\Sigma X_i^2 - (\Sigma X_i)^2} \tag{4}$$

$$\hat{\alpha} = \frac{\Sigma Y_i \Sigma X_i^2 - \Sigma X_i \Sigma X_i Y_i}{N\Sigma X_i^2 - (\Sigma X_i)^2} \tag{5}$$

Confidence limits at the 99% level were used for the present calculations.

$$\hat{c} - t_{c,\,n-2}\hat{\sigma}_{\hat{c}} > c > \hat{c} + t_{c,\,n-2}\hat{\sigma}_{\hat{c}} \qquad (6)$$

The statistic t is distributed as Student's t with n-2 degrees of freedom. The regression line passes through the origin with 99% probability if this interval includes zero.

APPENDIX D

SENSITIVITY LIMITS FOR Pt

Pt is determined by counting the 158 KeV radiation of ^{199}Au produced in the reaction $^{198}Pt\,(n,\gamma)\,^{199}Pt \xrightarrow{\beta^-} {}^{199}Au$. Sensitivity calculations must, however, consider the interfering reaction $^{197}Au\,(2n,\gamma)\,^{199}Au$.

We consider first the case for no interference from Au, calculating the minimum detectable concentration C as,

$$C(ppb) = \left(\frac{AW}{\phi\sigma aNw}\right) / \left(1 + \frac{\lambda_2}{\lambda_1-\lambda_2}\, e^{-\lambda_1 t_{ir}} - \frac{\lambda_1}{\lambda_1-\lambda_2}\, e^{-\lambda_2 t_{ir}}\right)$$

where the terms in the exponential are defined as in equation (4), p. 57.

and A = minimum detectable activity = 10 d/s in the 158 KeV region

W = physical atomic weight of ^{198}Pt

ϕ = neutron flux = 10^{13} n/cm^2/sec.

σ = reaction cross section for ^{198}Pt with neutrons

a = fractional atomic abundance of ^{198}Pt

N = Avogadro Number

w = sample weight = 100 mg.

t_{ir} = irradiation time = 14 days

For these conditions C, the minimum detectable activity is 0.12 ppb.

To take account of the interference from Au we note the following two conditions: (1) by experiment, we establish that for pure gold spectra about 30% of the total radiation is in the 158 KeV region (i.e. Compton from ^{198}Au plus the (2n, γ) contribution from ^{199}Au) and (2) we require that a minimum of 25% of the total radiation in the 158 KeV region be due to ^{199}Au produced from Pt in order that a statistically significant subtraction of the gold interference can be made (refer to Fig. 47, p. 68). These conditions permit about 30 d/s in the 158 KeV region from gold due to the reactions ^{197}Au (n, γ) ^{198}Au (Compton portion) plus ^{197}Au (2n, γ) ^{199}Au (interference), which in turn allow a total ^{198}Au activity of about 100 d/s. This, in turn, corresponds to a gold concentration of 0.0034 ppb. and a Pt/Au ratio of 0.12/0.0034 = 35.

Gold concentrations in the Strathcona cross-cut samples average 5 ppb. Therefore, as a 35/1 ratio of Pt/Au is required the minimum effective Pt concentration needed for measurement is approximately 175 ppb. It is noted that the lowest reported Pt value in the study is 244 ppb. (Table 5-4, Sample D4).